Lawrence Berkeley National Laboratory
Recent Work

Title
Photodissociation Dynamics of OC10

Permalink
https://escholarship.org/uc/item/7q6406jk

Journal
Journal of Chemical Physics, 105(18)

Author
Davis, H.F.

Publication Date
1996-04-01

Lawrence Berkeley Laboratory
UNIVERSITY OF CALIFORNIA

CHEMICAL SCIENCES DIVISION

Photodissociation Dynamics of OClO

H.F. Davis and Y.T. Lee

April 1996

DISCLAIMER

Photodissociation Dynamics of OClO

H. Floyd Davis* and Yuan T. Lee

Department of Chemistry
University of California, Berkeley

and

Chemical Sciences Division
Ernest Orlando Lawrence Berkeley National Laboratory
University of California
Berkeley, California 94720

April 1996

*Author to whom correspondence should be addressed at Department of Chemistry, Baker Laboratory, Cornell University, Ithaca, NY 14853-1301. Electronic mail: HFD1@Cornell.edu

ABSTRACT

Photofragment translational energy spectroscopy was used to study the dissociation dynamics of a range of electronically excited $OClO(^2A_2)$ vibrational states. For all levels studied, corresponding to OClO ($^2A_2 \leftarrow {}^2B_1$) excitation wavelengths between 350 and 475 nm, the dominant product ($>96\%$) was ClO ($^2\Pi$) + O(^3P). We also observed production of Cl + O$_2$ with a quantum yield of up to 3.9 ± 0.8 % near 404 nm, decreasing at longer and shorter wavelengths. The branching ratios between the two channels were dependent on the OClO $^2A_2$ excited state vibrational mode. The Cl + O$_2$ yield was enhanced slightly by exciting OClO ($^2A_2$) levels having symmetric stretching + *bending,* but diminished by as much as a factor of 10 for neighboring peaks associated with symmetric stretching + *asymmetric stretching.* Mode specificity was also observed in the vibrationally state resolved translational energy distributions for the dominant $ClO(^2\Pi)$ + O(^3P) channel. The photochemical dynamics of OClO possesses two energy regimes with distinctly different dynamics observed for excitation energies above and below $\sim$ 3.1 eV ($\lambda \sim$ 400 nm). At excitation energies below 3.1 eV ($\lambda >$ 400 nm), nearly all energetically accessible ClO vibrational energy levels were populated, and the Cl + O$_2$ channel was observed. Although at least 20% of the O$_2$ product is formed in the ground ($X^3\Sigma$) state, most O$_2$ is electronically excited ($a^1\Delta$). At E < 3.1 eV, both dissociation channels occur by an indirect mechanism involving two nearby excited states, OClO $^2A_1$ and $^2B_2$. Long dissociation timescales and significant parent bending before dissociation led to nearly isotropic polarization angular distributions ($\beta \sim$ 0). At excitation energies above 3.1 eV ($\lambda <$ 400 nm), the Cl + O$_2$ yield began to decrease sharply, with this channel becoming negligible at $\lambda <$ 370 nm. At these higher excitation energies, the ClO product was formed with relatively little vibrational energy and a large fraction of the excess energy was channeled into ClO + O translational energy. The photofragment anisotropy parameter (β) also increased, implying shorter dissociation timescales. The sharp change in the disposal of excess energy into the ClO products, the decrease of Cl + O$_2$ production, and anisotropic product angular distributions at E > 3.1 eV signify the opening of a new ClO + O channel. From our experimental results and recent *Ab-Initio* calculations, dissociation at wavelengths shorter than 380 nm to ClO + O proceeds via a direct mechanism on the optically prepared $^2A_2$ surface over a large potential energy barrier. From the $ClO(^2\Pi)$ + O(^3P) translational energy distributions, D_o(O-ClO) was found to be 59.0 ± 0.2 kcal/mole.

I. INTRODUCTION

Experimental studies of competitive dissociation pathways following electronic excitation of small molecules provide important insight into the topography of excited state potential energy surfaces. For most simple triatomics, (NO_2, SO_2, FNO, H_2O etc.) more than one chemical channel at commonly studied wavelengths is ruled out by thermodynamics.[1] However, there exists several small molecules which have, in addition to simple bond fission, decomposition channels involving the breaking and forming of more than one chemical bond. Formaldehyde is a benchmark system where two chemically distinct channels coexist, (i.e. H + HCO and H_2 + CO), and extensive experimental and theoretical work has provided considerable insight into the dynamics of these reactions.[2-4] Although there have been several studies of H_2 elimination from alkenes[5] and HCl loss from halogenated hydrocarbons,[6,7] molecular elimination channels in heavier systems[8,9] not involving at least one hydrogen atom is quite rare.

An interesting prospect in the excited state dynamics of molecules having multiple channels is to enhance a particular dissociation channel by selective excitation of the reactant. *Bond selective* photochemistry was demonstrated in C_2H_4BrI by selecting an ultraviolet excitation wavelength corresponding primarily to a $\sigma^* \leftarrow \sigma$ transition localized on the C-Br bond.[10] It was possible to preferentially break the stronger C-Br bond, leaving the weaker C-I bond relatively intact. Crim's group[11,12] and others[13,14] have carried out extensive studies of bond and mode specific chemistry using vibrational overtone excitation followed by electronic excitation to an excited potential energy surface. In many cases, the reactant vibrational excitation was selectively channeled into the product's vibrational degree(s) of freedom, and in favorable cases vibrationally mediated photodissociation facilitated access to regions of the excited potential energy surface favoring fission of a particular bond. For example, ultraviolet photodissociation of HOD ($4\nu_{OH}$) led to preferential OH bond fission, producing >15 times more OD than OH.[12]

The existence of vibrational structure in the electronic absorption spectra of fast evolving states provides another approach to studying the role of parent vibrational motion in molecular photodissociation. Reisler and coworkers[15] have demonstrated that parent ClNO bending is preferentially channeled into NO product rotational excitation, and studies of CH_3ONO photodissociation has shown that reactant NO stretching vibrations are preferentially deposited into product NO vibrations.[16,17] Recent studies of SO_2[18] photodissociation have revealed the existence of mode specific SO vibrational distributions from different SO_2 C($^1B_2$) vibrational levels. Hepburn et al.[19] demonstrated that the electronic state distribution of the sulfur atom product from CS_2 photodissociation depends on which band in the $^1B_2(^1\Sigma^+_u) \leftarrow X(^1\Sigma^+_g)$ absorption spectrum is pumped.

The studies mentioned above have demonstrated that selective excitation of well defined vibrational levels in predissociative excited states may have profound effects on product rotational, vibrational, and electronic state distributions. To date however, there have been few examples in which

chemical branching ratios are strongly affected by initial nuclear motion. Earlier, mode specific $Cl + O_2$: $ClO + O$ branching ratios from different initial $OClO(^2A_2)$ vibrational levels were illustrated.[20] Relative to pure symmetric stretching modes $(v_1,0,0)$, the Cl yield was slightly enhanced for combination bands containing one quantum of *bending* $(v_1,1,0)$ and significantly diminished for neighboring $OClO$ levels having *asymmetric stretching* excitation $(v_1-1,0,2)$. The $Cl + O_2$ yields from $OClO$ photodissociation reached a peak near 400 nm, with yields of 3.9%, 3.0%, and 0.4% for the $(5,1,0)$, $(5,0,0)$ and $(4,0,2)$ levels, respectively. (Fig. 1) This mode specificity, leading to nearly an order of magnitude change in $Cl + O_2$ yields for neighboring $OClO$ $(^2A_2)$ levels, is striking in light of the fact that the levels span an energy range of only a few hundred wavenumbers.[21] Since $OClO$ fluorescence is negligible in this wavelength range due to picosecond dissociation timescales,[21-27] and since no other channels (*e.g.* $Cl + O + O$) are thermodynamically accessible,[28-30] the $ClO + O$ yields ranged from 96.1% for $OClO$ $(5,1,0)$ to 99.6% for $OClO$ $(4,0,2)$. Apparently, asymmetric stretching in the initially prepared parent $OClO$ molecule enhances simple bond fission forming $ClO + O$, thereby diminishing $Cl + O_2$ production.

The decline in Arctic and Antarctic ozone due to chemical reactions catalyzed by atmospheric chlorine has sparked considerable interest in the chemistry of halogen oxides.[31-37] The concentration of ClO and $OClO$ in the Antarctic stratosphere reaches levels nearly two orders of magnitude higher than normal, and these levels anticorrelate with O_3 abundance.[32] It has been generally assumed[32] that near ultraviolet excitation of $OClO$ results in O-ClO bond fission (Fig. 2):

$$OClO\ (X\ ^2B_1) \rightarrow OClO\ (A^2A_2) \rightarrow ClO(X^2\Pi) + O(^3P). \qquad (1)$$
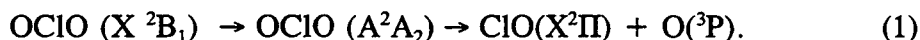
Since the newly generated O atom may combine with atmospheric O_2 to reform ozone, this channel leads to a net null cycle in the atmospheric ozone budget. However, the alternative channel regenerates a reactive Cl atom:

$$OClO \rightarrow Cl(^2P) + O_2(^3\Sigma_g^-,\ ^1\Delta_g,\ ^1\Sigma_g^+) \qquad (2)$$
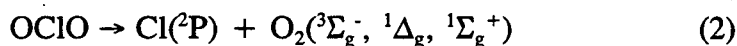
This channel leads to net destruction of atmospheric ozone.[38-41] According to recent estimates, if the quantum yield for channel 2 was >0.1 across the entire $OClO$ absorption spectrum, it would contribute as much as several percent to the currently observed levels of ozone depletion.[41] However, the relevance of $OClO$ photodissociation to the balance of ozone remains uncertain in the absence of complete quantum yield measurements over an range of excitation wavelengths.

The nature of the $OClO$ excited state potential energy surfaces and the coupling between them controls the branching between $ClO + O$ and $Cl + O_2$ production.[42-44] Spectroscopic studies[21-26,45] have shown that the $A^2A_2 \leftarrow X^2B_1$ absorption linewidths increase steadily with v_1 (symmetric stretch) above $v_1 = 3$ in electronically excited $OClO(^2A_2)$ due to decreasing excited state lifetimes. Interestingly, the

linewidths associated with excitation of symmetric stretching + *bending* $(\nu_1,1,0)$, or symmetric stretching + *asymmetric stretching* $(\nu_1,0,2)$, were broader at $\nu_1 = 3\text{-}7$ than those due to symmetric stretching excitation $(\nu_1,0,0)$ alone.[21] Although this suggests that the dissociation dynamics might be vibrationally mode specific, to date there have been no systematic studies of OClO photochemistry as a function of $^2A_2$ vibrational level.

In matrix isolation experiments at low temperature, Arkell and Schwager,[46] and others,[47-49] reported that photolysis of OClO led to formation of ClOO. Unlike symmetric OClO which can be readily synthesized and studied, the ClOO peroxy isomer remains poorly characterized because of its extreme reactivity due to a very weak Cl-O_2 bond ($D_o = 4.5$ kcal/mole).[50] Arkell and Schwager[46] suggested that the ClOO isomer resulted from recombination of the ClO + O fragment pairs in the matrix cage. Note that unlike OClO, the ClOO isomer is transparent at $\lambda > 300$ nm and will rapidly accumulate under conditions of steady state photolysis, giving the appearance that OClO $\rightarrow$ ClOO isomerization is dominant even if ClO + O are the nascent products. Under collision free conditions in the gas phase however, recombination of the fragments is not possible and the experimental branching ratios between ClO + O and Cl + O_2 must reflect the primary photochemistry.

To date, most previous studies in the gas phase[39,40,51-53] and in solution[54,55] have focussed on the most intense absorption peaks near 360 nm, where OClO (A^2A_2) symmetric stretching levels, $\nu_1 = 8\text{-}11$ are populated. Ruhl, Vaida and coworkers[39] photodissociated gaseous OClO using a focussed dye laser. Absorption of additional photons from the same pulse led to multiphoton ionization of the products. Although it was concluded that ClO(v'=4-6) + O(^3P) were the primary products, several features in the Cl$^+$ action spectrum near 362 nm were taken as evidence for Cl + O_2 production but the quantum yield was not determined. Lawrence and Apkarian[51] later studied the gas phase photodissociation of OClO at wavelengths in the range 359-368 nm, and were unable to see any evidence for Cl + O_2 formation. They set an upper limit to the Cl quantum yield of $<5 \times 10^{-4}$ (0.05%) in this wavelength region.

Subsequently, Bishenden and Donaldson (BD)[52,53] have investigated the photodissociation of OClO near 360 nm using 2+1 REMPI at 235 nm for detection of the Cl atomic product. They concluded that Cl atoms *are* formed upon single photon excitation of OClO near 360 nm, initially reporting a Cl yield of 0.15 (15%). We have studied OClO photodissociation dynamics using photofragment translational energy spectroscopy.[20] In addition to the dominant ClO + O channel, we observed Cl *and* O_2 from photodissociation of OClO near 400 nm. However, like Lawrence and Apkarian[51] we were unable to see any evidence for this channel near 360 nm, but as expected did observe strong ClO + O signal. We reported an upper limit of 0.2% for the Cl + O_2 yield at $\lambda \sim 360$ nm and concluded that the ClO + O channel accounts for > 99.8% of the absorption cross section.

BD has subsequently revised their earlier value of 15% to be an upper limit, with a lower limit being a few percent.[53] They have also reported that the ClO + O quantum yield near 360 nm was enhanced by excitation of combination bands having two quanta of asymmetric stretching (8,0,2) or

(9,0,2). Although this seems similar to our earlier observations of mode specific branching ratios at longer wavelengths, in our case the enhancement of ClO + O was accompanied by a diminished yield of Cl + O_2, and vice versa.[20] In the report by BD, on the other hand, the Cl REMPI spectra matched the OClO absorption spectrum for all OClO ($^2A_2$) levels near 360 nm. They thus concluded that the Cl + O_2 yield was *constant* (*i.e.*, at least a few percent) while the ClO + O yield was wavelength dependent. This result is difficult to rationalize however, since fluorescence must be negligible due to picosecond dissociation timescales, and other dissociation channels are thermodynamically closed. Since product flux must be conserved, enhancement in one dissociation channel should be accompanied by a decrease in the other.

Ab-Initio calculations on the ground and excited electronic states of OClO were first carried out by Gole in 1980.[42] His calculations confirmed that the photochemical dynamics of OClO involves interactions between several different excited electronic states. From earlier spectroscopic studies, it was known that absorption between 220 and 460 nm (Fig. 1) corresponds primarily to the parallel $^2A_2$ ← $^2B_1$ transition.[22-26] The $^2B_2$ and $^2A_1$ states lie at energies slightly below the prepared $^2A_2$ state.[42,43] Although the $^2A_1$ ← $^2B_1$ transition should be a dipole allowed, direct $^2B_2$ ← $^2B_1$ excitation is symmetry forbidden. The $^2A_1$, if accessed, should be strongly coupled by vibronic interactions to the "dark" strongly bent $^2B_2$ state which, according to Gole, could subsequently undergo concerted rearrangement in the matrix forming the peroxy Cl-O_2 isomer. Thus, direct excitation to the $^2A_1$ state followed by vibronic coupling to the $^2B_2$ was suggested as a possible mechanism for ClOO production, rather than geminate ClO + O recombination.[42] Although subsequent spectroscopic studies[21,45] have indicated that the $^2A_1$ state carries no oscillator strength in the near UV, as discussed in the next paragraph recent theoretical work[43] confirms the involvement of the $^2A_1$ state in OClO photodissociation.

Recently, Peterson and Werner carried out Ab-Initio calculations on OClO → ClO + O[43], and in the following paper, specifically address OClO → Cl + O_2.[44] Cuts of their potential energy surface[43] are reproduced in Fig. 3. Due to the existence of a potential energy barrier for dissociation to ClO + O along the $^2A_2$ asymmetric stretching coordinate, the low lying levels of OClO($^2A_2$) are bound along all three normal modes and dissociation requires the involvement of other states. From the recent calculations, it was concluded that the $^2A_2$ is coupled primarily to the $^2A_1$ by spin-orbit interactions. OClO ($^2A_1$) can subsequently dissociate through a nearly linear configuration to ClO($^2\Pi$) + O(^3P). Another decay mechanism for the $^2A_1$ state involves vibronic coupling to the strongly bent $^2B_2$ due to the presence of a conical $^2A_1/^2B_2$ intersection. OClO ($^2B_2$), in turn can decay by two alternative paths, to either ClO($^2\Pi$) + O(^3P) or Cl(^2P) + $O_2(^3\Sigma,^1\Delta)$.

II. EXPERIMENTAL

A. The molecular beam apparatus.

The experimental apparatus employs a molecular beam source which can be rotated through an angle of 90 degrees in a vertical plane perpendicular to the (horizontal) laser axis.[57] The seeded

supersonic molecular beam, described below, was collimated by two skimmers separated by a region of differential pumping, and was crossed by the unfocussed output (~ 3 mm dia.) from an excimer-pumped Lambda-Physik FL2002 dye laser (0.5-10 mJ, 20 ns, 50 Hz). A fraction of the photodissociation products recoiled out of the molecular beam into an electron bombardment ionizer located 36.8 cm away from the interaction region. After ionization by 200 eV electron impact, positive ions were extracted into a quadrupole mass filter (Extrel) and counted by a Daly-type ion detector. A multichannel scaler, triggered by the laser pulse, was used to record the product time of flight spectra at various angles between the molecular beam and detector.

B. The OClO molecular beam.

OClO was generated by passing 5% Cl_2/He at ~ 760 Torr through a U-tube containing $NaClO_2$ and glass beads, as described elsewhere.[20,58] Note that OClO is known to be explosive under certain conditions and should be handled with great care. The mixture flowed through teflon tubing to a piezoelectric driven pulsed molecular beam source.[59] After the $NaClO_2$ column was operated for some time, the $Cl_2 \rightarrow$ OClO conversion efficiency decreased and significant Cl_2 contaminant appeared in the beam. After some experimentation using various $NaClO_2$ samples, this behavior was attributed to the drying of the column over the course of the experimental run. Apparently, the heterogeneous conversion of Cl_2 to OClO requires the presence of some H_2O. The conversion efficiency could be increased reliably to $\sim 100\%$ by presaturating the Cl_2/He mixture with water by bubbling through room temperature water and then flowing this mixture through the $NaClO_2$ tube. Since the presence of water vapor was undesirable due to OClO-H_2O cluster formation, the OClO/H_2O/He mixture was passed through a -10° C trap to remove H_2O before entering the molecular beam source.

For TOF data recorded at small angles between the beam and detector axis, some time dependent background was observed in experiments using the pulsed beam when the laser was turned off. This signal results from the time dependent intensity fluctuation of OClO background near the beam axis due to the pulsed nature of the beam. When this signal was present, parallel experiments were conducted with the laser on and off and difference spectra were employed for the analysis.

C. Data Analysis

The product time of flight spectra were analyzed using a version of the program CMLAB2[60,61] running on a personal computer. The data analysis involved an iterative forward convolution method, described elsewhere.[60] Using the known apparatus functions and the measured molecular beam velocity distribution, a trial P(E) and CM angular distribution (β parameter)[62,63] was used to calculate the TOF distribution for a fragment mass at a given molecular beam- detector angle. The calculated TOF were compared to the experimental data and then an improved P(E) was generated to better simulate the data. This procedure was continued iteratively using data obtained at several detector angles until good agreement was achieved between the experimental and simulated TOF.

The photofragment anisotropy[62,63] (β parameter) was measured for a number of excitation wavelengths. To reduce saturation effects, TOF spectra were obtained at low pulse energies ($\leq$ 0.5 mJ). The polarization of the laser was rotated with respect to the detector axis using a quartz double Fresnel rhomb (Optics for Research). TOF spectra were recorded and then integrated for different polarization angles in 30 degree increments.

III. RESULTS AND ANALYSIS

A. Primary Channels from (5,1,0) Level

Time of flight (TOF) data was recorded with the mass spectrometer set at Cl^+, ClO^+, O^+, and O_2^+. Because the detector is located away from the molecular beam axis, only the photofragments are detected in our experiments. The Newton diagram in velocity space for the Cl-containing fragments from dissociation of OClO $^2A_2$ (5,1,0) at 404 nm is shown in Fig. 4. Excitation at 404 nm (Fig. 2) prepares OClO ($^2A_2$) levels lying 11.7 kcal/mole above D_o(O-ClO); ClO($X^2\Pi$) may be produced in vibrational levels up to v"= 4. We observe Cl^+ signal (m/e =35) from two different sources. The dominant source is from fragmentation of ClO (from ClO + O channel) in the electron bombardment ionizer, and the minor source is from the Cl + O_2 channel. Since the reaction OClO $\rightarrow$ Cl($^2P_{3/2}$) + $O_2(^3\Sigma)$ is nearly thermoneutral (Fig. 2), and because a large potential energy barrier exists along the reaction coordinate, a relatively large translational energy release is anticipated. For each excitation wavelength, TOF data was obtained for each product species at several different angles and the entire data set was used in the analysis. By observing both momentum matched counterfragments (i.e. ClO + O or Cl + O_2) and by determining the TOF at several different angles, we can monitor both product channels with comparable sensitivity and can directly measure the Cl(^2P) + O_2 : ClO + O(^3P) branching ratios.

The TOF data obtained with the mass spectrometer tuned to m/e = 51 (ClO^+) and m/e = 35 (Cl^+) at 20° is shown in the upper panels of Fig. 5. The solid lines are the calculated TOF based on the optimized product translational energy distribution P(E), described below. The large slow component at 200-600 μs is identical to that seen for ClO^+ and results from fragmentation of ClO to Cl^+ in the ionizer. The small, fast contribution seen at ~ 120 μs in the Cl data is from the Cl + O_2 channel. In the inset to the Cl TOF at 20° (Fig. 5), the vertical scale for the Cl + O_2 peak is expanded by a factor of 15 at T = 140 -200 μsec. The bottom panel of Figure 5 shows the O_2^+ TOF resulting from the Cl + O_2 channel. Figure 6 shows the O^+ TOF recorded at 40° and 70°. This signal results exclusively from O atoms from the ClO + O channel since the ClO is constrained to θ < 40°. Contribution from fragmentation of O_2 (from the Cl + O_2 channel) to O^+ in the detector is negligible.

The entire data set for each wavelength was fitted to a single P(E) for each channel. The P(E) for the ClO + O channel was primarily derived from the O^+ data since the TOF for the faster light fragment showed the most resolvable structure. The solid lines in the TOF spectra were calculated

using the translational energy distributions (P(E)'s) shown in Fig 7. The maximum calculated translational energies for formation of vibrationally excited diatomic molecules are indicated. The structure in the P(E) for the ClO + O(^{3}P) channel clearly corresponds to a progression in ClO X^{2}Π (v"). From conservation of energy:

$$E_{photon} + E_{int,OClO} = D_o(O-ClO) + E_{trans,ClO+O} + E_{int,ClO} + E_{int,o} \qquad (3)$$

Pulsed expansion of 10% OClO in He at 1 atm should result in substantial rotational cooling. Since the laser was tuned to peaks assigned to the OClO ^{2}A$_2$(v_1,v_2,v_3) ← ^{2}B$_1$(0,0,0) transition, hot-band contributions are negligible so E$_{int, OClO}$ ~ 0. For all spectra reported here, the laser was tuned to OClO peaks corresponding to absorption of the ^{35}Cl isotope.[21] At λ > 274 nm only O(^{3}P$_J$) is thermodynamically accessible: the ground spin orbit state of oxygen atom is ^{3}P$_2$ and excited levels lie at 158 cm^{-1} (^{3}P$_1$) and 227 cm^{-1} (^{3}P$_0$).[28] The O(^{3}P) fine structure splitting is smaller than the spacing between ClO product vibrational energy levels (850 cm^{-1}) and the two ClO(X^{2}Π$_{1/2,3/2}$) spin orbit levels (350 cm^{-1}).[29] Thus we are only able to resolve ClO vibrational structure but some finer detail can be partially resolved at low translational energies where our resolution is greatest (*e.g.* Fig. 7). Since we resolve ClO vibrational structure, the data can be used to check for possible dependence of the ClO fragmentation pattern on its vibrational level. From momentum conservation, the O atom carries the same P(E) information as the ClO fragment. If highly vibrationally excited ClO levels were, for example, more extensively fragmented in the ionizer, the observed intensities of the slowest ClO products would be smaller than predicted from a P(E) derived independently from the O atom TOF. Since good agreement was found between the P(E) derived from the O and ClO TOF data, we conclude that the ClO fragmentation pattern is not very sensitive to vibrational level for v = 1-5, apparently because this level of ClO internal excitation is relatively small and ClO$^+$ is a rather strongly bound ion.

The P(E) for the Cl + O$_2$ channel (Fig. 7-lower) is structured, showing two distinct components. Since the only accessible excited Cl atomic state[28] is ^{2}P$_{1/2}$ at 350 cm^{-1}, the structure and width of the P(E) primarily reflects the O$_2$ internal state distribution. In Fig. 7, the maximum translational energy for formation of various vibrational levels of O$_2$(^{3}Σ), O$_2$(^{1}Δ), and O$_2$(^{1}Σ) are indicated. By energy conservation, the contribution at 41 < E < 67 kcal/mole must correspond to production of Cl + O$_2$(^{3}Σ). As discussed later, the sharp rise below 41 kcal/mole is attributed to dominant production of O$_2$ a^1Δ.

Figure 8 shows the Cl$^+$ TOF spectrum showing the relative contribution for both channels while varying the photolysis laser pulse energy. The signal intensity is proportional to the pulse energy from 0.5-10 mJ/pulse, as expected for a 1 photon process. More importantly, the *shape* of the TOF and the relative contribution from the two channels were constant over this range of laser energies, demonstrating that multiphoton effects are negligible under our experimental conditions.

B. ClO:Cl Detection Sensitivity

The relative detection sensitivity for ClO and Cl was determined directly by photodissociation[64] of ClOCl:

$$ClOCl \rightarrow Cl(^2P) + OCl(^2\Pi) \qquad (4)$$

The TOF data for ClO^+ and Cl^+ resulting from 423 nm photodissociation of ClOCl at 20 and 50 degrees is shown in Fig. 9. As expected, one peak was seen in the ClO TOF whereas two peaks appeared for $m/e = 35$ (Cl^+). The slower peak at Cl^+ results from fragmentation of ClO in the ionizer, and the fast peak in the Cl^+ TOF results from the Cl atom recoiling from ClO. The P(E) for the ClO + Cl channel, obtained by fitting all three TOF spectra, is shown in Fig. 10. The anisotropy parameter (β) was found to be $\sim$-1.0 by measuring the Cl signal intensity as a function of laser polarization angle (Fig. 10-Lower). This result is consistent with recent calculations[65] indicating that the absorption in this wavelength region corresponds to a perpendicular $B_1 \leftarrow A_1$ transition.

According to equation (4) equal numbers of Cl and ClO products must be formed from ClOCl photolysis. After fitting the two peaks to a single P(E) and after properly accounting for the differing transformation Jacobians between the lab and CM reference frames for the two fragments, we obtain the relative detection sensitivity $S_{expt} = 0.32$ for the ClO and Cl fragments from ClOCl dissociation. Using this quantity, the measured ClO fragmentation pattern, and the relative contributions for the two channels in the Cl TOF from OClO photodissociation, we may calculate the Cl:ClO branching ratios for OClO photodissociation.

The relative detection sensitivity[8,66] S_{expt} is given by:

$$S_{expt} = \frac{\sigma_{ion}(ClO)}{\sigma_{ion}(Cl)} \times \frac{F(Cl^+/ClO)}{F(Cl^+/Cl)} = 0.32 \qquad (5)$$

In equation 5, $\sigma_{ion}(ClO)$ and $\sigma_{ion}(Cl)$ are the 200 eV electron impact ionization cross sections for ClO and Cl, respectively. The fraction of ionized ClO fragments to yield Cl^+ is $F(Cl^+/ClO)$ and the fraction of ionized Cl fragments yielding Cl^+ is $F(Cl^+/Cl) = 1$. Since all of the parameters in equation 9 may be determined directly (see below), we may also calculate S (S_{calc}) using values for σ and F, and compare it to our experimental value (S_{expt}). By monitoring the ClO fragment from OClO photodissociation at Cl^+, ClO^+ and O^+, we found that $F(Cl^+/ClO) = 0.24$. The following empirical relationship[8,66,67] relates the peak ionization cross section , σ_{ion}($Å^2$) to molecular polarizability , α ($Å^3$):

$$\sigma_{ion} = 36\sqrt{\alpha} - 18 \qquad (6)$$

Using the known[68] atomic polarizabilities and approximating the ClO polarizability as the sum of its

constituent atomic polarizabilities, we calculate $\sigma_{ClO} = 43.3$ Å^2 and $\sigma_{Cl} = 34.0$ Å^2. Inserting these quantities into equation (6), we find that $S_{calc} = 0.30$, which is within 6 % of the experimental value. We have used the experimental value (S_{expt}) in all calculations below.

C. Determination of Cl:ClO Branching Ratio

The Cl:ClO branching ratio from OClO photolysis was determined from the m/e $=$ 35 (Cl$^+$) TOF spectra. The relative contributions from the two channels in the Cl$^+$ TOF data at 20° (Fig. 5- Top) provides the apparent branching ratio (R_{app}), uncorrected for the detection sensitivities at m/e $= 35$. For OClO (5,1,0), $R_{app} = 0.125$. The actual branching ratio R is obtained from R_{app} by multiplication by the detection sensitivity S(=0.32):

$$R = \frac{\phi(Cl+O_2)}{\phi(ClO+O)} = R_{app} \times S \quad (7)$$

In equation 7, $\phi(Cl + O_2)$ and $\phi(ClO + O)$ are the photochemical quantum yields. After inserting R_{app} and S, we find that R $= 0.040$ for OClO (5,1,0). Since OClO fluorescence is negligible at these wavelengths due to picosecond dissociation timescales,[24,25] $\phi(Cl+O_2) + \phi(ClO+ O) = 0.99$ -1.0, so we conclude $\phi(Cl+O_2) = 0.039$ and $\phi(ClO+O) = 0.961$. The relative Cl + O$_2$ quantum yields for different OClO vibrational levels should be accurate to within $\pm 10\%$. From the good agreement between the experimental and calculated value of S, the uncertainty in the relative detection efficiency for Cl and ClO is also $\pm 10\%$. Thus the total uncertainty in our Cl + O$_2$ quantum yield should not exceed $\pm$ 20% of the stated value.

D. Mode Specificity at λ > 400 nm

The O$^+$ TOF (60°) for the cluster of OClO ($^2A_2 \leftarrow {}^2B_1$) absorption peaks near 410 nm are shown in Fig. 11. Except for the laser wavelength, the data for each TOF spectrum was obtained under identical experimental conditions. The significantly different shapes for each TOF reflect the strong dependence of ClO vibrational distribution on the initial OClO ($^2A_2$) vibrational level. In Fig. 12, the Cl$^+$ TOF spectra recorded at 20° are shown for the same group of OClO absorption peaks-- in the insets the vertical scale is expanded by a factor of 15 to reveal structure in the TOF for the Cl + O$_2$ channel. The Cl + O$_2$ yields are tabulated in Table II. The data was fitted using the same procedure outlined above, using data shown in Fig. 11 and 12, as well as that obtained at other angles. The optimized translational energy distributions for the ClO + O channel are shown in Fig. 13. As shown in figure 12, although the Cl yield under the (5,1,0) peak is slightly greater than that seen under the (5,0,0), this channel is nearly absent under the (4,0,2). Thus, near 400 nm, the Cl + O$_2$ yield is strongly diminished by parent OClO asymmetric stretching excitation. Note however that the *shapes* of the Cl + O$_2$ TOFs

are nearly independent of the OClO vibrational mode, indicating that the O_2 internal state distributions are not significantly dependent on OClO $^2A_2$ vibrational level. Indeed, the P(E) obtained for the Cl + O_2 channel from the (5,1,0) level (Fig. 7-Lower) also provided a satisfactory fit for the (5,0,0) and (4,0,2) TOF spectra.

From the translational energy distributions such as those shown in Fig. 13, we have estimated the ClO vibrational energy distributions for each OClO $(^2A_2)$ state. In cases where the vibrational structure is fairly well resolved (e.g., (5,1,0)), vibrational distributions were determined from the relative areas under each vibrational component. In other cases, the ClO + O P(E) distributions were each fit to a sum of Gaussians. The widths of the vibrational contours in the P(E) are a convolution of the ClO rotational, ClO spin orbit, and O spin orbit distributions. Since these individual contributions are unknown, ClO rotational distributions cannot be extracted from our data. The approximate ClO vibrational energy distributions are summarized in Tables I and II, together with $<f_v>$, the fraction of available energy deposited into ClO vibration:

$$\langle f_{v}\rangle = \frac{\Sigma_v \ N_v E_v}{E_{avl}} \qquad (8)$$

In equation 8, N_v is the relative yield of each vibrational level v of energy E_v above zero (for v=0), and E_{avl} is the total available energy where $E_{avl} = E_{h\nu} - D_o(O\text{-}ClO)$.

The O^+ TOF for the cluster of OClO peaks near 420 nm is shown in Fig. 14. Again, the ClO internal state distributions are strongly dependent on the initial OClO vibrational mode (Fig. 15). As shown in Fig. 16, the yield of Cl + O_2 products decreases somewhat, and can only barely be seen in the unexpanded TOF spectra. Interestingly, the Cl + O_2 channel is not diminished to as large an extent under the (3,0,2) relative to its neighbors as it was for the (4,0,2). Also, the yield under the (3,1,2) is significant, in contrast to the (4,1,2) where very little Cl + O_2 was observed. Furthermore, the Cl + O_2 yield for the (4,0,0) level seems anomolously small relative to that for the (3,0,0) and (5,0,0) levels. The shape of the Cl + O_2 component for the (3,1,2) band is similar to that seen for the (5,0,0) and (5,1,0), with the intensity of the fastest component near 110 μs ($O_2^3\Sigma$) approximately half that of the slower component ($O_2^1\Delta$). However, for the (4,0,0) and (4,1,0) bands, the intensities of both of these peaks are nearly identical showing that the yield of ground state O_2 ($^3\Sigma$) relative to excited $^1\Delta$ has increased for these OClO $^2A_2$ vibrational levels.

At longer wavelengths, we observed a steadily decreasing contribution from the Cl + O_2 channel. As summarized in Tables I and II, a relatively large fraction of available energy continues to be channeled into ClO vibrational excitation at these longer wavelengths. The O^+ TOF spectra in Fig. 17 was obtained by excitation of the (1,1,0), (1,0,0) and (0,0,0) bands near 470 nm; the P(E) is shown in Fig. 18. Although weak OClO $(^2A_2)$ fluorescence has been previously observed[25,26] in this wavelength region, photodissociation is known to occur on the picosecond timescale.[23-27] This,

combined with our observation of strong ClO + O signal with negligible production of Cl + O_2 shows that ClO + O is dominant even for the vibrationless OClO $^2A_2$ (0,0,0) level. Owing to the relatively small absorption cross sections and small Cl yields near the $^2A_2$ band origin, we have not attempted to study the Cl + O_2 channel near 470 nm.

E. Determination of D_o(O-ClO) ·

Provided that at least some of the ClO photofragments are formed in their ground rovibrational states and that some ground state $O(^3P_2)$ is produced, by measuring the maximum translational energy at a well defined excitation energy we obtain D_o(O-ClO).[57] Substituting $E_{int, OClO} \sim 0$ into equation 3, and assuming that the fastest products correspond to production of internally cold $ClO(^2\Pi_{3/2})$ + $O(^3P_2)$:

$$D_o(O\text{-}ClO) = E_{photon} - E_{trans,max,ClO+O} \quad (9)$$

Since OClO $^2A_2$ (0,0,0) lies only slightly above D_0(O-ClO), the maximum measured ClO + O translational energy release following excitation near the $^2A_2$ origin facilitates a precise determination of D_o(O-ClO). Using equation 9, D_o(O-ClO) was consistently calculated to be 59.0 ± 0.2 kcal/mole for decay of OClO vibrational levels ranging from 1-13 kcal/mole above D_o(O-ClO). Since the thermochemistry of the ClO and O are very well established,[28,69] we can calculate the standard enthalpy of formation for OClO at 0 K. According to the JANAF tables[28], $\Delta H^\circ_f(Cl)$ = 119.621 ± 0.006 kJ/mole (0 K) and $\Delta H^\circ_f(O)$ = 246.79 ± 0.10 kJ/mole (0 K). Spectroscopic studies on the ClO radical[69] led to a value for D_o(Cl-O) = 265.38 ± 0.033 kJ/mole, and so $\Delta H^\circ_f(ClO)$ = 101.03 ± 0.14 kJ/mole (0 K). Using our value for D_o(O-ClO), $\Delta H^\circ_f(OClO)$ (0 K) = 100.9 ± 1.0 kJ/mole (24.12 ± 0.24 kcal/mole) and using the heat capacity correction from the JANAF tables[28], $\Delta H^\circ_f(OClO)$ (298 K) = 98.43 ± 1.0 kJ/mole (23.53 ± 0.24 kcal/mole). Our result is in good agreement with a recent determination[70] of $\Delta H^\circ_f(OClO)$ (298 K)=96.65 ± 4.18 kJ/mole, but considerably reduces the uncertainty.

Using D_o(O-O), D_o(Cl-OO), D_o(ClO) and D_o(O-ClO), the enthalpy of isomerization (reaction 10) may be computed:

$$OClO(X^2B_1) \rightarrow ClOO(X^2A') \qquad \Delta H(0\ K) = -0.30 \pm 0.25\ kcal/mole. \qquad (10)$$
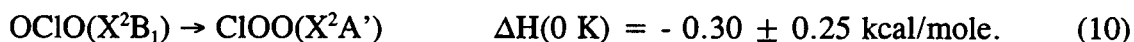
Although the enthalpies of formation of the two isomers are nearly identical, each is separated by a large potential energy barrier.[44]

F. Photodissociation at λ < 400nm.

In Fig. 19, the O^+ TOF spectra (30°) for the cluster of peaks near 395 nm are shown. The slow contribution in the O^+ TOF data near 300 μsec results from fragmentation of the ClO product to O^+ in

the ionizer. Note that the O^+ TOF spectra are very similar for all initial OClO vibrational levels; *i.e.*, the ClO vibrational energy distributions are not as strongly dependent on OClO vibrational mode as was the case at lower excitation energies. The translational energy distributions for the ClO + O channel is shown in Fig. 20. Note that the ClO vibrational distributions for all levels except (6,1,0) are much colder than at longer wavelengths, with the dominant ClO vibrational level now v"=0 with a large translational energy release. Indeed, the fraction of excess energy channeled into ClO vibration decreases sharply from 0.41 for the (5,0,0) level to 0.21 for OClO (6,0,0). (Tables I and II) Apparently, the ClO products become vibrationally cold with dominant production of v = 0 and v = 1 at wavelengths shorter than 390 nm. In addition, the relative contribution from the Cl + O_2 channel begins to diminish. For example, upon tuning from the (5,0,0) level to (6,0,0), the Cl yield decreases from 3.2 to 2.0%. Similarly, the yield decreases from 3.9 to 2.4% upon tuning from (5,1,0) to (6,1,0). These general trends continue as the excitation energy is further increased. As can be seen in Fig. 21, the Cl + O_2 channel is only barely observable from OClO vibrational levels near 375 nm, even in the expanded figures.

G. Polarization Dependence Studies.

The polarization angular dependence is shown in Fig. 22 for a range of OClO ($^2A_2$) vibrational levels. The CM product angular distribution is given[62,63] by:

$$f(\theta) = (1/4\pi)[1 + \beta P_2(\cos \theta)] \qquad (11)$$

where $P_2(\cos\theta)$ is the second order Legendre polynomial in cos θ. In equation 11, β can range from 2.0 for a purely parallel dissociation to -1.0 for a perpendicular process, and $\beta = 0$ indicates an isotropic CM angular distribution. The ClO + O product polarization angular distributions were nearly isotropic ($\beta \sim 0$) at wavelengths longer than 400 nm for OClO vibrational levels having zero quanta of asymmetric stretching. For example, the (5,0,0) angular distribution is isotropic to within the signal to noise. The angular distribution recorded for the neighboring (4,0,2) level, however, is slightly anisotropic, with $\beta \sim 0.2$.

We have not carried out a detailed study of the polarization dependence over a wide range of wavelengths since, as explained below (Section IV.C), most of the polarization dependence is washed out due to the strongly bent OClO geometry and relatively long dissociation timescales. However, a few conclusions are obvious from the polarization measurements shown in Fig. 22: 1) We always observe positive values for β, consistent with the parallel polarized nature of the $^2A_2 \leftarrow ^2B_1$ electronic transition. 2) β steadily increases upon tuning to the blue but remains much less than the limiting value of 2.0 even at 360 nm. 3) For a given excitation energy, dissociation of OClO ($^2A_2$) combination bands having asymmetric stretching excitation leads to more anisotropic angular distributions than those associated with pure symmetric stretching.

H. ClO and Cl TOF Spectra near 360 nm.

We have examined the dissociation dynamics near 360 nm in considerable detail. In particular, we looked for the Cl + O_2 channel first discussed by Vaida *et. al.*[39], and subsequently described by Bishenden and Donaldson.[52,53] The Cl yield reported by the latter workers range from a lower limit of a few percent to as high as 15%. The ClO and Cl TOF spectra, obtained at 30° for the (10,0,0) band at 360 nm are shown in Fig. 23. The dye laser beam was vertically polarized, 3 mm dia., and 1 mJ/pulse. The dominant features at t = 200 - 600 μs have the same shape, and are identical after accounting for the slightly different transmission times of the two different masses through the mass spectrometer. The Cl TOF corresponds to the Cl^+ daughter ions resulting from fragmentation of ClO (produced from the ClO + O channel) upon electron impact ionization. In the inset to the Cl TOF spectrum in Fig. 23, the vertical axis is expanded by a factor of 100 to enhance the region where Cl + O_2 channel is most likely to be observed. The solid line in the inset in Fig. 23 is the calculated TOF assuming a yield of 0.2% for Cl + O_2 production, using the Cl + O_2 P(E) determined at 404 nm, and that shown in Fig. 24 for the ClO + O channel. Since the observed contribution lies below the solid line, the Cl + O_2 product channel that we observed near 404 nm cannot account for more than 0.2% in this wavelength region.

As shown in the inset in Fig. 23 (solid points), some very weak fast Cl signal appears to be present near T = 100-130 μs, lying below our upper limit of 0.2%. However, the power dependence studies shown in Fig. 25 suggest that this fast contribution results primarily from a multiphoton effect. The dominant, broad feature in the Cl TOF spectra, peaking at T = 255 μs, maintains constant shape with increasing laser pulse energy. Since this dominant contribution depended linearly on laser pulse energy (up to ~2.5 mJ/pulse), it corresponds to a single photon process. At pulse energies above 2.5 mJ, the general shape of this dominant contribution remained nearly constant, even though we calculated (using the known absorption cross sections) that the OClO(A←X) transition must be strongly saturated. In the insets to Fig. 25, the solid line corresponds to the calculated contribution for the Cl + O_2 channel assuming a yield of 0.2%. Since our experimental data (solid points) shows that the contribution from the faster component *increases* relative to the dominant 255 μs peak at higher pulse energies, it must result from a multiphoton process; likely photodissociation of vibrationally excited ClO by a 360 nm photon. The data obtained at 1 mJ/pulse (Figs. 24,25) indicates that the upper limit to the Cl + O_2 yield is 0.2%. We have not attempted to reduce this limit further due to the decreased signal to noise ratio at smaller laser pulse energies and the expectation that an upper limit of 0.2% for the Cl + O_2 channel already renders it insignificant from an atmospheric standpoint. As discussed below, polarization dependence studies failed to turn up any evidence for production of Cl + O_2 at other polarization angles.

We have considered the possibility that a channel producing Cl + O_2 near 360 nm might involve a different reaction mechanism than at the longer wavelengths, possibly producing highly internally excited O_2. If this were the case, less energy would be available for Cl + O_2 translational energy and

these products might be constrained to angles within 30° of the OClO molecular beam and would not appear in Figs. 23 or 25. To investigate this possibility, we have recorded the ClO and Cl TOF spectrum at an angle of 13 degrees from the molecular beam, as shown in Fig. 26. Again, the solid line is the calculated TOF using the P(E), in Fig. 24. If Cl + O_2 was formed with low CM translational energy release, their laboratory velocities (v) would be comparable to the OClO beam velocity (~ 1260 m/s), and would appear at T $\sim$ 315 μs. Although our ability to detect products formed with low CM velocities (u) is considerably enhanced by the v^2/u^2 factor in the CM $\rightarrow$ LAB product intensity transformation, no significant Cl^+ contribution was observed in excess of that expected from fragmentation of ClO in the ionizer.

It is appropriate to consider whether or not it is possible for Cl + O_2 to be constrained to beam-detector angles even smaller than 13°, and still remain undetected in our experiment. At 360 nm, the excess energy available to the Cl + O_2 products from OClO photodissociation is 26,100 cm^{-1} (~ 74.5 kcal/mole). For Cl + O_2 products to escape detection at 13° would require that they be formed with $E_{trans} < 0.7$ kcal/mole. For the $Cl(^2P_{3/2})$ + O_2 channel, translational energies below 0.7 kcal/mole would require that the O_2 be formed with 73.8 - 74.5 kcal/mole of internal excitation, implying *exclusive* production of $O_2(^3\Sigma$, v=19, J=24-30), $O_2(^1\Delta$, v= 13, J>39), O_2 ($^1\Delta$, v=14, J=0-10), O_2 ($^1\Sigma$, v=9, J>40) or O_2 ($^1\Sigma$, v=10, J=0-11).[28,29] We believe that such narrow O_2 rovibrational state distributions, peaking within 0.7 kcal/mole of the maximum available energy, is exceedingly unlikely. Therefore, Cl + O_2, if produced, could not escape detection in our experiment because of insufficient recoil energy. There has been considerable reference in the literature to "photochemical isomerization" of OClO to ClOO following electronic excitation of OClO near 360 nm.[38-41] Under collisionless conditions in the gas phase, if the ClOO isomer (D_0 Cl-OO = 4.5 kcal/mole) were formed, it would rapidly dissociate to Cl + O_2 or isomerize back to OClO and decay to ClO + O. Radiative processes are too slow for appreciable production of bound ClOO in the gas phase.

The polarization angular dependence observed for the Cl^+ resulting from decomposition of OClO (10,0,0) prepared at 360 nm was shown in Fig. 22. The solid line fit to the data indicates β = 0.5 $\pm$ 0.2. A positive value for β is consistent with the parallel nature of the OClO ($^2A_2 \leftarrow$ $^2B_1$) transition which is believed to carry all of the oscillator strength in this wavelength region.[21,45] The polarization dependence of the Cl^+ TOF spectra from OClO(10,0,0) was also found to be consistent with β = 0.5 $\pm$ 0.2, as expected since the signal results exclusively from fragmentation of ClO to Cl^+ in the ionizer. As shown in Fig. 27, the shapes of the Cl TOF spectra recorded at various laser polarization angles remained nearly constant and no additional components attributable to Cl + O_2 production was observed at any polarization angle for OClO (10,0,0).

In Fig. 28, the time of flight distributions for O atoms from the ClO + O channel is shown for neighboring OClO vibrational levels near 370 nm. Note that there are considerable differences in the shapes of these TOF spectra. The ClO + O internal state distributions are thus *mode specific*, albeit less so than at wavelengths near 400 nm. The translational energy distributions derived from this data

are shown in Fig. 29. In all four spectra, the translational energy distributions P(E) peak near 13 kcal/mole, indicating that a large fraction of the excess energy appears in ClO + O translational energy release. This behavior contrasts that for wavelengths near 400 nm where a relatively large fraction of excess energy appears as ClO vibrational energy, with most thermodynamically accessible ClO levels populated. As shown in Figs. 30 and 31, near 360 nm the ClO is also produced in low vibrational levels (v = 1-3), with very little contribution for v $\geq$ 4 ($E_{trans} <$ 10 kcal/mole). In the translational energy distributions shown in Figs. 29 and 31, we have normalized the P(E) distributions for neighboring levels to unit area since (as discussed below), $\phi_{ClO + O} >$ 0.998. A notable observation in Fig. 29 is that the ClO internal state distribution from OClO (8,0,2) is narrower than the others, peaking more sharply at 13.5 kcal/mole, with P(E) reaching 0.23. However, for all of the neighboring OClO vibrational levels shown in Fig. 29, the P(E) remains well below 0.20. As shown in Figs. 30 and 31, we observed analogous behavior for the absorption peaks near 360 nm, with the (9,0,2) level leading to more sharply peaking translational energy distribution. We conclude that at 360 - 370 nm, asymmetric stretching excitation in the initially prepared OClO($^2A_2$) levels leads to narrower ClO rovibrational energy distributions.

IV. DISCUSSION

A. Dynamics at $\lambda >$ 380 nm

Due to a substantial potential energy barrier for dissociation of the "bright" $^2A_2$ surface to ClO + O (Fig. 3[43]) along the asymmetric stretching coordinate, the photodissociation of OClO at E < 3.1 eV must be indirect, involving interactions with one or more lower lying states.[43] The narrow linewidths of the absorption features in this energy region indicates that dissociation timescales are many picoseconds.[21-27] This long decay lifetime, combined with substantial bending of the parent OClO molecule (see below) leads to product angular distributions which are nearly isotropic.

Detailed linewidth studies by McDonald and Innes[23], an later by Michielsen $et.$ $al.$[22] showed that decay lifetimes are independent of rotational level but dissociation of the F_1 spin component (J = N + ½) is approximately twice as fast as that for F_2 (J = N - ½). It was argued[23] that the ground $^2B_1$ electronic state was unlikely to be the perturber because even near the $^2A_2$ (0,0,0) origin, the $^2B_1$ level density would be high and this should tend to smooth out any dependence of linewidth on spin component. It was concluded that the dissociation mechanism involves spin orbit interactions between the $^2A_2$ and the nearby $^2B_2$ or $^2A_1$ states. The insensitivity of linewidth on OClO rotational level,[22,23] was taken as evidence that the perturbing levels have nuclear geometries similar to the $^2A_2$.

Analysis of high resolution spectra near the OClO ($^2A_2$) band origin showed that the linewidths associated with bending (v_2) were more than twice as broad as pure symmetric stretching. However, linewidths were independent of symmetric stretching level (v_1) for v_1 = 0-3.[22,23] The optically prepared

$^2A_2$ and the nearby $^2B_2$ form a Renner-Teller pair, becoming orbitally degenerate ($^2\Pi_g$) in their linear configurations. Since interactions between Renner-Teller pairs are expected to be enhanced by bending, the $^2B_2$ was favored as the spin orbit perturber in the early studies.[22,23] However, the recent *ab-initio* calculations[43] indicate that the $^2B_2$ interacts directly with the $^2A_2$ only at considerably higher energies, whereas the $^2A_1$ crosses the $^2A_2$ near the $^2A_2$ equilibrium angle. It was thus concluded[43] that the $^2A_1$ is the spin orbit perturber of the $^2A_2$.

As shown in Fig. 3, Peterson and Werner's calculations[43] show that the $^2A_1$, like the $^2A_2$, is bound at E < 3.1 eV with respect to dissociation to ClO + O along the asymmetric stretching coordinate for bond angles near equilibrium (100°). However, those theoretical calculations (see Fig. 3) indicated the existence of a very small barrier to linear OClO along the $^2A_1$ bending coordinate, with the energy of linear OClO lying lower than the bent form. The height of the barrier to achieve linearity (for fixed OClO bond length) appeared to lie very close to the energy of the $^2A_2$ origin (~ 2.8 eV).[43] The calculations indicated that dissociation to ClO + O can subsequently proceed via a nearly linear $^2A_1$ transition state with the height of the barrier for dissociation estimated to be lower than that to achieve linearity. Our results are consistent with these conclusions. Our finding that ClO + O production is by far the dominant channel for all $^2A_2$ levels down to the (0,0,0) level confirms that the $^2A_1$ lies below OClO $^2A_2$ (0,0,0). Furthermore, our observation of strong ClO + O signal even from OClO (0,0,0) indicates that interactions between the $^2A_1$ and $^2A_2$ are significant in the region of the $^2A_2$ origin, consistent with a crossing between these levels near the $^2A_2$ minimum.

At excitation energies below 3.1 eV (λ > 400 nm), the ClO is formed vibrationally excited with large populations of nearly all thermodynamically accessible vibrational levels. The width of each vibrational peak in the TOF spectra is a convolution of the ClO rotational and spin orbit distribution, and is further broadened by the distribution of O(^{3}P) spin orbit levels. The ClO($X^2\Pi_{1/2,3/2}$) spin orbit levels are separated by 350 cm^{-1} and the excited spin orbit O (^3P_J) levels lie at 158 cm^{-1} (J=1) and 227 cm^{-1} (J=0). Since we are unable to resolve these fine structure levels, the ClO rotational distributions cannot be obtained from the widths of the vibrational envelopes for the ClO + O P(E). However, from the fact that each vibrational contour peaks well away from the maximum theoretical translational energy, it is clear that the ClO rotational distributions peak well away from J"=0. Because the ClO vibrational spacing ($\sim$ 2.4 cm^{-1} at low v") is clearly well resolved in our TOF data, the ClO rotational envelopes must be considerably narrower than the 350 cm^{-1} vibrational spacing. We thus conclude that at excitation wavelengths longer than 400 nm, the ClO products are formed vibrationally hot with only a modest degree of rotational excitation.

Michielsen and coworkers found that decay lifetimes at ν_1 = 0-3 were independent of symmetric stretching level (ν_1).[22] Their additional finding that OClO predissociation rates are enhanced by parent bending is clearly important to unravelling the dynamics in the low energy region. Peterson and Werner[43] compared one dimensional cuts of the symmetric stretching potentials for the four OClO electronic states at fixed angles of 106.4° and 117.4°, corresponding to the equilibrium bond angles for

the prepared $^2A_2$ and ground $^2B_1$ state, respectively. They noted that OClO bending has a strong effect on the energies of the $^2A_2/^2A_1$ crossings, consistent with the observation that OClO decay lifetimes are diminished with bending excitation. An additional reason for the enhancement seen with parent bending is that initial $^2A_2$ bending provides nuclear motion facilitating increased access to regions of the $^2A_1$ surface favorable to decay to ClO + O. As noted above, this corresponds to nearly linear nuclear configurations where the potential energy barrier is lowest. Our observation of highly vibrationally excited ClO with modest rotational excitation in this low energy region of the OClO (A←X) absorption spectrum appears to support the hypothesis that a large fraction of the ClO + O products originate from a nearly linear OClO ($^2A_1$) transition state.

As noted in the results section, the P(E) for the Cl + O_2 channel is bimodal (Fig. 7). From energy conservation, the fastest component, lying in the energy range 41-67 kcal/mole, must correspond to production of ground state O_2 $X^3\Sigma$ in vibrational levels ranging from 1-6. The rise near E = 41 kcal/mole corresponds exactly to the expected maximum translational energy release for O_2 $a^1\Delta$(v"=0) or O_2 $X^3\Sigma$ (v"=6). Since it seems unlikely that the $O_2(^3\Sigma)$ vibrational energy distribution would be so bimodal and highly inverted to rise sharply above v = 6, we attribute the rise below E = 41 kcal/mole to formation of O_2 ($^1\Delta$, v"=0). We conclude that approximately 20% of the O_2 is ground state ($^3\Sigma$) formed in vibrational levels between 0 - 5. From the sharp rise below 41 kcal/mole, the dominant O_2 products are in the electronically excited $^1\Delta$ state. The exact location of this peak indicates that the O_2 ($^1\Delta$) is primarily formed in v"= 0-4. Note that the maximum in the P(E) for the Cl+ O_2 channel lies at 32 kcal/mole, slightly higher than the maximum allowed translational energy release for production of Cl + $O_2(^1\Sigma)$, ruling out the possibility that the sharp rise corresponds to these products. Of course, some contribution from this channel may be hidden under the dominant Cl + $O_2(^1\Delta)$ peak at slightly lower translational energies.

Owing to the presence of a conical intersection between the $^2A_1$ and $^2B_2$ states near the minimum in the $^2A_1$ bending potential, vibronic interactions mediated by b_2 asymmetric stretching should be appreciable.[43] The $^2B_2$ electronic state is an optically dark level, not accessible by a direct dipole transition from the ground state. As discussed elsewhere[42-44], all available evidence indicates that Cl + O_2 production primarily involves decomposition from OClO $^2B_2$ levels. Due to the O=O bonding and Cl-O antibonding character of the b_2 orbital, the $^2B_2$ is strongly bent with an equilibrium OClO angle of ~ 90°.[43] In C_{2v} symmetry, OClO($^2B_2$) correlates to Cl (^2P) + O_2 ($^1\Delta$), consistent with our finding that $^1\Delta$ is the dominant electronic state of the O_2 products. However, the 20% yield of ground state $O_2(^3\Sigma)$ observed in our experiment indicates that C_{2v} symmetry is broken to some degree, facilitating a crossing to the ground electronic state as the products separate.

An interesting observation is that the O_2 translational energy distributions were essentially identical for many OClO $^2A_2$ levels. For example, we were able to fit the Cl + O_2 distributions from the (5,0,0), (4,0,2), and (5,1,0) levels with the same P(E). This relative insensitivity to initial vibrational state suggests that the O_2 state distributions are primarily determined rather late in the

decomposition process, as the Cl + O_2 are departing. However, a survey of the Cl TOF spectra over a wider range of excitation wavelengths does reveal some interesting effects. As can be seen in Fig. 16, for example, at slightly lower energies near the (4,1,0), the relative contribution from the slower, $O_2(^1\Delta)$ channel is nearly the same as the faster $O_2(^3\Sigma)$ peak. Thus the yield of electronically excited O_2 ($^1\Delta$) relative to the ground state diminishes as the excitation energy is decreased towards that of the potential energy barrier for this channel. This is predicted by the theoretical calculations.[44] As discussed in the following paper, the potential energy barrier for Cl + O_2 production on the $^2B_2$ surface is strongly dependent on OClO geometry, with substantial decrease in the barrier height for non-C_{2v} geometries.[44] The relative contribution of ground state $O_2(^3\Sigma)$ therefore increases upon decreasing the excitation energy towards the top of the potential energy barrier as a larger fraction of products result from non-C_{2v} trajectories. It is important to note, however, that since OClO ($^2B_2$) is nearly unbound in asymmetric stretching[43], *i.e.*, in the reaction coordinate for production of ClO + O; asymmetric excitation in the $^2B_2$ state will diminish the <u>*total*</u> yield of Cl + O_2 products in favor of ClO + O production. Thus the nuclear motion associated with the initially prepared OClO vibrational mode plays a critical role in controlling the identity of the products. Only those OClO $^2B_2$ levels very near C_{2v} reach Cl + O_2. Any asymmetric vibrational excitation promotes decay to ClO + O, consistent with the shorter dissociation timescales and therefore more strongly anisotropic angular distributions, as well as strongly diminished Cl + O_2 yields.

The possibility that OClO symmetric bending might lead to a dramatic enhancement in Cl + O_2 production rates has been raised[21b] in connection with the atmospheric significance of OClO photochemistry. It was suggested that the absence of OClO ($^2A_2$) peaks associated with two quanta of bending (e.g. 5,2,0) might be attributable to extreme broadening of those peaks due to very short lifetimes resulting from rapid decomposition to Cl + O_2. We have looked for enhanced Cl + O_2 production at the calculated band positions for OClO $^2A_2$ (5,2,0) and (4,2,0), but saw no evidence for significant Cl + O_2 at these wavelengths. This, along with our finding that ClO + O remained dominant for all OClO levels (including those with bending), shows that the Cl + O_2 channel is never greatly enhanced with OClO($^2A_2$) bending excitation. Thus the lack of activity for OClO combination bands having two quanta of bending is more likely explained by symmetry effects operative in the three normal modes, as discussed qualitatively by Brand, *et. al.*[71]

B. Change in Dynamics near 400 nm

Upon tuning to wavelengths shorter than 400 nm, significant changes are observed in both product channels. Whereas most energetically accessible ClO vibrational energy levels are populated with strongly mode specific distributions at longer wavelengths, upon tuning to shorter wavelengths the ClO becomes vibrationally cold, with most excess energy channeled into relative translational energy. In this same energy region, the Cl + O_2 channel diminishes significantly. Interestingly, Richard and Vaida observed a considerable increase in the OClO absorption linewidths above 3.1 eV.[21] In

particular, a plot of the absorption linewidths (Ref. 21b Fig. 3) show a rapid increase from 0.3 cm^{-1} for OClO (5,0,0) to ~0.9 cm^{-1} for OClO (7,0,0).

All of the changes noted above clearly indicate the onset of a new ClO + O decomposition mechanism at E > 3.1 eV. Our experimental observations and the theoretical calculations[43,44] provide strong evidence that this change is associated with the opening of the ClO + O channel on the $^2A_2$ surface. At energies above the barrier to ClO + O, the magnitude of the coupling of OClO ($^2A_2$) to the ClO + O continuum increases sharply, and dissociation timescales decrease. The photochemical dynamics and branching ratios are governed by the strength of the coupling of the prepared $^2A_2$ state to the available decay channels.[43,44] As the reaction rate constant for dissociation to ClO + O on the bright $^2A_2$ surface increases, the nonadiabatic behavior ultimately leading to Cl + O$_2$ production become negligible and so this channel closes. The large translational energy release and production of vibrationally cold ClO are signatures of the existence of a substantial potential energy barrier for ClO + O production with strong ClO-O repulsion in the exit channel. Our data indicates that ClO produced from OClO photodissociation near 360 nm is in low vibrational levels (v"=1-3), with negligible production of v" > 4. This clearly disagrees with previous conclusions that the ClO is primarily formed in v"=4-6 in this wavelength region.[39,40]

C. Polarization Dependence Studies

Photodissociation of OClO near 360 nm leads to production of ClO + O with a translational energy distribution peaking near 13 kcal/mole (Fig. 31), corresponding to a most probable center of mass O atom velocity of 2360 m/s. The effect of the initial tangential velocity of the O atom due to OClO parent rotation is thus negligible in the present case. However, β is reduced considerably from the maximum possible value of 2.0, primarily because the direction of O atom product recoil (along the Cl-O bond axis) does not lie along the axis of the transition dipole. OClO is a strongly bent molecule with an equilibrium bond angle of 117.4° for the ground ($^2B_1$) state, and 106.2° for the excited ($^2A_2$) level.[21] The OClO ($^2A_2 \leftarrow {}^2B_1$) transition moment lies parallel to the OClO a axis, ie., in the OClO plane perpendicular to the C$_{2v}$ axis. Thus the Cl-O bond axis, along which the O atom departs, lies 31-37° from the direction of the ($^2A_2 \leftarrow {}^2B_1$) transition dipole moment. The second factor which diminishes β is that the OClO parent molecule has a dissociation lifetime of at least several hundred femtoseconds[21-27] so the parent molecule will undergo a fraction of a rotation before dissociating, as in NO$_2$ photodissociation.[63]

The photofragment anisotropy parameter (β) is related to parent lifetime (τ) by the following expression:[63]

$$\beta = 2 P_2 (\cos\chi) \left(\frac{1 + \omega^2 \tau^2}{1 + 4\omega^2 \tau^2} \right) \qquad (12)$$

In equation 12, χ is the angle between the recoil velocity vector of the fragment and the parent

transition dipole moment, and ω is the frequency of parent rotation. Estimating T = 15 K and using the moment of inertia for OClO, we calculate ω = 6.4 x 10^{11} s^{-1}. The ground state OClO bond angle (Θ = 117.4°) corresponds to χ = 31.3° and that of the excited state (Θ = 106.2°) corresponds to χ = 36.9°. Upon substituting these values into equation 12, it is apparent that the large value of χ leads to substantial reduction in β. Indeed, even in the limit of τ = 0 (instantaneous dissociation), assuming dissociation from a ground state geometry (χ = 31.3°), the maximum value for β is 1.19. If the molecule dissociates from the excited state geometry (χ = 36.9°) the maximum in β is only 0.92. Thus because χ is not well defined, it is difficult to extract OClO lifetime information from our anisotropy measurements using equation 12. However, if we assume that OClO dissociates from a geometry close to that of the excited $A(^2A_2)$ state (106.2°), the following β values are calculated: β = 0.72 (τ = 500 fs); β = 0.49 (τ = 1 ps). Therefore, our observed value of 0.5 ± 0.2 near 360 nm is consistent with a dissociation timescales in the range 0.5 - 2 ps for OClO (10,0,0). As expected, our inferred timescales near 360 nm are somewhat longer than those measured directly by Zewail's group at higher excitation energies (λ < 350 nm).[56]

D. Absence of Cl + O_2 near 360 nm

Our study, as well as that by Lawrence and Apkarian[51] indicate that the strong Cl signal reported near 360 nm by BD[52,53] cannot be attributable to production of Cl + O_2. However, since their Cl REMPI action spectra[52,53] followed the known OClO absorption spectrum, the signal must result from OClO photodissociation. Previously, we suggested that this Cl signal results from photodissociation of the dominant ClO products to Cl + O by the focussed 235 nm REMPI probe laser.[20] At 235 nm, the ClO (v=0) absorption cross section[72] is ~ 2 x 10^{-18} cm^2, and the Cl + O product yield is unity.[72,73] In the quantum yield measurement described in Ref. 52, Cl atoms were detected by 2 + 1 REMPI using ~ 0.3 mJ of 235 nm radiation focussed by a 7.5 cm focal length lens. Assuming a beam waist diameter < 0.5 mm, the fluence is > 1.8 x 10^{17} $photons/cm^2$. Using the ClO (v=0) absorption cross section, our calculations indicate that > 36% of the ClO produced in the first step will be photolyzed to Cl + O. These Cl atoms would be produced and ionized within the same laser pulse. Consequently, a large contribution to the Cl signal is to be expected from ClO photodissociation at 235 nm under the experimental conditions employed in Refs. 52 and 53.

E. Nature of the Mode Specificity Near 360 nm

Following our report[20] of mode specific Cl:ClO yields near 400 nm, a similar effect was reported by BD near 360 nm.[53] Specifically, the enhanced ClO intensities from OClO (8,0,2) and (9,0,2) was taken as evidence that the quantum yields for this channel are enhanced with OClO asymmetric stretching excitation. Surprisingly, the Cl REMPI spectra resembled the OClO absorption spectrum, leading those workers to concluded that the Cl + O_2 yield was constant. This conclusion, if correct, together with conservation of product flux dictates the existence of another photochemical channel which

decreases when OClO asymmetric stretching levels are excited. However, since the following arguments lead to the conclusion that $\phi_{Cl + O_2} + \phi_{ClO + O} \geq 0.9998$ near 360 nm, no other photochemical channels can be significant: 1) The quantum yield for $OClO(^2A_2)$ fluorescence is negligible (*i.e.*, <2 x 10^{-4}) due to picosecond dissociation timescales.[21-27] 2) Formation of Cl + O + O is energetically closed.[28] 3) The $ClOO(^2A'')$ isomer (D_o = 4.5 kcal/mole[50]), if produced, would be formed above D_o and would rapidly dissociate to Cl + O_2. 4) OClO $(^2A_2)$ levels excited near 360 nm lie above the barrier for dissociation to ClO + O. Other OClO electronic states $(^2A_1, ^2B_2$ or $^2B_1)$ are dissociative at these energies[43] so metastable or fluorescent OClO levels cannot be significant. From these considerations, we conclude that enhancement in the ClO + O yield *must* be accompanied by a decrease in Cl + O_2 production, independent of reaction mechanism(s). Since this requirement is not fulfilled in Ref. 53, the claim of mode specific Cl:ClO branching ratios near 360 nm must be in error.

Flesch and coworkers[74] have recently carried out a photodissociation study of OClO and its molecular aggregates. They detected ClO following OClO photodissociation by single photon ionization at 10.91 eV, just above the adiabatic ClO ionization potential of 10.87 eV. They, like BD, observed enhanced ClO signal from OClO vibrational modes having asymmetric stretching excitation $(v_1,0,2)$ near 360 nm. However, they attributed this behavior to different ClO vibrational energy distributions from each OClO parent $^2A_2$ vibrational level.[74] They postulated that since ClO ionization cross sections are likely to depend on vibrational level, the ClO detection sensitivities will not be constant for ClO products from different parent OClO vibrational states.

Our work confirms that the ClO vibrational distributions from OClO photodissociation at 360 - 370 nm are indeed mode specific. Most notably, the ClO translational energy distributions are narrower and more sharply peaking for OClO asymmetric stretching levels than for neighboring peaks. The exact peak locations in the P(E) shown in Fig. 29 indicates that decay of OClO (8,0,2) leads to enhanced production of ClO (v"=2,J"<15½) or ClO(v"=1,J">35½), relative to neighboring OClO absorption peaks. Similar behavior is seen for OClO (9,0,2), as shown in Fig. 31. Since there is no resolvable structure in the OClO (8,0,2) or (9,0,2) P(E)'s, and because the $O(^3P_J)$ spin orbit distributions are unknown, we cannot distinguish between production of ClO v=1 and 2 from the P(E)'s shown in Fig. 29 and 31. However, it is clear from our data that if *the most probable* ClO levels are monitored state specifically (*e.g.*, using 2 + 1 REMPI) while scanning the OClO excitation laser at 360 - 370 nm, the ClO signal will appear to be enhanced for OClO (8,0,2) and (9,0,2), relative to neighboring peaks. Such behavior results from the narrower P(E) and sharper peaking of the ClO rovibrational state distribution, rather than from increased ClO:Cl branching ratios.[52,53] Since the ClO absorption cross section into the dissociative $A(^2\Pi)$ continuum[72,73] should not vary significantly for ClO (v"=1-3), a constant fraction of ClO products are photolyzed by the 235 nm probe laser producing a Cl REMPI spectrum which follows the OClO absorption spectrum, as reported in Ref. 53.

V. CONCLUSIONS

We have studied the photodissociation of OClO using photofragment translational energy spectroscopy and have obtained branching ratios for the two photochemical channels over a wide range of wavelengths. The dominant channel ($\geq$ 96 %) is production of ClO + O. Although the vibrational distributions of the ClO product are strongly dependent on the initial OClO vibrational level, at $\lambda >$ 400 nm essentially all thermodynamically accessible vibrational levels are produced. The preferential formation of vibrationally excited ClO is rationalized in terms of the recent *Ab-Initio* calculations which indicated that the bright $^2A_2$ state is bound with respect to dissociation at E < 3.1 eV but interacts via spin orbit coupling to a nearby $^2A_1$ which dissociates to ClO + O via a nearly linear transition state. The minor Cl + O_2 channel, which to date has received considerable attention due to its potential for atmospheric ozone depletion, was clearly observed. As expected from orbital symmetry considerations, the O_2 was primarily formed in the $^1\Delta$ state from concerted decomposition involving an OClO transition state near C_{2v} symmetry. At excitation energies above 3.1 eV ($\lambda <$ 400 nm), the Cl + O_2 channel diminishes with the ClO + O yield reaching unity at $\lambda <$ 380 nm. These observations, combined with the sharp decrease in ClO vibrational excitation, large translational energy release, and more anisotropic product angular distributions reflect the onset of a new OClO dissociation mechanism involving direct predissociation of OClO ($^2A_2$) levels over a large potential energy barrier.

VI. ACKNOWLEDGEMENTS

VII. REFERENCES

1.   H. Okabe, *Photochemistry of Small Molecules,* J. Wiley and Sons, Inc.,1978.
2.   a) C.B. Moore and J.C. Weisshaar, Ann. Rev. Phys. Chem. **34**, 525 (1983).
      b) W.H. Green Jr., C.B. Moore and W.F. Polik, Ann. Rev. Phys. Chem. **43**, 591 (1992).
      c) R.D. van Zee, C.D. Pibel, T.J. Butenhoff, and C.B. Moore, J. Chem. Phys. **97**, 3235 (1992).
      d) K.L. Carleton, T.J. Butenhoff and C.B. Moore, J. Chem. Phys. **93**, 3907 (1990).
3.   a) T.J. Butenhoff, K.L. Carleton, R.D. van Zee, and C.B. Moore, J. Chem. Phys. **94**, 1947 (1991).
      b) W.H. Miller, R. Hernandez, C.B. Moore and W.F. Polik, J. Chem. Phys. **93**, 5657 (1990).

4. J. D. Goddard, Y. Yamaguchi and H.F. Schaefer III, J. Chem. Phys. **75**, 3459 (1981).

5. a) E.F. Cromwell, A. Stolow, M.J.J. Vrakking, and Y.T. Lee, J. Chem. Phys. **97**, 4029 (1992).

    b) B.A. Balko, J. Zhang and Y.T. Lee, J. Chem. Phys. **97**, 935 (1992).

6. a) Aa. S. Sudbo, P.A. Schulz, Y.R. Shen and Y.T. Lee, J. Chem. Phys. **69**, 2312 (1978).

    b) D. Krajnovich, F. Huisken, Z.Zhang, Y.R. Shen, and Y.T. Lee, J. Chem. Phys. **77**, 5977 (1982).

7. J.W. Hudgens, J. Chem. Phys. **68**, 777 (1978).

8. H. F. Davis, B. Kim, H.S. Johnston, and Y.T. Lee, J. Phys. Chem. **97**, 2172 (1993).

9. H.F. Davis, P.I. Ionov, S.I. Ionov, and C. Wittig, Chem. Phys. Lett. **215**, 214 (1993).

10. a) L.J. Butler, E.J. Hintsa, S.F. Shane and Y.T. Lee, J. Chem. Phys. **86**, 2051 (1987).

    b) L.J. Butler, E.J. Hintsa and Y.T. Lee, J. Chem. Phys. **84**, 4104 (1986).

11. a) R.B. Metz, J.D. Thoemke, J.M. Pfeiffer and F.F. Crim, J. Chem. Phys. **99**, 1744 (1993).

    b) A. Sinha, J.D. Thoemke and F.F. Crim, J. Chem. Phys. **96**, 372 (1992).

    c) M.C. Hsiao, A. Sinha and F.F. Crim, J. Phys. Chem. **95**, 8263 (1991).

    d) A. Sinha, M.C. Hsiao and F.F. Crim, J. Chem. Phys. **94**, 4928 (1991).

    e) F.F. Crim, Science **249**, 1387 (1990).

12. a) R.L. VanderWaal and F.F. Crim, J. Phys. Chem. **93**, 5331 (1989).

    b) R.L. VanderWaal, J.L. Scott and F.F. Crim, J. Chem. Phys. **92**, 803 (1990).

    c) R.L. VanderWaal, J.L. Scott, F.F. Crim, K. Weide and R. Schinke, J. Chem. Phys. **94**, 3548 (1991).

13. M.J. Bronikowski, W.R. Simpson and R.N. Zare, a) J. Phys. Chem. **97**, 2194, 1993; b) J. Phys. Chem. **97**, 2204 (1993).

14. I. Bar, Y. Cohen, D. David, S. Rosenwaks, J.J. Valentini, J. Chem. Phys. **93**, 2146 (1990).

15. a) C.X.W. Qian, A. Ogai, L Iwata and H. Reisler, J. Chem. Phys. **89**, 6547 (1988).

    b) Y.Y. Bai, A. Ogai, C.X.W. Qian, L. Iwata, G.A. Segal and H. Reisler, J. Chem. Phys. **90**, 3903 (1989).

    c) A. Ogai, C.X.W. Qian, L. Iwata and H. Reisler, J. Chem. Phys. **93**, 1107 (1990).

16. a) U. Bruhlmann, M. Dubs and J. R. Huber, J. Chem. Phys. **86**, 1249 (1987); b) E. Kades, M. Rosslein, and J. R. Huber, Chem. Phys. Lett., **209**, 275 (1993); c) S.A. Reid, J. T. Brandon, and H. Reisler, Chem. Phys. Lett., **209**, 22 (1993).

17. S. Hennig, V. Engel, R. Schinke, M. Nonella, and J.R. Huber, J. Chem. Phys. **87**, 3522 (1987).

18. P. Felder, B.M. Haas and J.R. Huber, Chem. Phys. Lett. **204**, 248 (1993)

19. C. Starrs, M.N. Jego, A. Mank and J.W. Hepburn, J. Phys. Chem. **96**, 6526 (1992).

20. H. F. Davis and Y.T. Lee, J. Phys. Chem. **96**, 5681 (1992).

21. a) E.C. Richard, and V. Vaida, J. Chem. Phys. **94**, 153 (1991).

b) E.C. Richard, and V. Vaida, J. Chem. Phys. **94**, 163 (1991).

22. S. Michielsen, A.J. Merer, S.A. Rice, F.A. Novak, K.F. Freed, and Y. Hamada, J.Chem.Phys. **74**, 3089 (1981).

23. P.A. McDonald and K.K. Innes, Chem. Phys. Lett. **59**, 562 (1978).

24. Y. Hamada, A.J. Merer, S. Michielsen, and S.A. Rice, J. Mol. Spectrosc. **86**, 499 (1981).

25. R.F. Curl Jr., K. Abe, J. Bissinger, C. Bennett and F.K. Tittel, J. Mol. Spect. **48**, 72 (1973).

26. K. Sakurai, J. Clark, and H.P. Broida, J. Chem. Phys. **54**, 1217 (1971).

27. K.J. Brockmann and D. Haaks, in Methods of Laser Spectroscopy, edited by Y. Prior, A. Ben-Reuven, and M. Rosenbluh (Plenum, New York, 1986).

28. M.W. Chase Jr., C.A. Davies, J.R. Downey, D.J. Frurip, R.A. McDonald and A.N. Syverud, J. Phys. Chem. Ref. Data.14, Supp. 1. (*JANAF Thermochemical Tables, 3rd. ed.-* 1985).

29. K.P. Huber and G. Herzberg, *Molecular Spectra and Molecular Structure IV. Constants of Diatomic Molecules,* Van Nostrand Reinhold Co. (1979).

30. S. Abramowitz and M.W. Chase, Jr. Pure and Appl. Chem. **63**, 1449 (1991).

31. J.C. Farman, B.G. Gardiner, J.D. Shanklin, Nature **294**, 733 (1981).

32. a) S. Solomon, R.W. Sanders, and H.L. Miller Jr., J. Geophys. Res. **95**, 13807 (1990).

    b) S. Solomon, R.W. Sanders, M.A. Carroll, and A.L. Schmeltekopf, J. Geophys. Res. **94**, 11393 (1989)..

    c) S. Solomon, G.H. Mount, R.W. Sanders, and A.L. Schmeltekopf, Geophys., Res., **92**, 8329 (1987).

33. R.J. Salawitch, S.C. Wofsy, M.B. McElroy, Planet. Space Sci. **36**, 213 (1988).

34. L.T. Molina and M.J. Molina, J. Phys. Chem. **91**, 433 (1987).

35. M.B. McElroy, R.J. Salawitch, S.C. Wofsy, J.A. Logan, Nature **321**, 759 (1986).

36. a) A.A. Turnipseed, J.W. Birks, and J.G. Calvert, J. Phys. Chem. **95**, 4356 (1991).

    b) A.J. Hills, R.J. Cicerone, J.G. Calvert, and J.W. Birks, Nature **328**, 405 (1987).

37. a) S.P. Sander and R.R. Friedl, J. Phys. Chem. **93**, 4764 (1989)

    a) R.R. Friedl and S.P. Sander J. Phys. Chem. **93**, 4756 (1989).

    c) S.P. Sander and R.R. Friedl, Geophys. Res. Lett. **15**, 887 (1988).

    d) W.B. DeMore and E. Tschuikow-Roux, J. Phys. Chem. **94**, 5856 (1990).

    e) J.G. Anderson, D.W. Toohey, and W.H. Brune, Science **251**, 39 (1991)

    f) R.J. Salawitch, S.C. Wofsy, et. al., Science **261**, 1146 (1993).

38. V. Vaida, S. Solomon, E.C. Richard, E. Ruhl, and A. Jefferson, Nature **342**, 405 (1989).

39. E. Ruhl, A. Jefferson and V. Vaida, J. Phys. Chem. **94**, 2990 (1990).

40. V. Vaida, E.C. Richard, A. Jefferson, L.A. Cooper, R. Flesch and E. Ruhl, Ber. Bunsen-Ges. Phys. Chem. **96**, 391 (1992).

41. V. Vaida and J.D. Simon, Science, **268**, 1443 (1995)

42. J.L. Gole, J. Phys. Chem. **84**, 1333 (1980).

43. K. A. Peterson and H.-J. Werner, J. Chem. Phys. **96**, 8948 (1992).

44. K. A. Peterson and H.-J. Werner, J. Chem. Phys., next paper.

45. A. Wahner, G.S. Tyndall, and A.R. Ravishankara, J. Phys. Chem. **91**, 2734 (1987).

46. A. Arkell and I. Schwager, J. Am. Chem. Soc. **89**, 5999 (1967).

47. a) F.J. Adrian, J. Bohandy and B.F. Kim, J. Chem. Phys. **85**, 2692 (1986).
    b) F.J. Adrian, J. Bohandy and S.K. Sur, J. Am. Chem. Soc. **106**, 8014 (1984)

48. K. Johnsson, A. Engdahl and B. Nelander, J. Phys. Chem. **97**, 9603 (1993).

49. H.S.P. Muller and H. Willner, J. Phys. Chem. **97**, 10589 (1993).

50. J.M.Nicovich, K.D. Kreutter, C.J. Shackelford, and P.H. Wine, P.H.; Chem.Phys. Lett. **179**, 367 (1991).

51. W.G. Lawrence, K.C. Clemitshaw, and V.A. Apkarian, J. Geophys. Res. **95**, 18591 (1990).

52. E. Bishenden, J. Haddock, and D.J. Donaldson, a) J. Phys. Chem. **95**, 2113 (1991); b) J. Phys. Chem. **96**, 6513 (1992).

53. E. Bishenden, and D.J. Donaldson, a) J. Chem. Phys. **99**, 3129 (1993); b) J. Chem. Phys. **101**, 9565 (1994).

54. R.C. Dunn, E.C. Richard, V. Vaida and J.D. Simon, J. Phys. Chem. **95**, 6060 (1991).

55. R.C. Dunn, B.N. Flanders, V. Vaida and J.D. Simon, Spectrochimica Acta **48A**, 1293 (1992).

56. T. Baumert, J.L. Herek, and A.H. Zewail, J. Chem. Phys. **99**, 4430 (1993).

57. A.M. Wodtke, and Y.T Lee, J. Phys. Chem. **89**, 4744 (1985).

58. R.I. Derby and W.S. Hutchinson, Inorg. Synth. **4**, 152 (1953).

59. D. Proch and T. Trickl, Rev. Sci. Instrum. **60**, 713 (1989).

60. T.K. Minton, G.M. Nathanson, and Y.T. Lee, J. Chem. Phys. **86**, 1991 (1987).

61. X. Zhao, Ph.D. Thesis, Univ. of Calif., Berkeley, 1988. (LBL-26332).

62. a) R. Zare, J. Photochem. **4**, 1 (1972); b) C.J. Jonah, Chem. Phys. **55**, 1915 (1971).

63. G.E. Busch and K.R. Wilson, J. Chem. Phys. a) **56**, 3626 (1972); b) **56**, 3638, (1972), c) V. P. Hradil, T. Suzuki, S.A. Hewitt, P.L. Houston, and B.J. Whitaker, J. Chem. Phys. **99**, 4455 (1993).

64. J.J. Renard and H.I. Bolker, Chemical Reviews **76**, 487 (1976).

65. J. E. Del Bene, J.D. Watts, and R.J. Bartlett, Chem. Phys. Lett. **246**, 541 (1995).

66. a) D. Krajnovich, L.J. Butler and Y.T. Lee, J. Chem. Phys. **81**, 3031 (1984); b) A.M. Wodtke, E. J. Hintsa and Y.T. Lee, J. Phys. Chem. **90**, 3549 (1986).

67. R. E. Center and A.J. Mandl, Chem. Phys. **57**, 4104 (1972).

68. Weast, R.C., Ed., *CRC Handbook of Chemistry and Physics,* CRC Press, Inc. Boca Raton, Fla. (1987).

69. S. A. Barton, J.A. Coxon, and U.K. Roychowdhury, Can. J. Phys., **62**, 473 (1984), and references cited therein.

70.   R. Flesch, E. Ruhl, K. Hottmann, and H. Baumgartel, J. Phys. Chem. **97**, 837 (1993).

71.   J.D.C. Brand, R.W. Redding, A.W. Richardson, J. Mole Spectrosc. **34**, 399 (1970).

72.   a) M. Mandelman and R.W. Nicholls, J. Quant. Spectrosc. Radiat. Trans. **17**, 483 (1977); b) F.G. Simon, W. Schneider, G.K. Moortgat, and J. P. Burrows, J. Photochem. Photobiol. A: Chem. **55**, 1 (1990).

73.   H.F. Davis and Y.T. Lee, J. Phys. Chem., **100**, 30 (1996)

74.   R. Flesch, B. Wassermann, B. Rothmund, and E. Ruhl, J. Phys. Chem. 98, 6263 (1994).

VIII. FIGURE CAPTIONS

1.   OClO absorption spectrum (204K), from Ref. 45. Upper Figure: Most intense peaks correspond to progression in ν_1 (labeled). Lower Figure: OClO ($^2A_2$) vibrational assignments near 360 nm. Vibrational assignments from Ref. 21.

2.   Energy level diagram for OClO ground and excited states, and its photodissociation products.

3.   Cuts of OClO potential energy surfaces calculated by Peterson and Werner, reproduced from reference 43.

4.   Newton diagram in velocity space for Cl-containing fragments resulting from decomposition of OClO (5,1,0) prepared at 404nm. Arrow denotes initial OClO beam velocity, and circles are calculated recoil velocities for formation of ground vibrational state fragments.

5.   Upper: ClO Product TOF spectrum (20°) recorded at m/e= 51 for OClO $^2A_2$ (5,1,0) level. Middle: Cl Product TOF spectrum recorded under identical conditions. Dominant slower peak results from fragmentation of ClO to Cl in ionizer. Inset shows expanded vertical scale (x15). Bottom: O_2 TOF spectrum recorded under identical experimental conditions. In all figures, solid line is optimized fit to experimental data.

6.   O atom TOF spectra recorded at indicated angles for ClO + O channel from (5,1,0) level. Structure corresponds to vibrational excitation of ClO counter fragment.

7.   Translational energy distributions for O(^3P) + ClO and Cl(^2P) + O_2 channels from OClO $^2A_2$ (5,1,0) level. The calculated maximum relative translational energies for production of internally excited diatomics are indicated.

8.   Power dependence for Cl TOF spectra recorded at 20 degrees for photodissociation of OClO^A

(5,1,0).

9.   ClO and Cl TOF spectra for ClOCl photodissociation at 423 nm.

10.   Photodissociation of ClOCl. Top: Dependence of ClO signal intensity with laser polarization angle. Bottom: ClO + Cl product translational energy distribution for photodissociation of ClOCl at 423 nm.

11.   TOF spectra recorded at m/e = 16 (O^+) for OClO $^2A_2$ (5,0,0), (4,0,2), (5,1,0), and (4,1,2). Solid line is calculated fit to the data using P(E) shown in Fig. 13.

12.   TOF spectra recorded at m/e = 35 (Cl^+) for OClO $^2A_2$ (5,0,0), (4,0,2), (5,1,0), and (4,1,2). Solid line is calculated fit. Note that the Cl + O_2 channel is strongly suppressed for OClO $^2A_2$ levels having asymmetric stretching excitation.

13.   Translational energy distributions for O(^{3}P) + ClO channel from OClO $^2A_2$ (5,0,0), (4,0,2), (5,1,0) and (4,1,2) levels. The calculated maximum relative translational energies for production of internally excited ClO is indicated.

14. O^+ TOF recorded at 40° for OClO absorption peaks near 410 nm.

15.   Translational energy distributions for O(^{3}P) + ClO channel from OClO $^2A_2$ (4,0,0), (3,0,2), (4,1,0) and (3,1,2) levels.

16. Cl^+ TOF recorded at 20° for OClO absorption peaks near 410 nm..

17. O^+ TOF recorded at 20° for OClO absorption peaks near 470 nm.

18.   ClO + O translational energy distributions for OClO vibrational levels near 470 nm.

19. O^+ TOF recorded at 40° for OClO absorption peaks near 395 nm. Slower peak near 280 nm results from fragmentation of ClO to O^+ in ionizer.

20.   ClO + O translational energy distribution for ClO + O channel from indicated OClO $^2A_2$ levels.

21. Cl^+ TOF spectra for OClO peaks near 380 nm. Note that the Cl + O_2 channel is nearly absent in this energy region.

22. Dependence of ClO + O channel (monitored at ClO$^+$) to laser polarization angle for several OClO $^2A_2$ vibrational levels.

23. TOF spectra for ClO and Cl resulting from excitation to the (10,0,0) peak of OClO($^2A_2$) near 360 nm. Dominant Cl$^+$ peak is daughter ion from fragmentation of ClO in electron impact ionizer detector. Inset: vertical scale expanded by factor of 100. Solid line in the inset is calculated contribution assuming 0.2 % yield of Cl + O_2.

24. ClO + O translational energy distribution [P(E)] for products from decomposition of $^2A_2$ (10,0,0) vibrational level prepared by excitation of OClO at 360 nm..

25. Cl TOF spectra from decay of $^2A_2$ (10,0,0) vibrational level recorded at various laser pulse energies. Shape of dominant contribution (T=220-700 μs) is independent of energy (*i.e.* a one photon process). Fast contribution (T=100-200 μs) increases at higher pulse energy (*i.e.* a multiphoton process). Solid line corresponds to upper limit of 0.2 % for Cl + O_2 channel, determined at 1 mJ/pulse.

26. ClO and Cl TOF spectra recorded at 13° for decay of $^2A_2$ (10,0,0) vibrational level. TOF spectra are identical, with no contribution from Cl + O_2 channel.

27. Cl TOF spectra at various laser polarization angles, θ_p. θ_p = 0 degrees corresponds to laser polarization along the detector axis. θ_p = 90 degrees corresponds to vertical laser polarization. Shape of TOF spectra is nearly the same for each polarization angle with no evidence for Cl + O_2 channel.

28. O$^+$ TOF spectra (30°) from indicated OClO ($^2A_2$) vibrational levels near 370 nm. Note that the shapes for different vibrational levels are different, with narrowest TOF for OClO (8,0,2).

29. Translational energy distributions P(E) for ClO + O channel from indicated OClO $^2A_2$ vibrational levels pumped near 370 nm, normalized to unit area. Mode specific ClO vibrational distributions are evident with enhanced contribution for E_{trans} ~ 13 kcal/mole from the (8,0,2) level.

30. O$^+$ TOF spectra (30°) from indicated OClO vibrational levels near 360 nm. Note that the shapes for different vibrational levels are different, with narrowest TOF for OClO $^2A_2$ (9,0,2).

31. Translational energy distributions P(E) for ClO + O channel from indicated OClO $^2A_2$

vibrational levels pumped near 360 nm, normalized to unit area. Mode specific ClO vibrational distributions are evident with enhanced contribution for $E_{trans} \sim$ 14 kcal/mole from the (9,0,2) level.

TABLE I: ClO Vibrational State Distributions from Various OClO Levels

Band ν_1 ν_2 ν_3	E (cm^{-1})	E$_{avl}$ (cm^{-1})	ClO Vibrational Populations (% in v')						$<f_v>$ %
			0	1	2	3	4	5	
0 0 0	21 016	372	100	-	-	-	-	-	.00
1 0 0	21 724	1080	60	40	-	-	-	-	.31
1 1 0	22 007	1363	50	50	-	-	-	-	.31
2 0 0	22 423	1779	38	62	-	-	-	-	.29
2 1 0	22 704	2060	24	51	25	-	-	-	.41
3 0 0	23 117	2473	39	33	25	3	-	-	.31
2 0 2	23 280	2636	13	47	37	3	-	-	.26
3 1 0	23 393	2750	17	52	28	3	-	-	.36
4 0 0	23 804	3160	21	17	46	16	-	-	.42
3 0 2	23 958	3314	17	49	22	12	-	-	.33
4 1 0	24 077	3433	11	28	37	21	4	-	.44
3 1 2	24 225	3581	11	23	36	15	15	-	.47
5 0 0	24 486	3842	23	16	24	25	12	-	.41
4 0 2	24 633	3989	34	36	10	15	5	-	.25
5 1 0	24 754	4110	17	24	25	13	20	-	.39
4 1 2	24 896	4252	36	18	18	11	16	-	.30
6 0 0	25 162	4518	42	22	12	10	14	-	.24
5 0 2	25 304	4660	50	29	4	6	10	-	.17
6 1 0	25 425	4781	25	21	21	15	17	1	.32
5 1 2	25 564	4920	43	32	4	10	11	-	.19
7 0 0	25 832	5188	26	42	12	6	10	4	.23
6 0 2	25 970	5326	17	45	16	9	6	6	.24
7 1 0	26 093	5449	17	37	20	8	7	11	.28
6 1 2	26 229	5585	15	38	24	10	6	7	.26
8 0 0	26 497	5853	14	46	16	12	12	-	.23

TABLE II: ClO Vibrational State Distributions and Cl Yields from Various OClO Levels

Band ν_1 ν_2 ν_3	ClO Vibrational Populations (% in v')						$<f_v>$ %	Cl(%)
	0	1	2	3	4	5		
0 0 0	100	-	-	-	-	-	0.00	-
1 0 0	60	40	-	-	-	-	0.31	-
2 0 0	38	62	-	-	-	-	0.29	1.8
3 0 0	39	33	25	3	-	-	0.31	2.9
4 0 0	21	17	46	16	-	-	0.42	0.9
5 0 0	23	16	24	25	12	-	0.41	3.2
6 0 0	42	22	12	10	14	-	0.24	2.0
7 0 0	26	42	12	6	10	4	0.23	0.6
8 0 0	14	46	16	12	12	-	0.23	0.6
1 1 0	50	50	-	-	-	-	0.31	-
2 1 0	24	51	25	-	-	-	0.41	1.0
3 1 0	17	52	28	3	-	-	0.36	2.6
4 1 0	11	28	37	21	4	-	0.44	2.1
5 1 0	17	24	25	13	20	-	0.39	3.9
6 1 0	25	21	21	15	17	1	0.32	2.4
7 1 0	17	37	20	8	7	11	0.28	1.4
2 0 2	13	47	37	3	-	-	0.26	1.0
3 0 2	17	49	22	12	-	-	0.33	. 1.3
4 0 2	34	36	10	15	5	-	0.25	0.4
5 0 2	50	29	4	6	10	-	0.17	1.3
6 0 2	17	45	16	9	6	6	0.24	0.5
3 1 2	11	23	36	15	15	-	0.47	2.5
4 1 2	36	18	18	11	16	-	0.30	1.0
5 1 2	43	32	4	10	11	-	0.19	1.3
6 1 2	15	38	24	10	6	7	0.26	1.1

Fig. 1

OClO $(A\ ^2A_2)$

OClO$(X\ ^2B_1)$

404 nm

$Cl(\overline{^2P_J}) + O_2(^1\Sigma_g^+)$

$Cl(^2P_J) + O_2(^1\Delta_g)$

$Cl(^2P_J) + O_2(^3\Sigma_g^-)$

$ClO(\overline{^2\Pi_i,\ v'}) + O(^3P_J)$

Energy (kcal/mol)

Fig. 2

Fig. 3

$\underline{Cl}(^2P_J) + O_2(^3\Sigma^-_g)$

$\underline{Cl}(^2P_J) + O_2(^1\Delta_g)$

$\underline{Cl}(^2P_J) + O_2(^1\Sigma^+_g)$

$\underline{ClO}(^2\Pi_i) + O(^3P_J)$

OClO

1000 m/s

0° 10° 20° 30° 40° 50° 60°
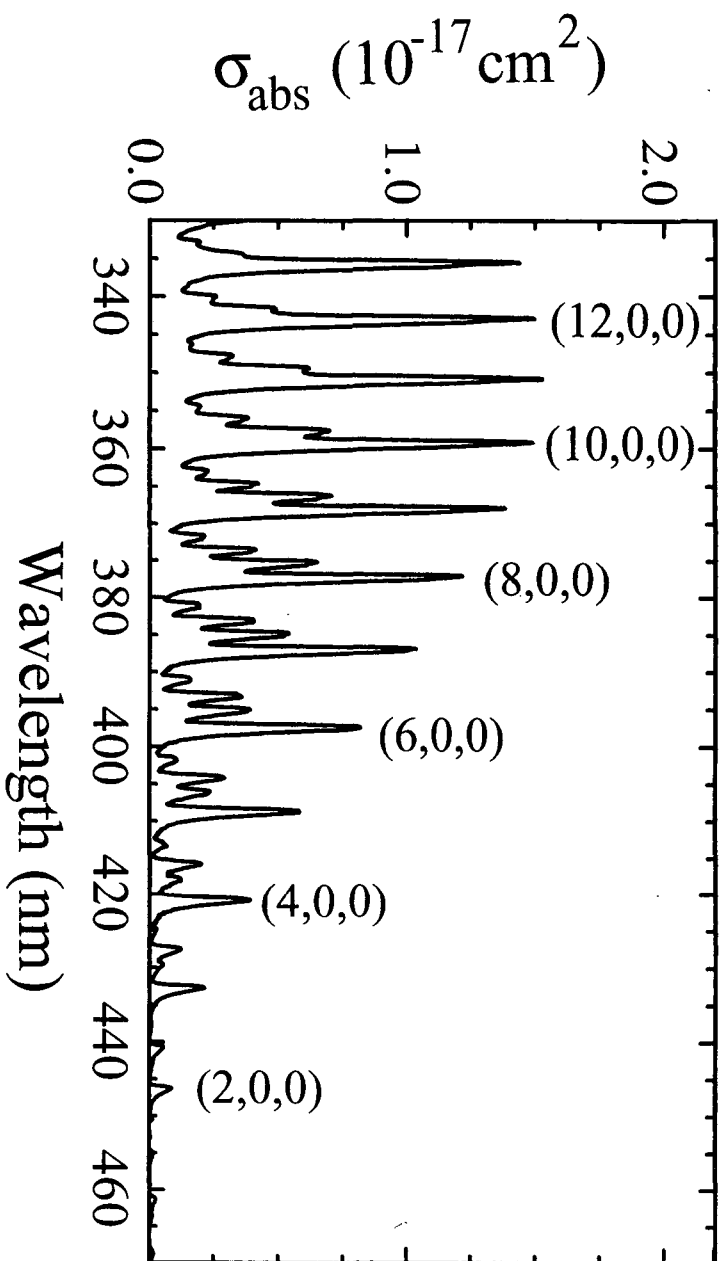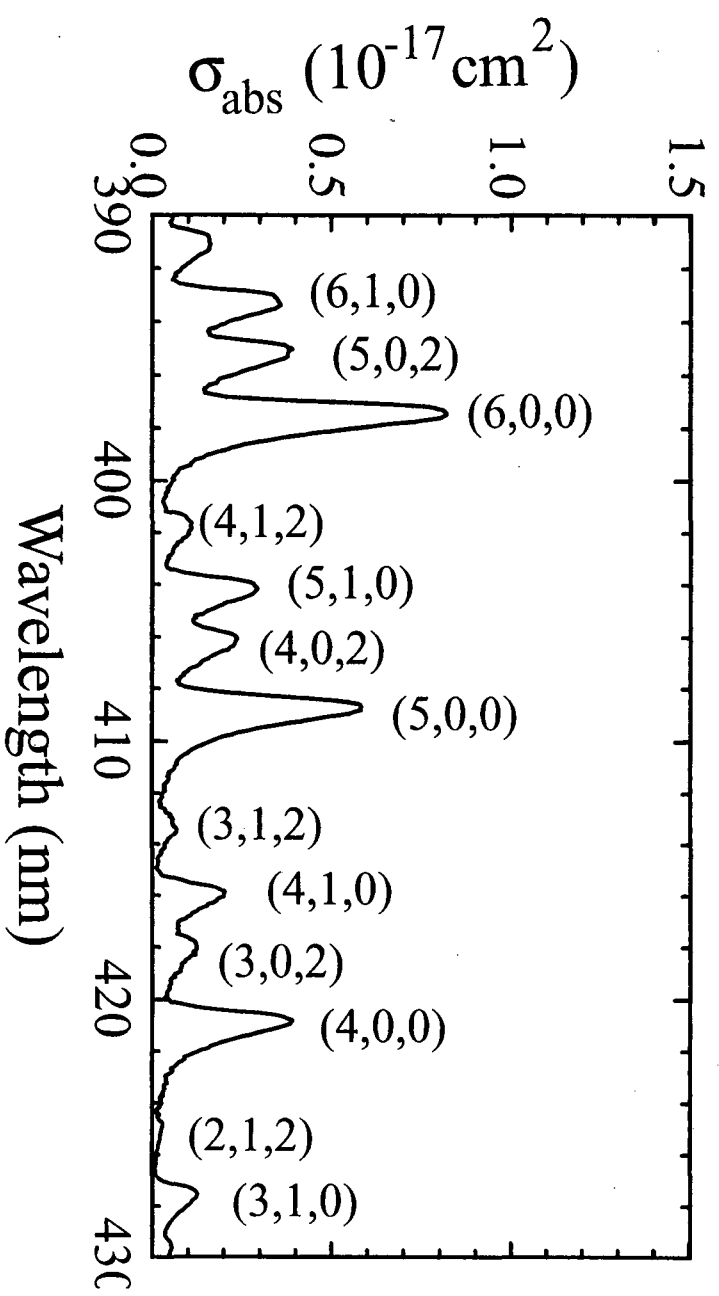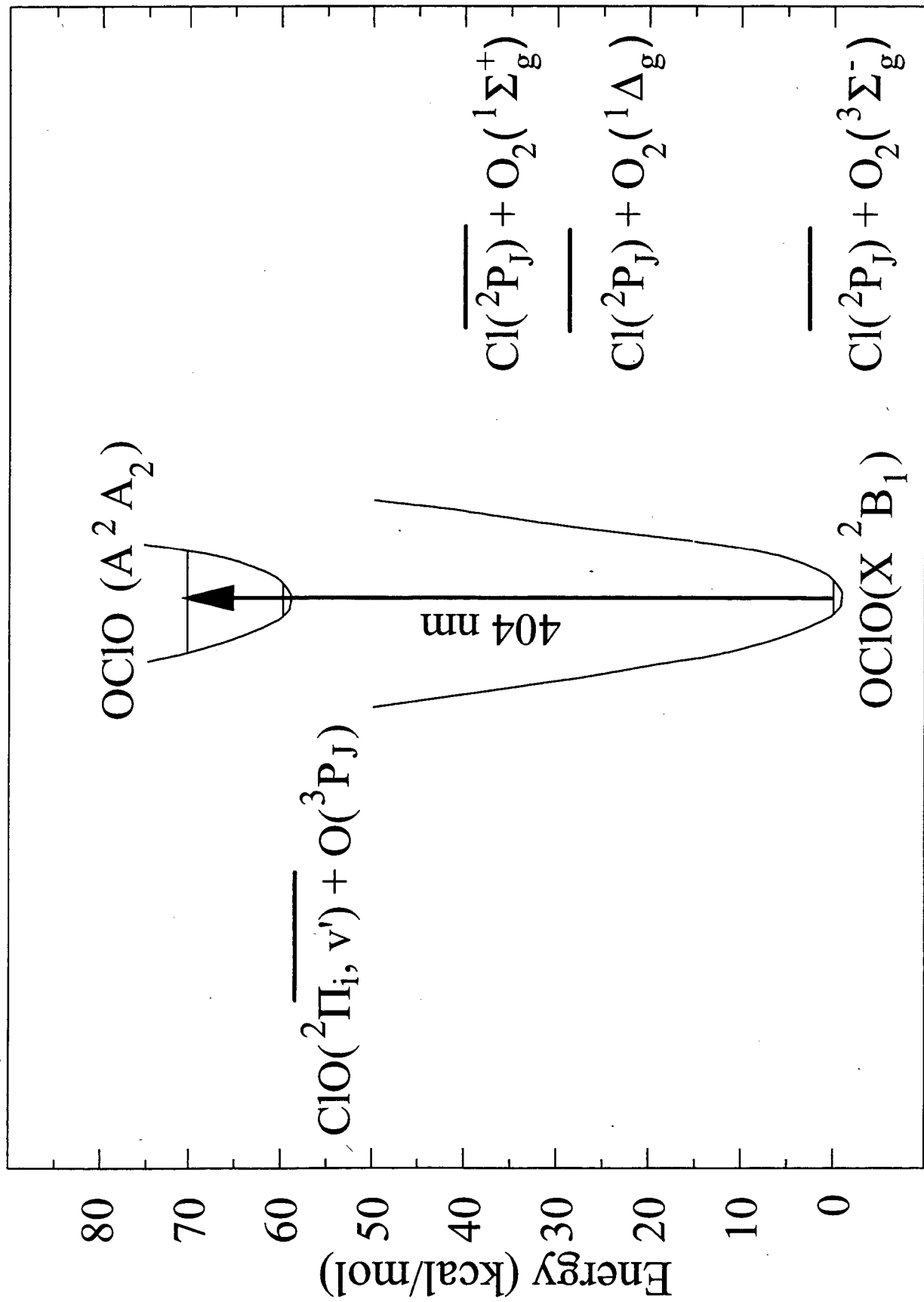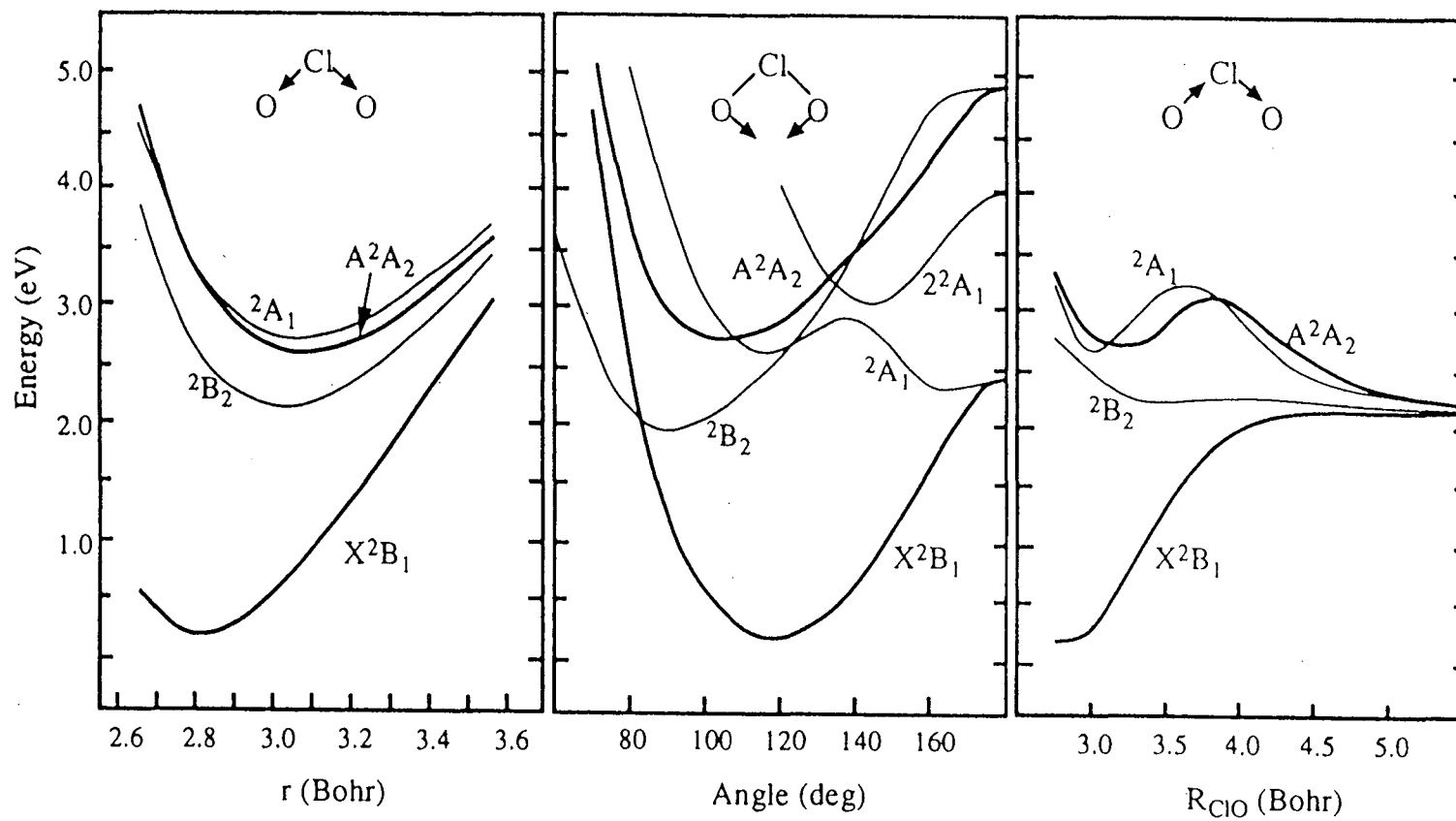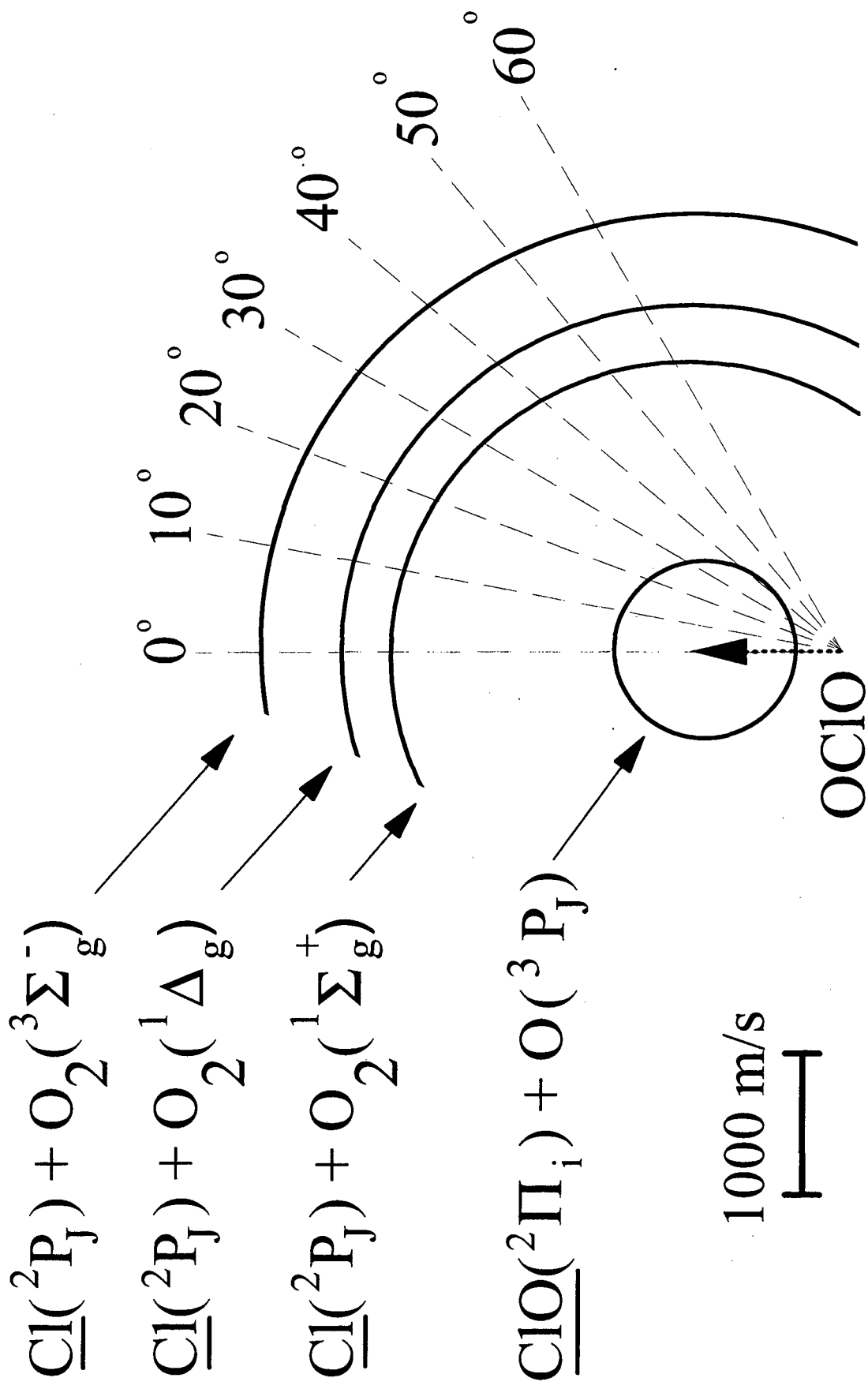
Fig. 4

Fig. 5

Fig. 6

Fig. 7

Fig. 8

Fig. 9

$\beta = -1.0$

Fig. 10

Fig. 11

Fig. 12

The figure contains four stacked panels showing N(T) versus Flight Time, T (μsec) from 0 to 600.

Panel (5,0,0): 3.2% Cl + O₂

Panel (4,0,2): 0.4% Cl + O₂

Panel (5,1,0): 3.9% Cl + O₂
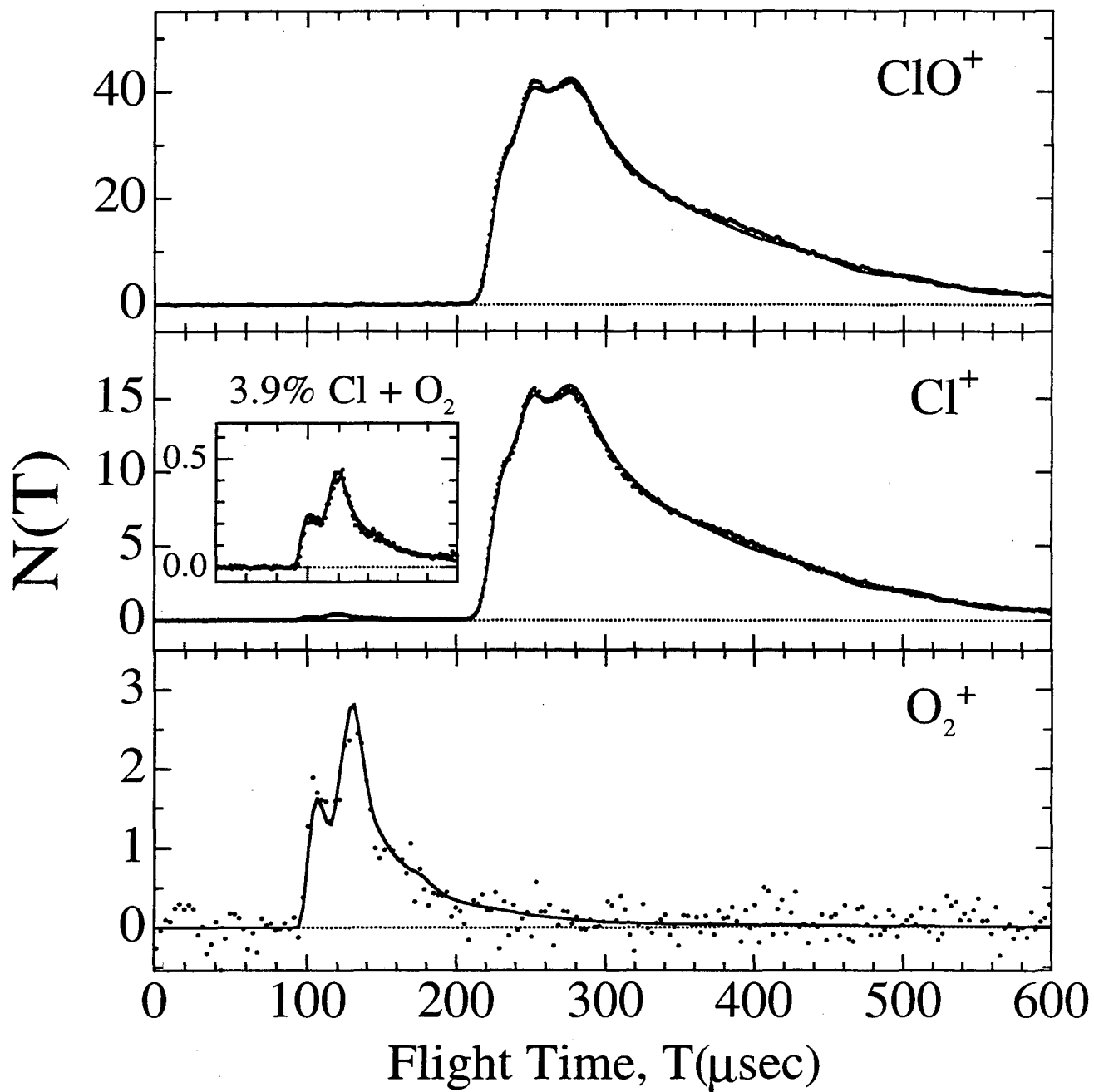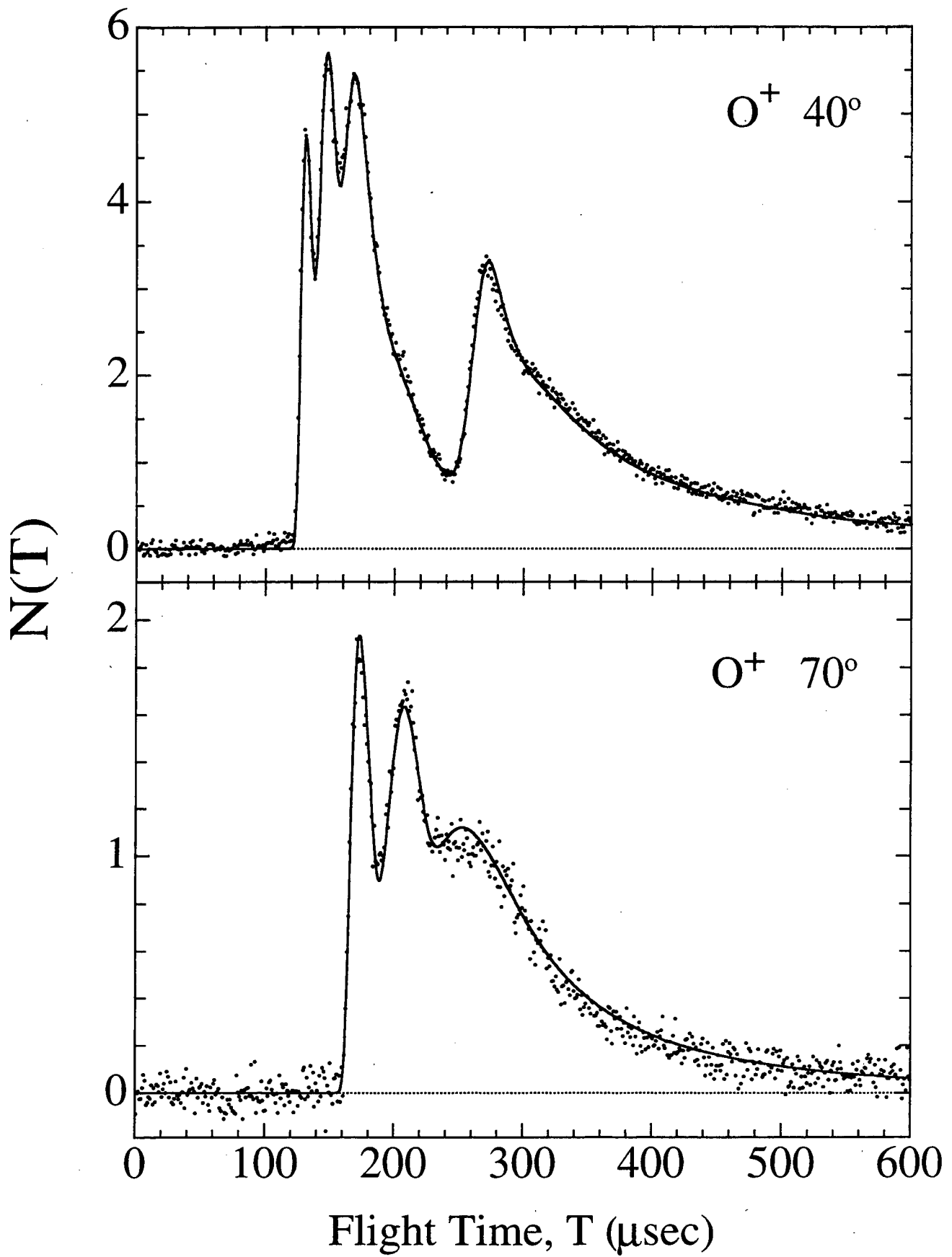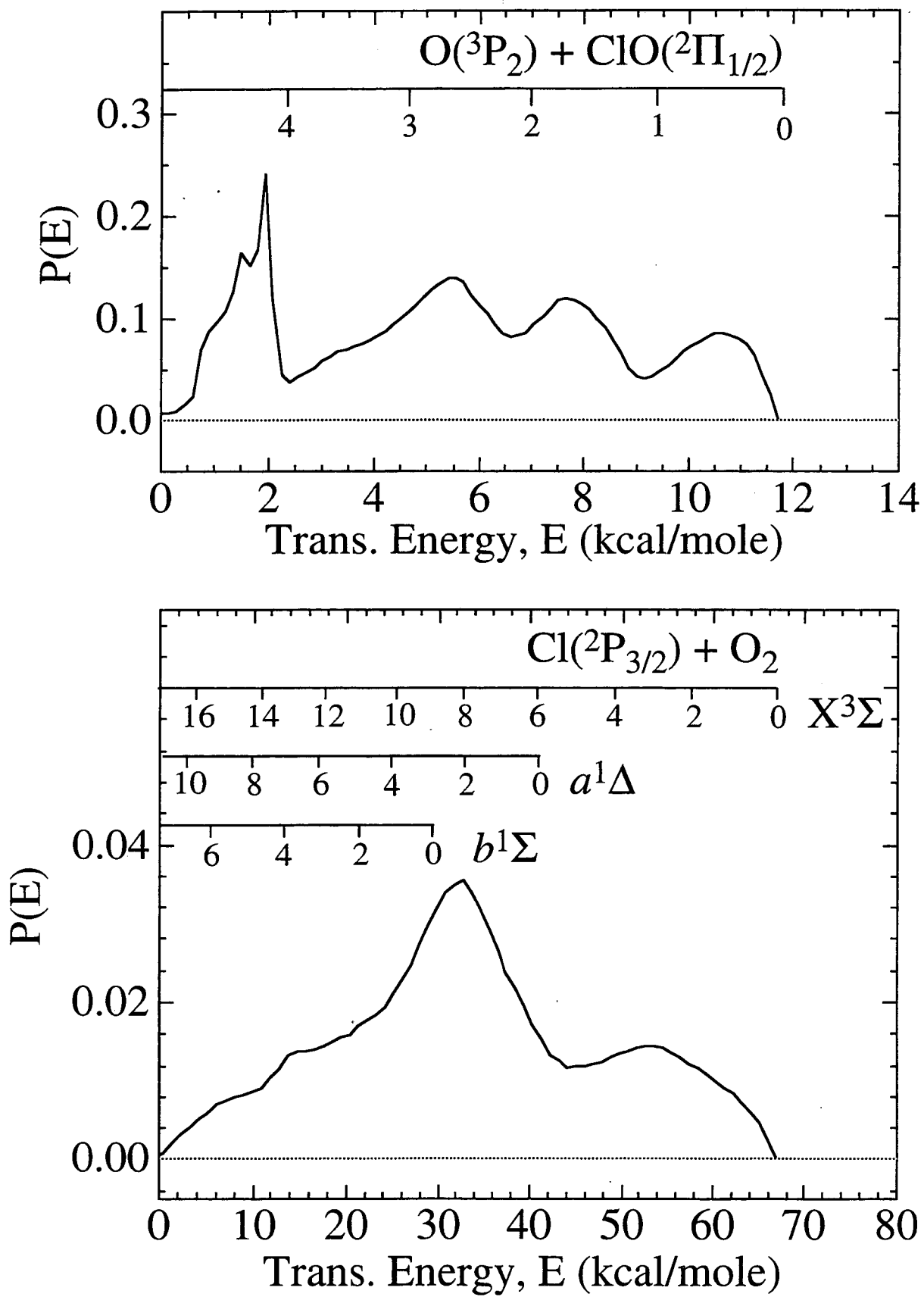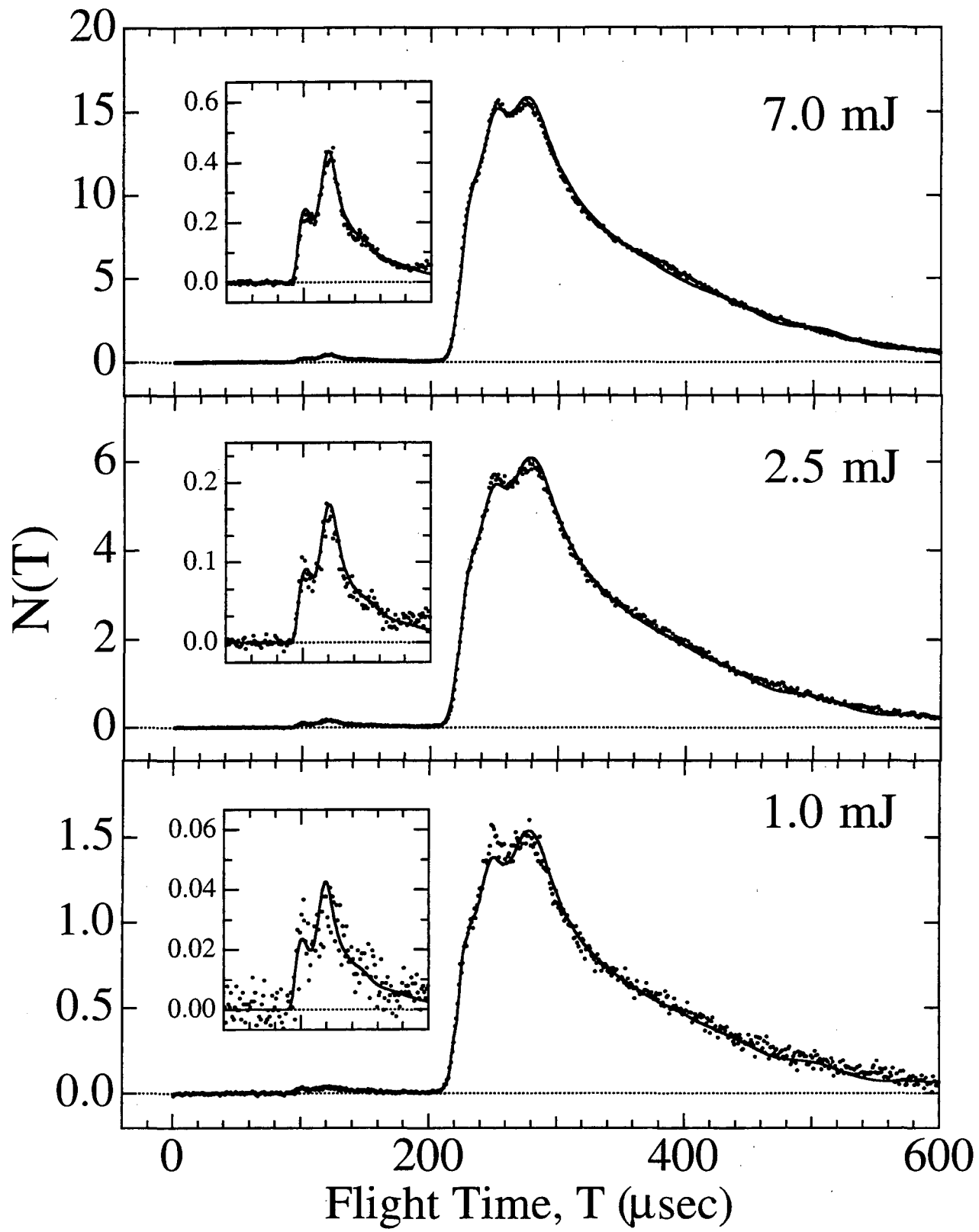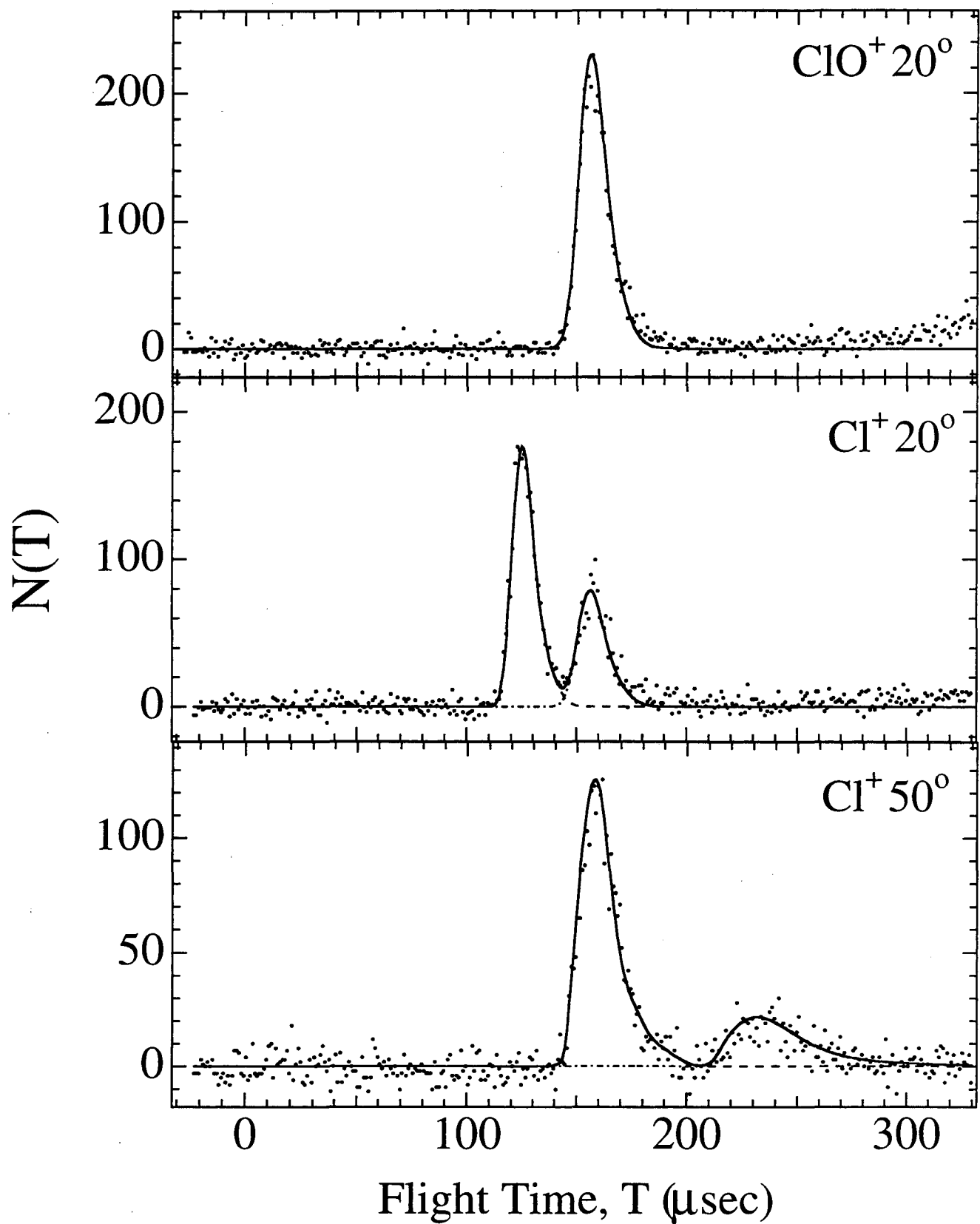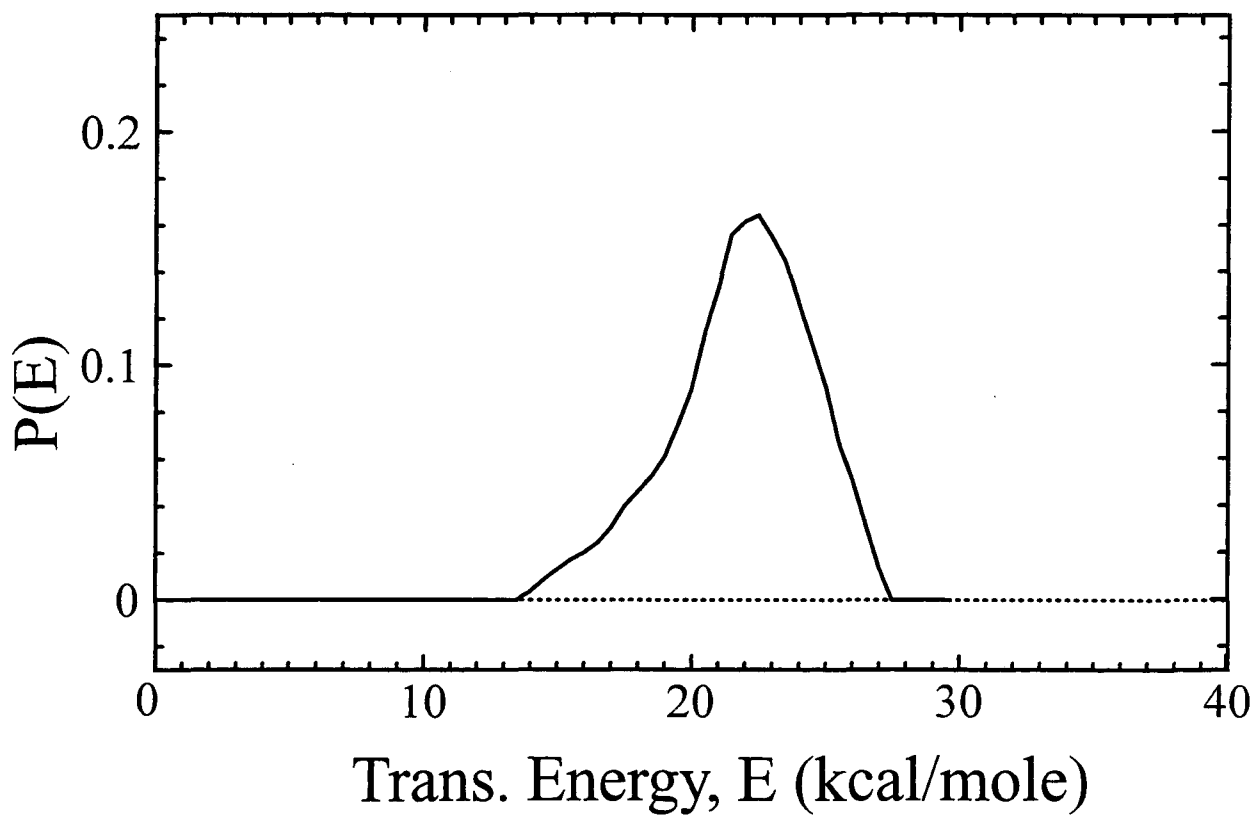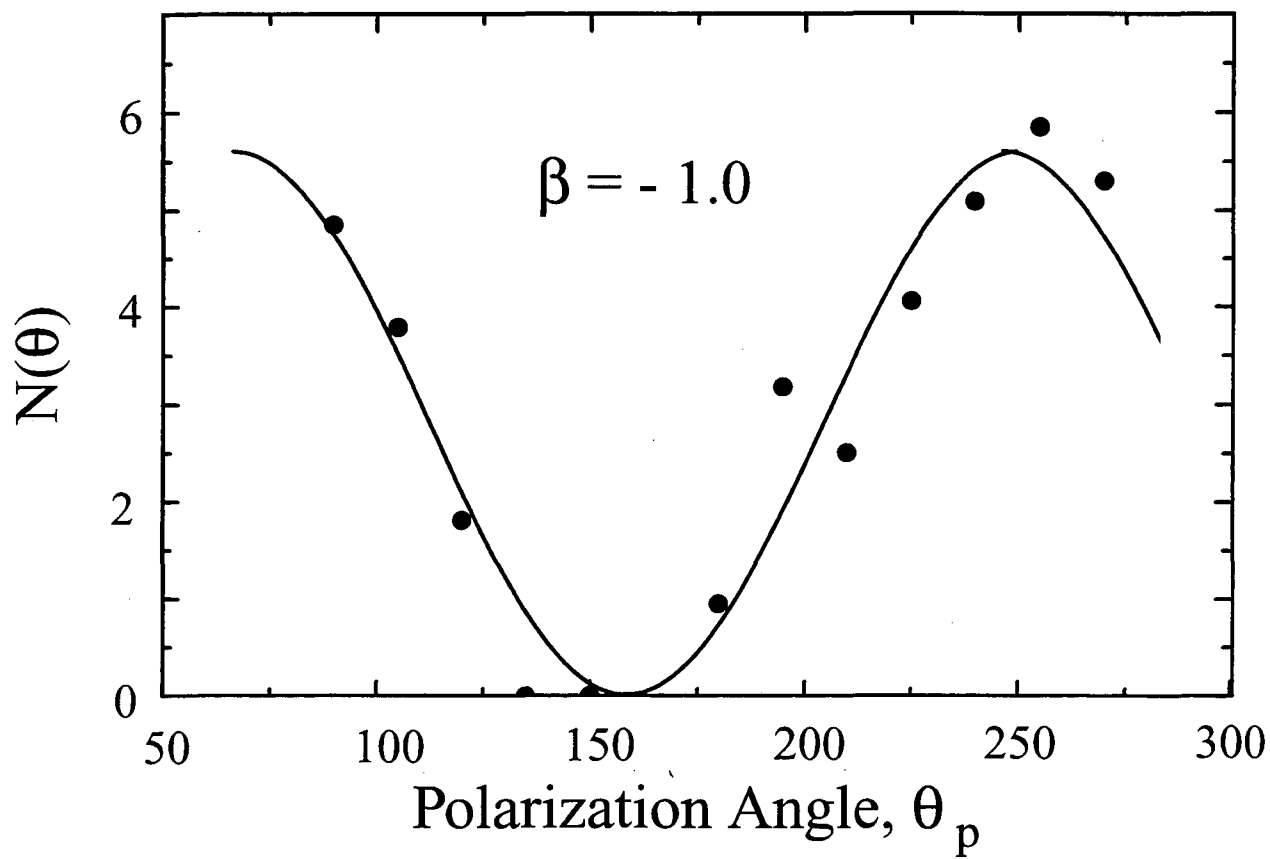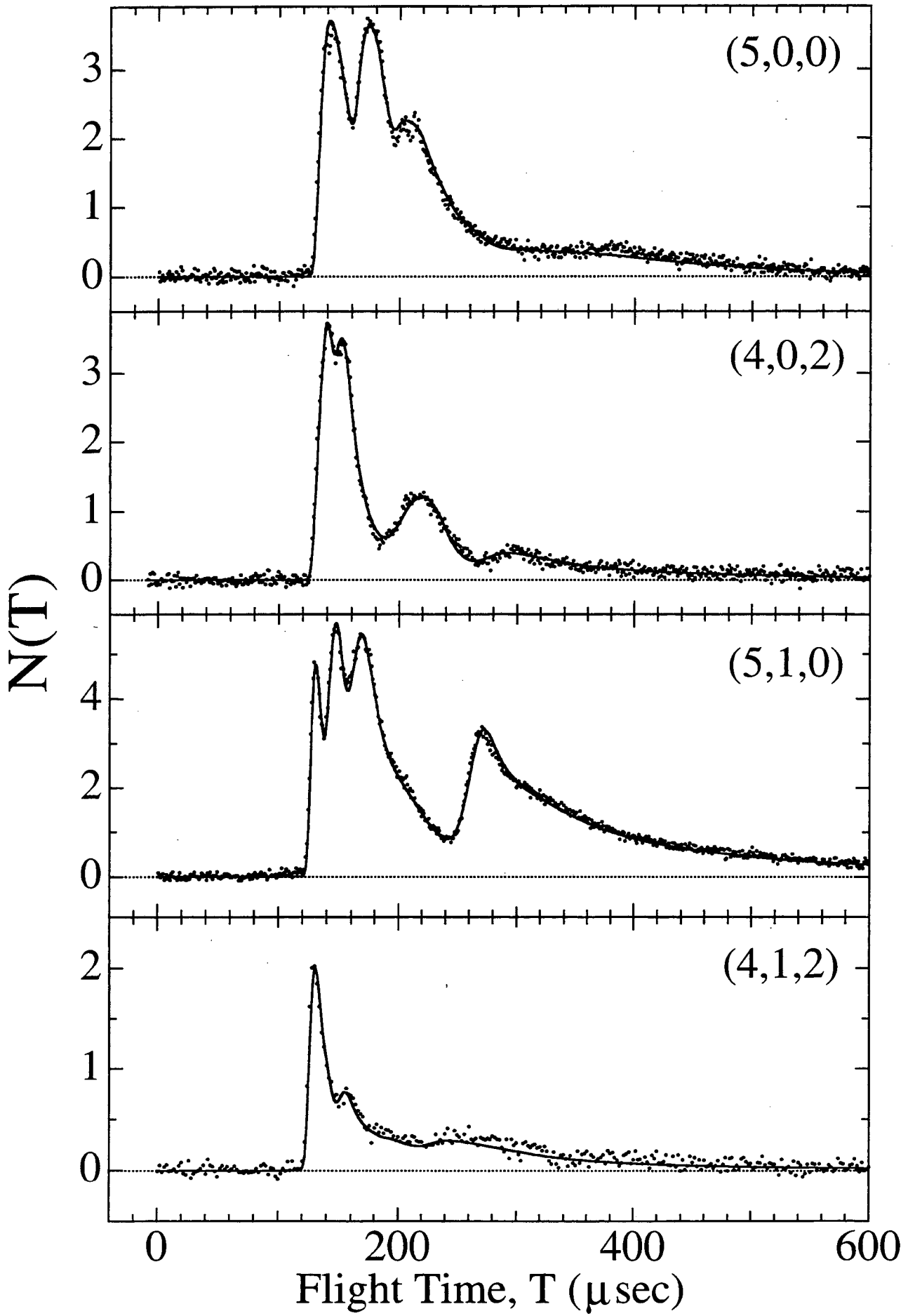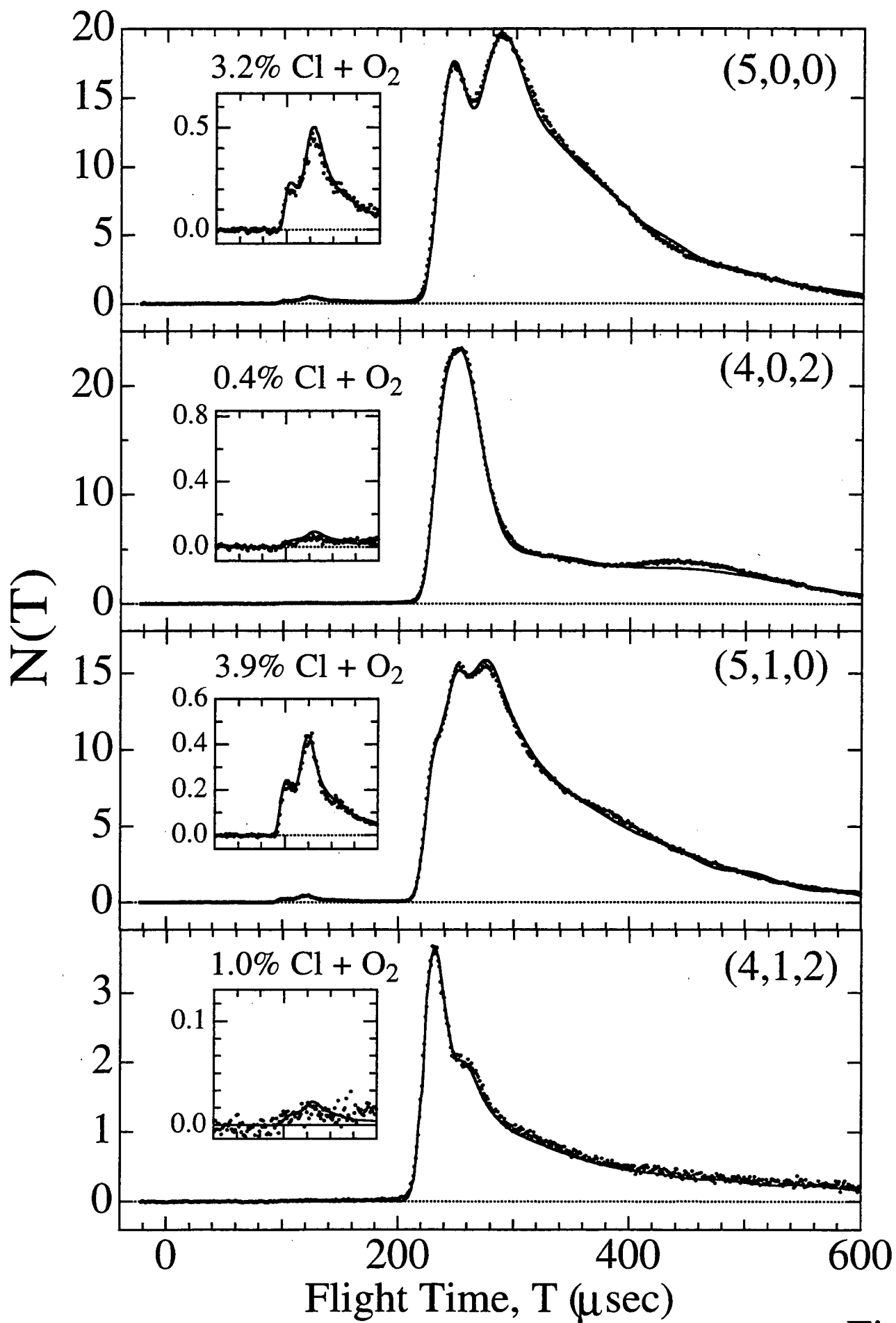
Panel (4,1,2): 1.0% Cl + O₂
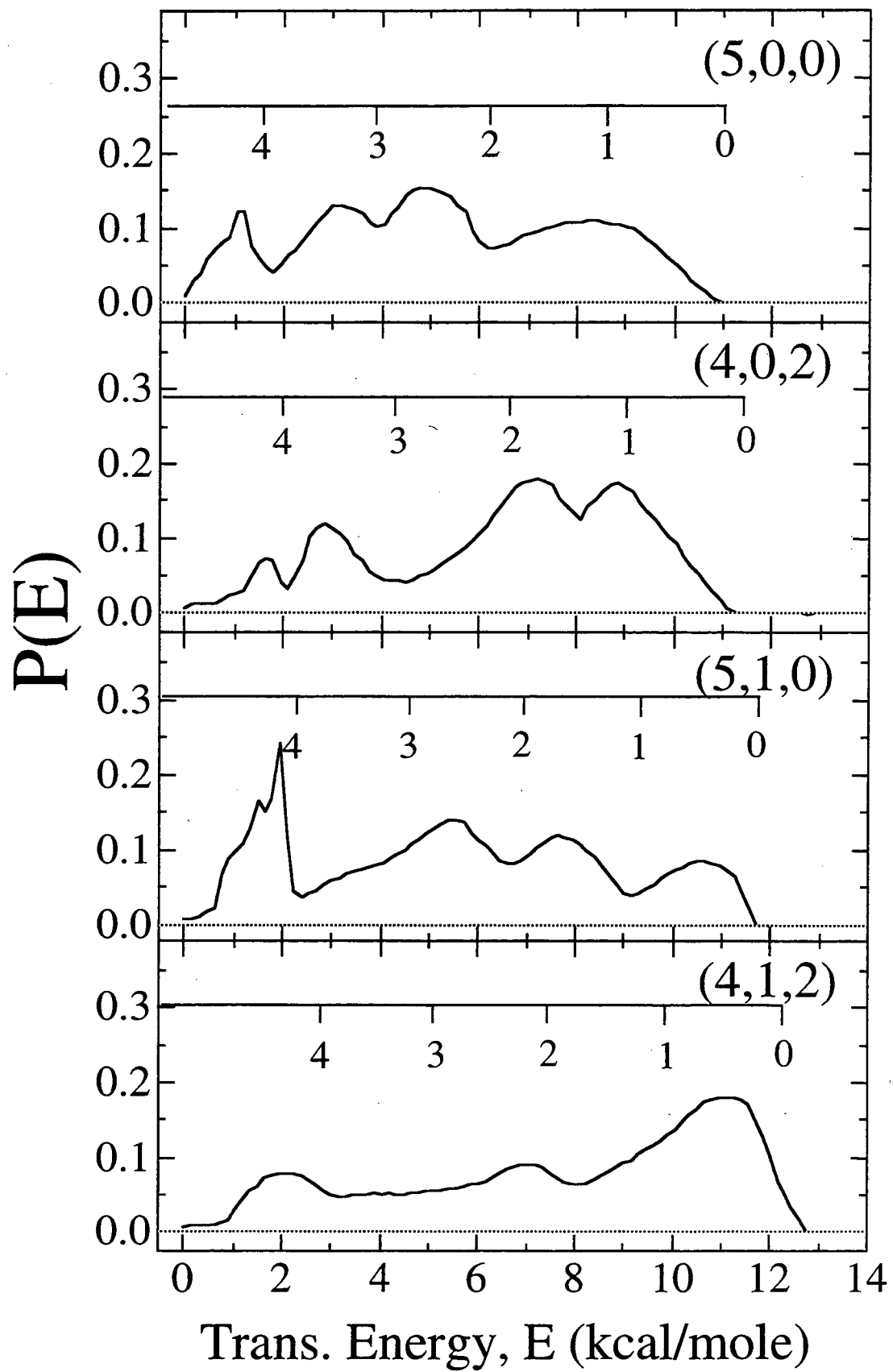
Fig. 13
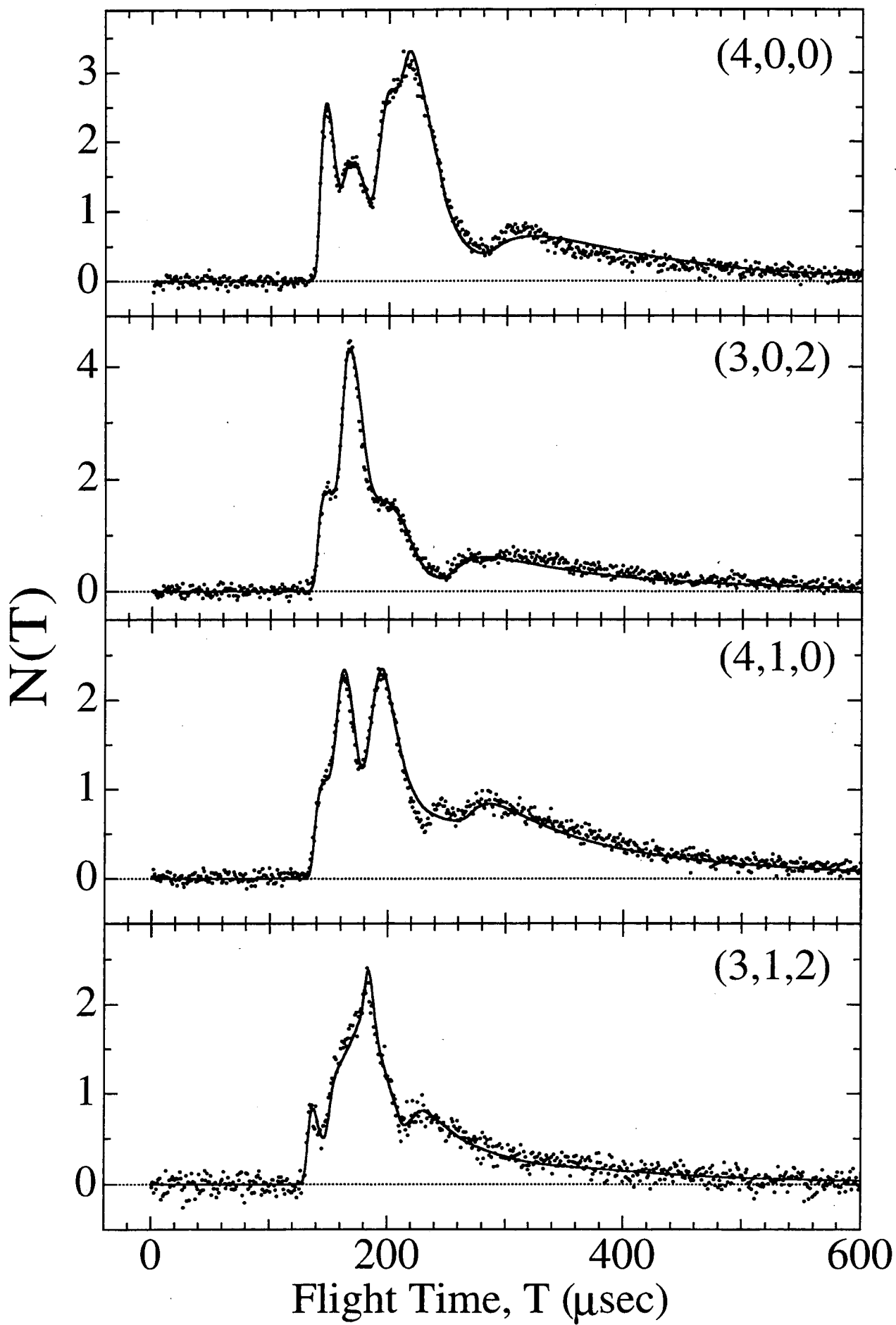
Fig. 14
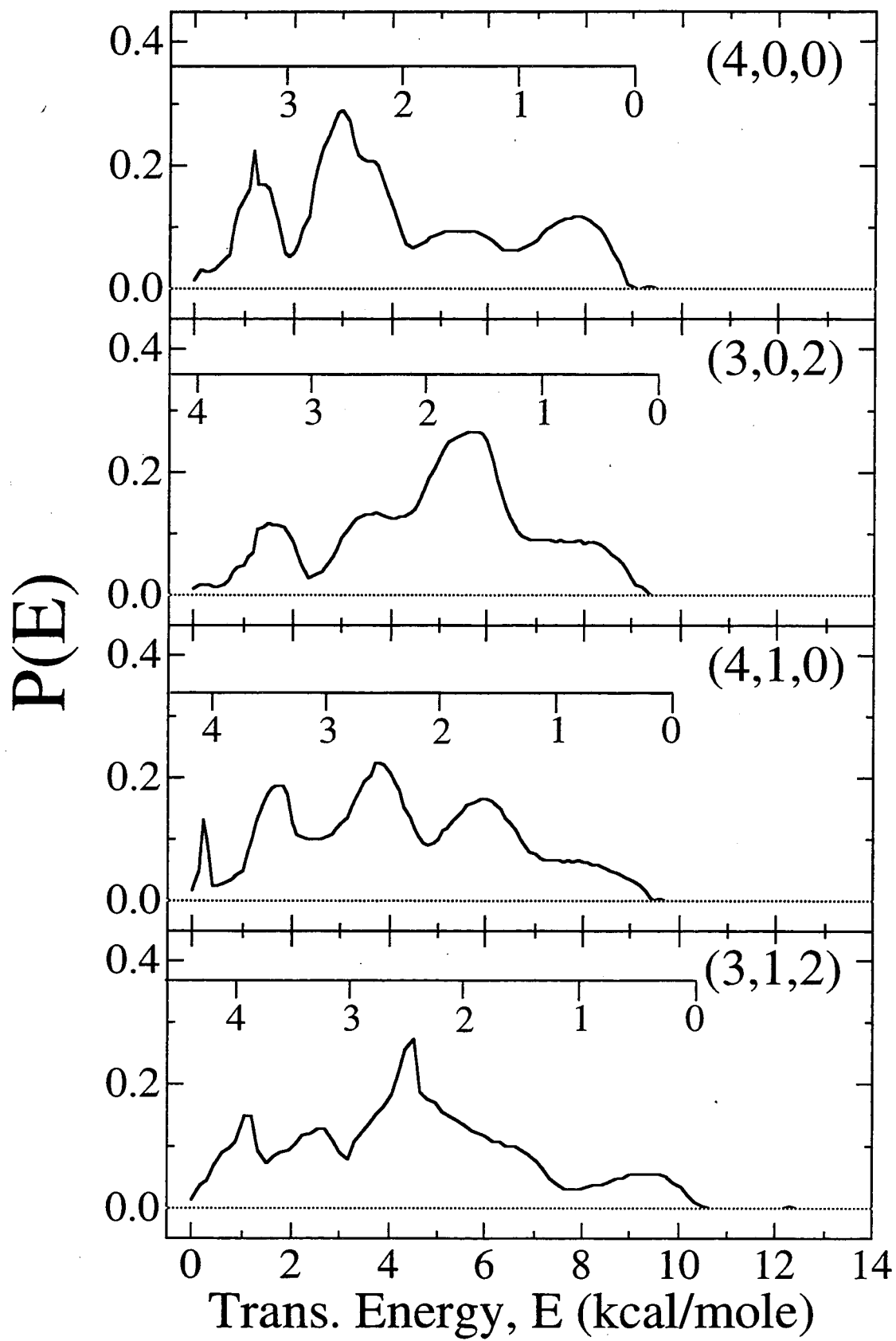
Fig. 15
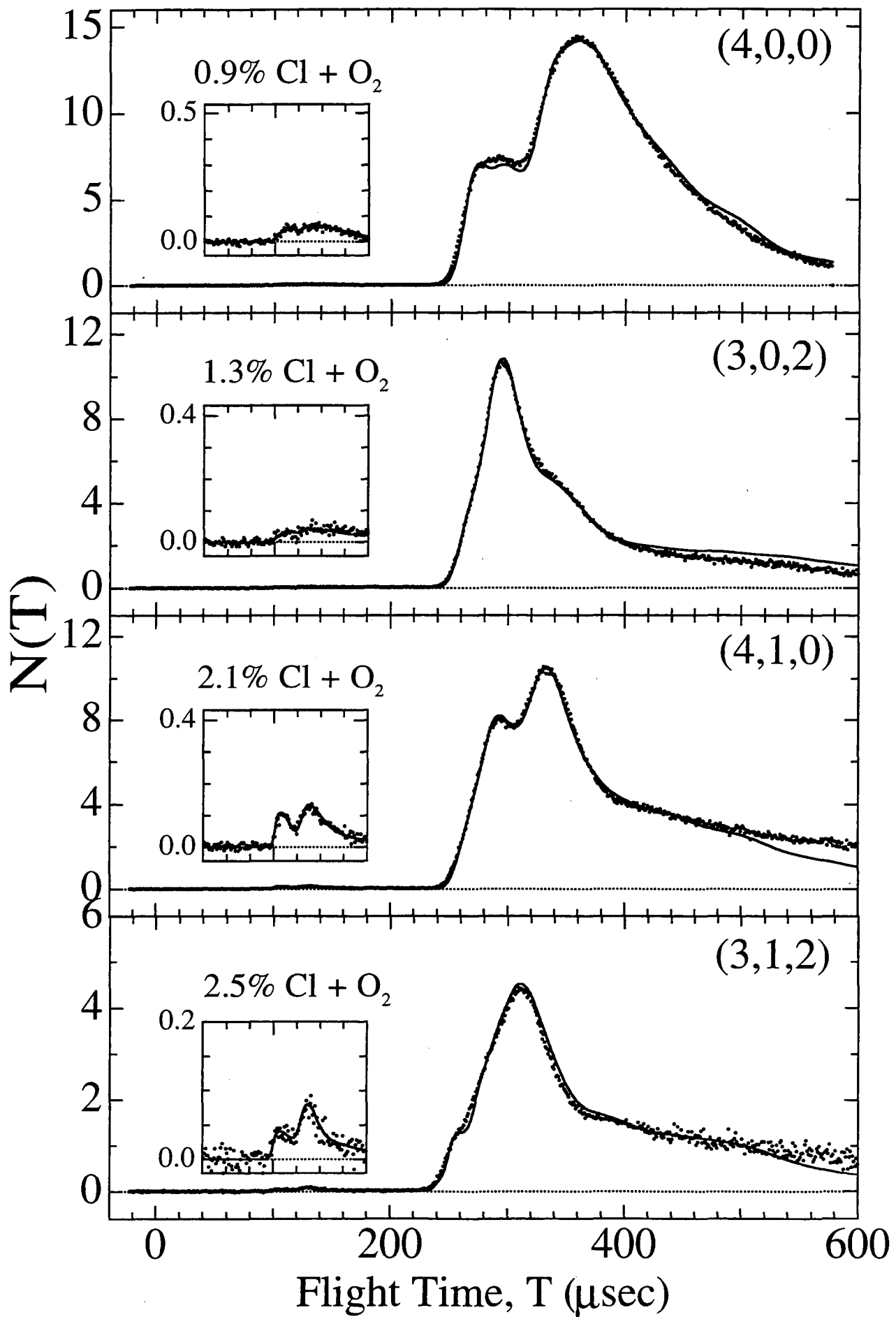
Fig. 16
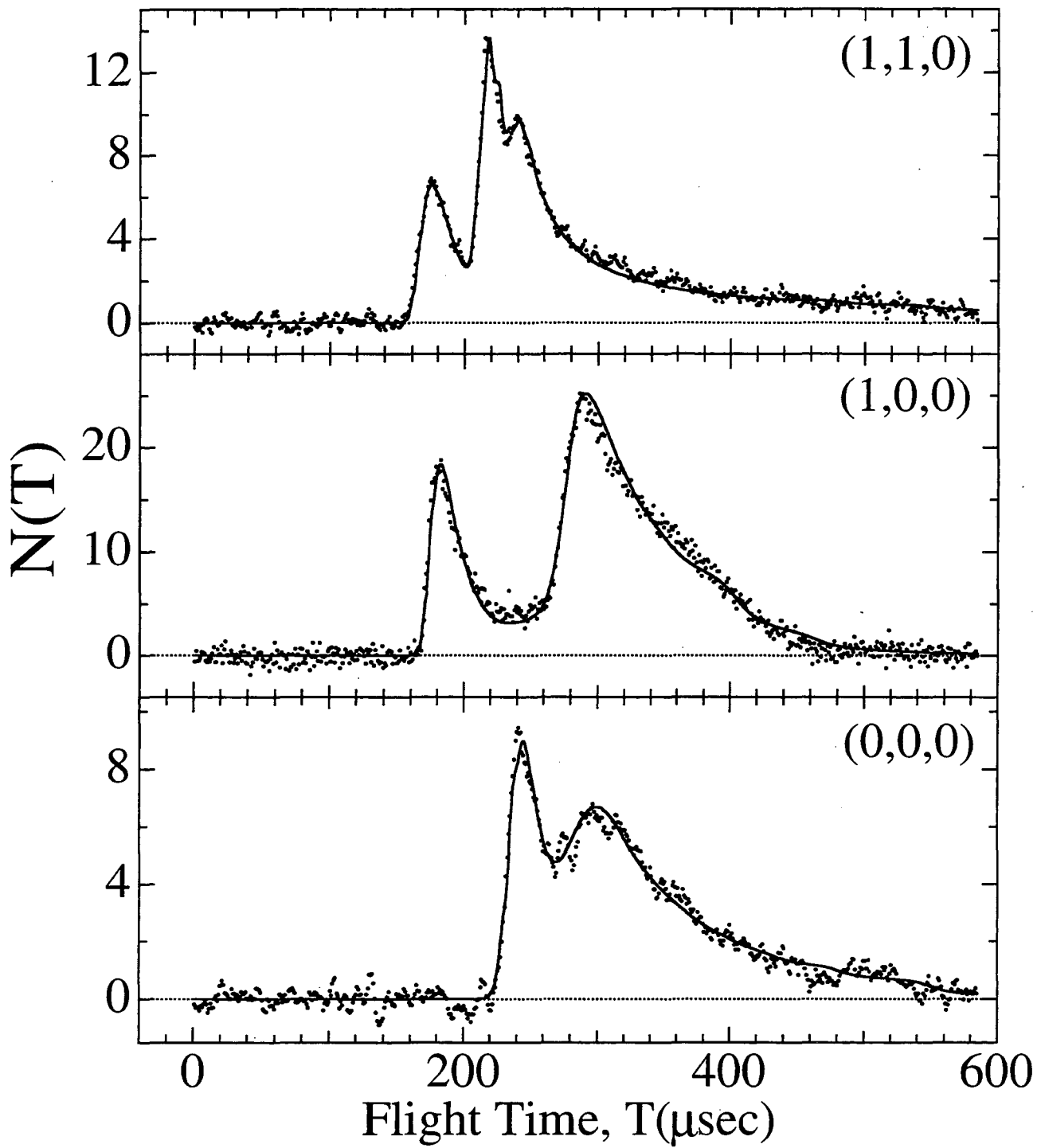
Fig. 17

Fig. 18

Fig. 19

Fig. 20

Fig. 21

(5,0,0)

(4,0,2)

(7,0,0)

(6,0,2)

(8,1,0)

(10,0,0)

N(ϕ)

Polarization Angle (ϕ)

Fig. 22

Fig. 23

ClO(v'') + O

(10,0,0)
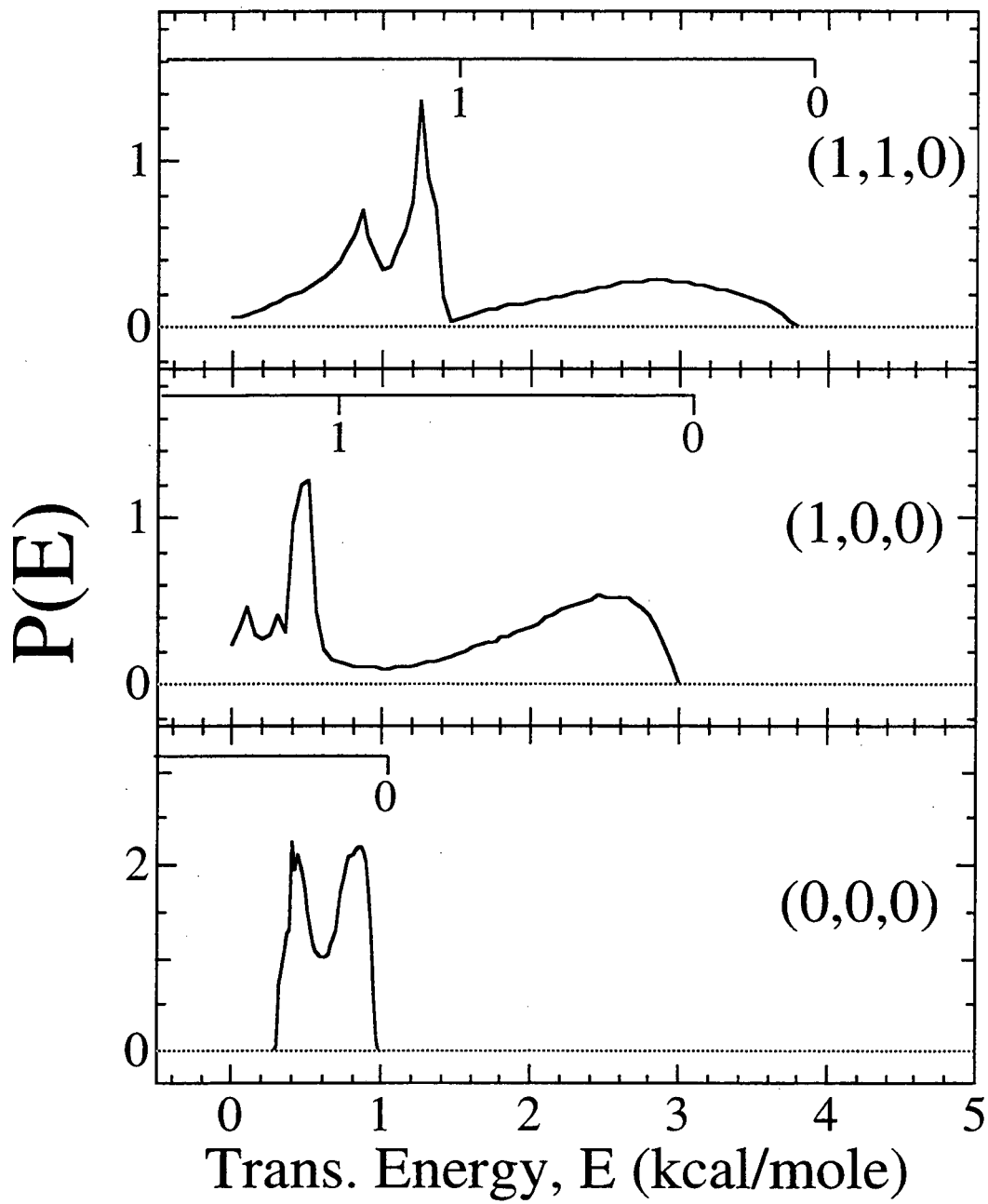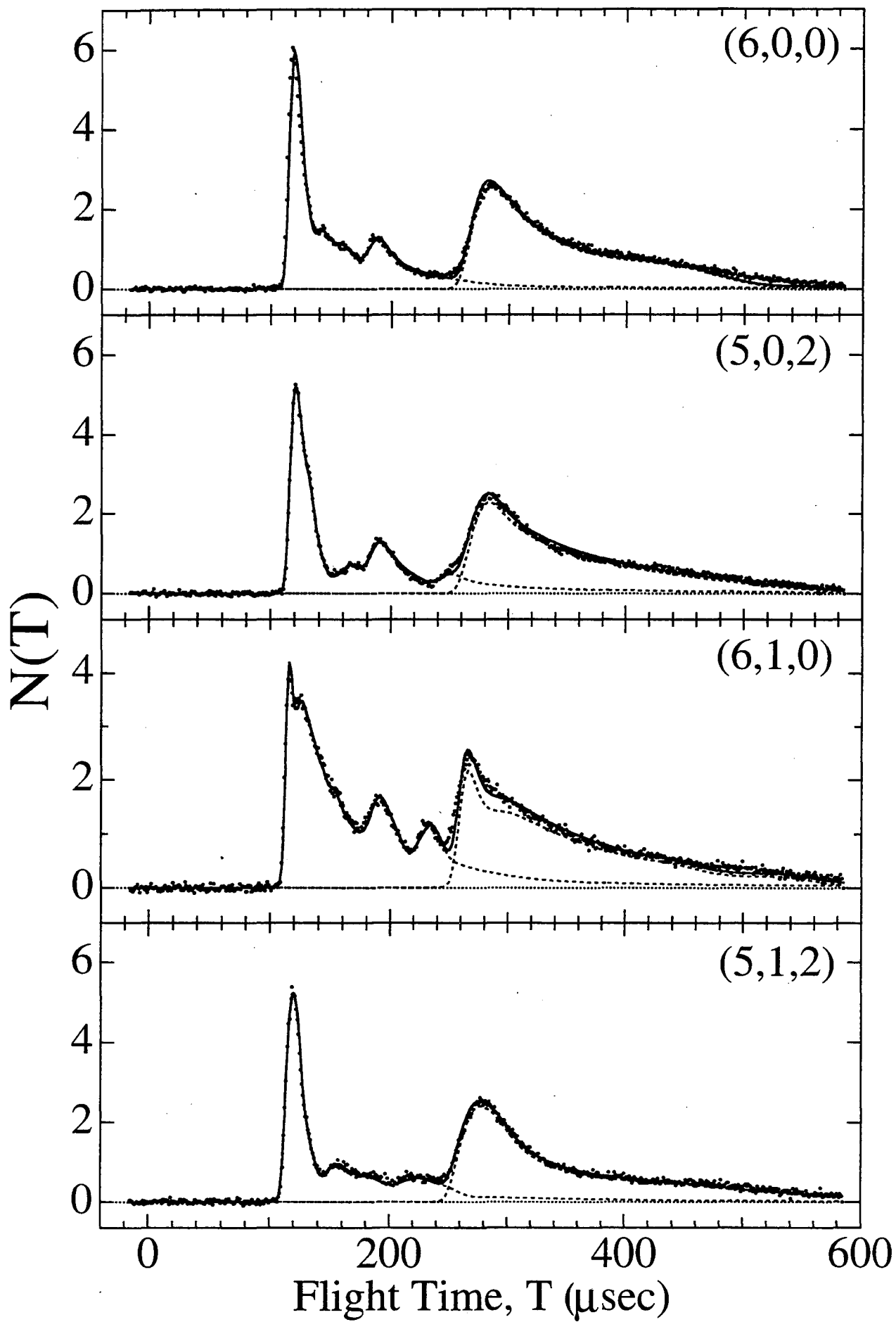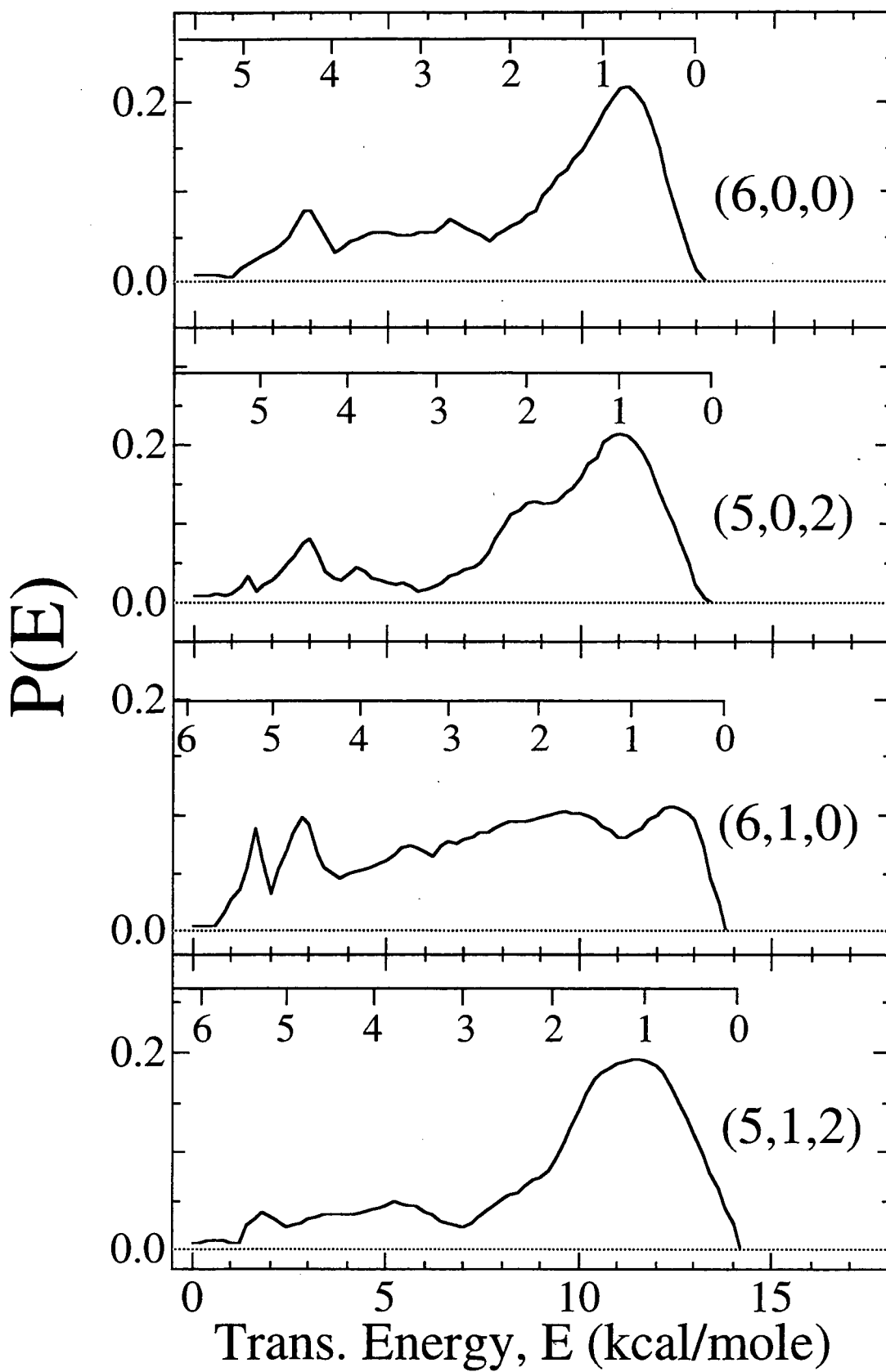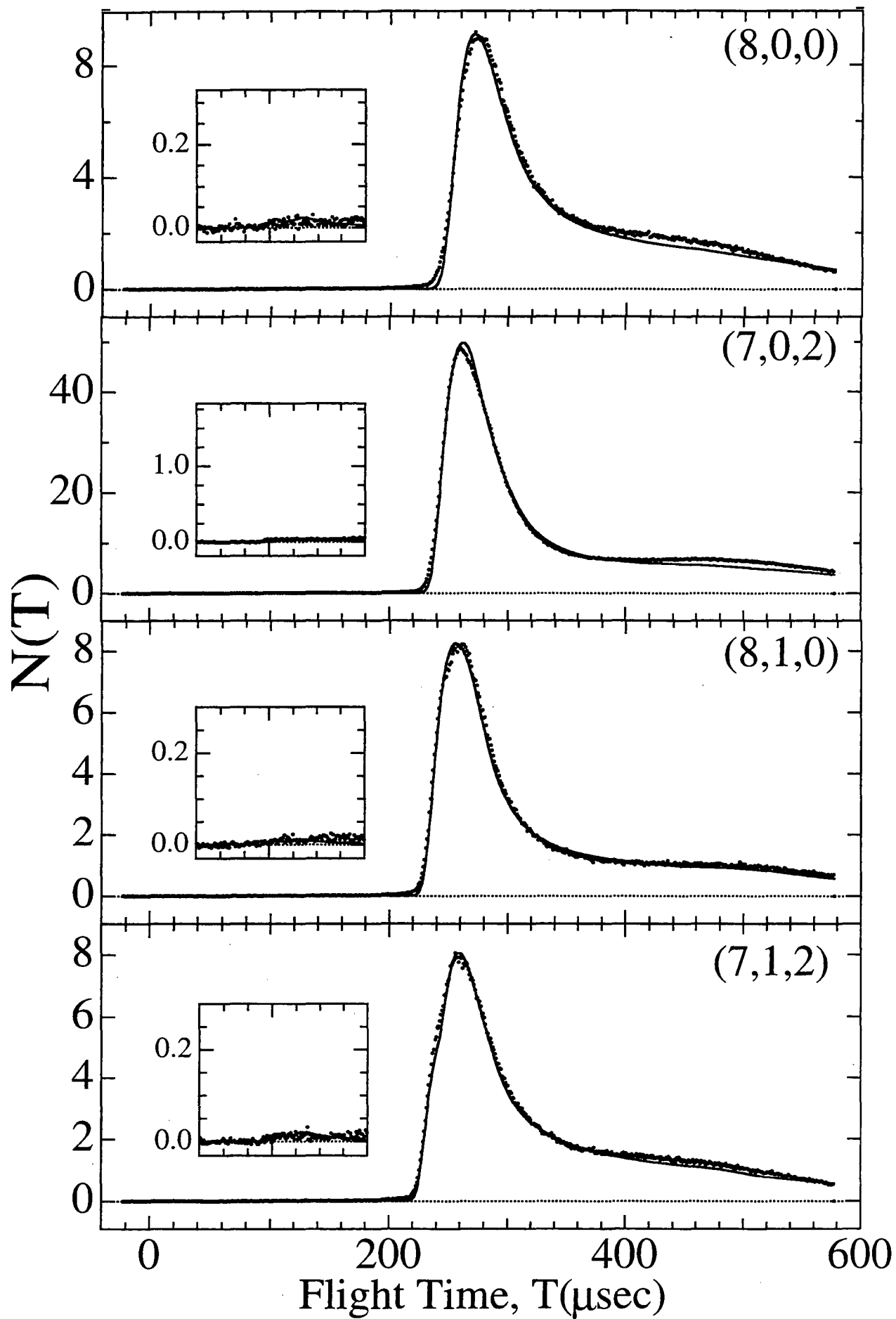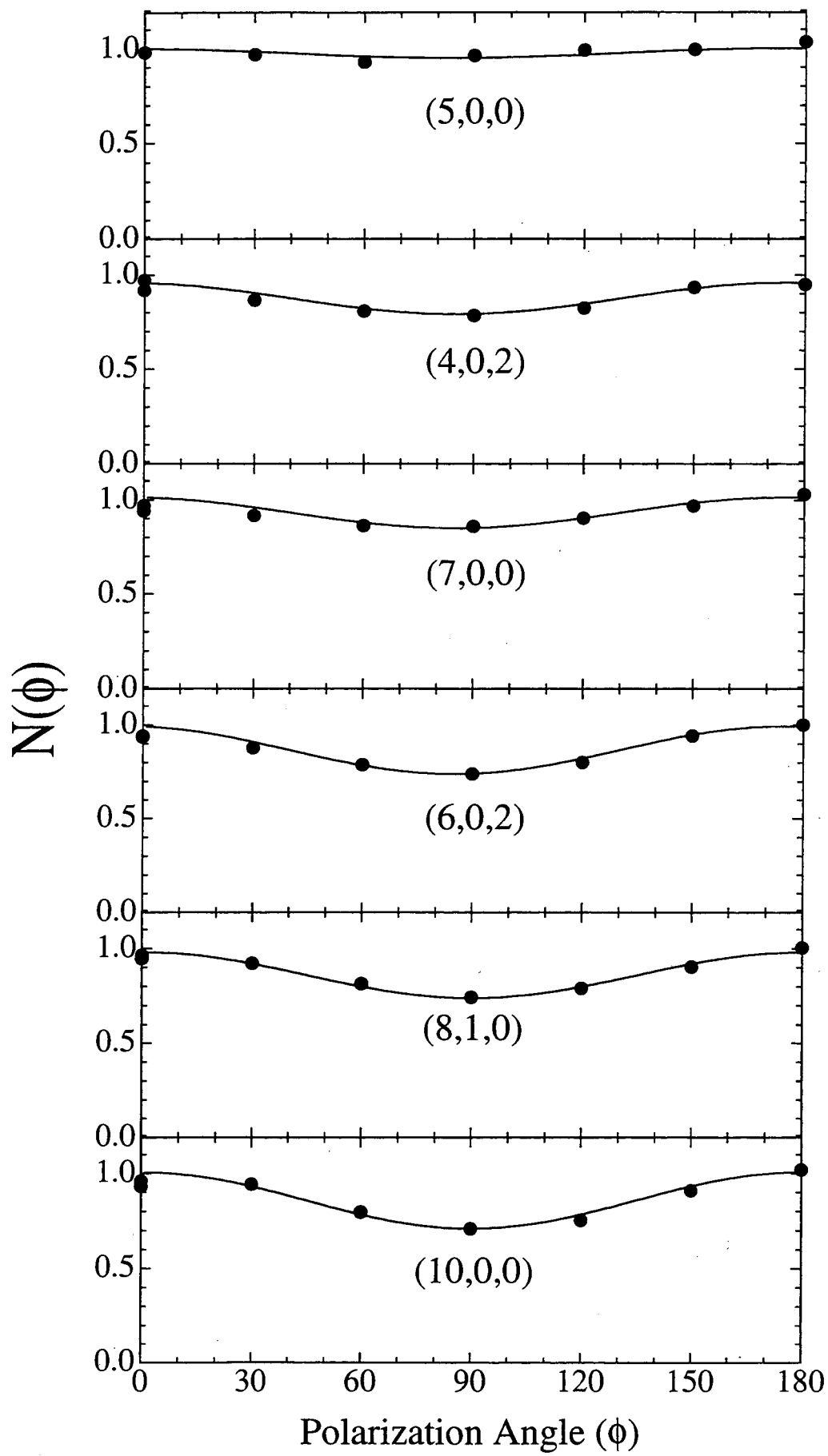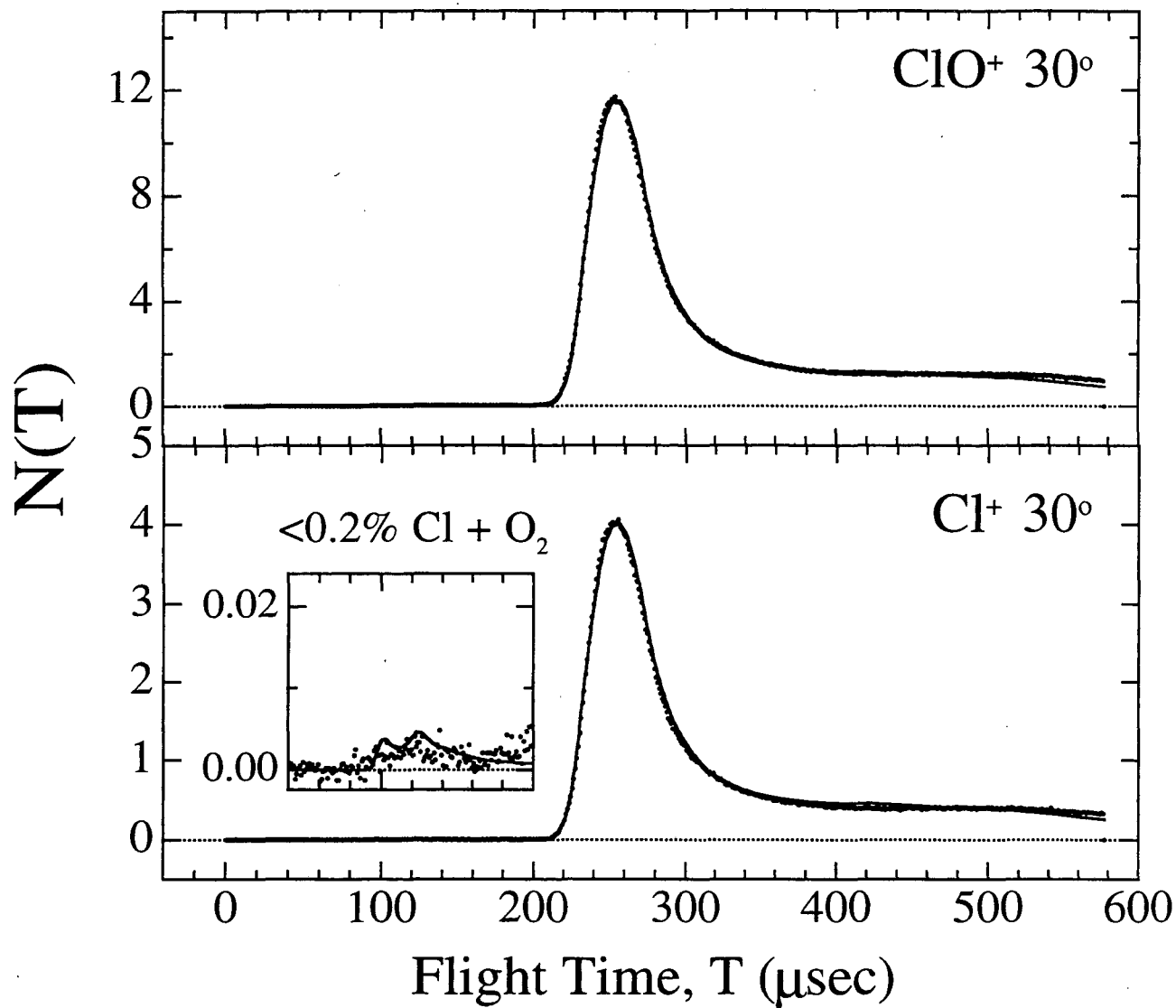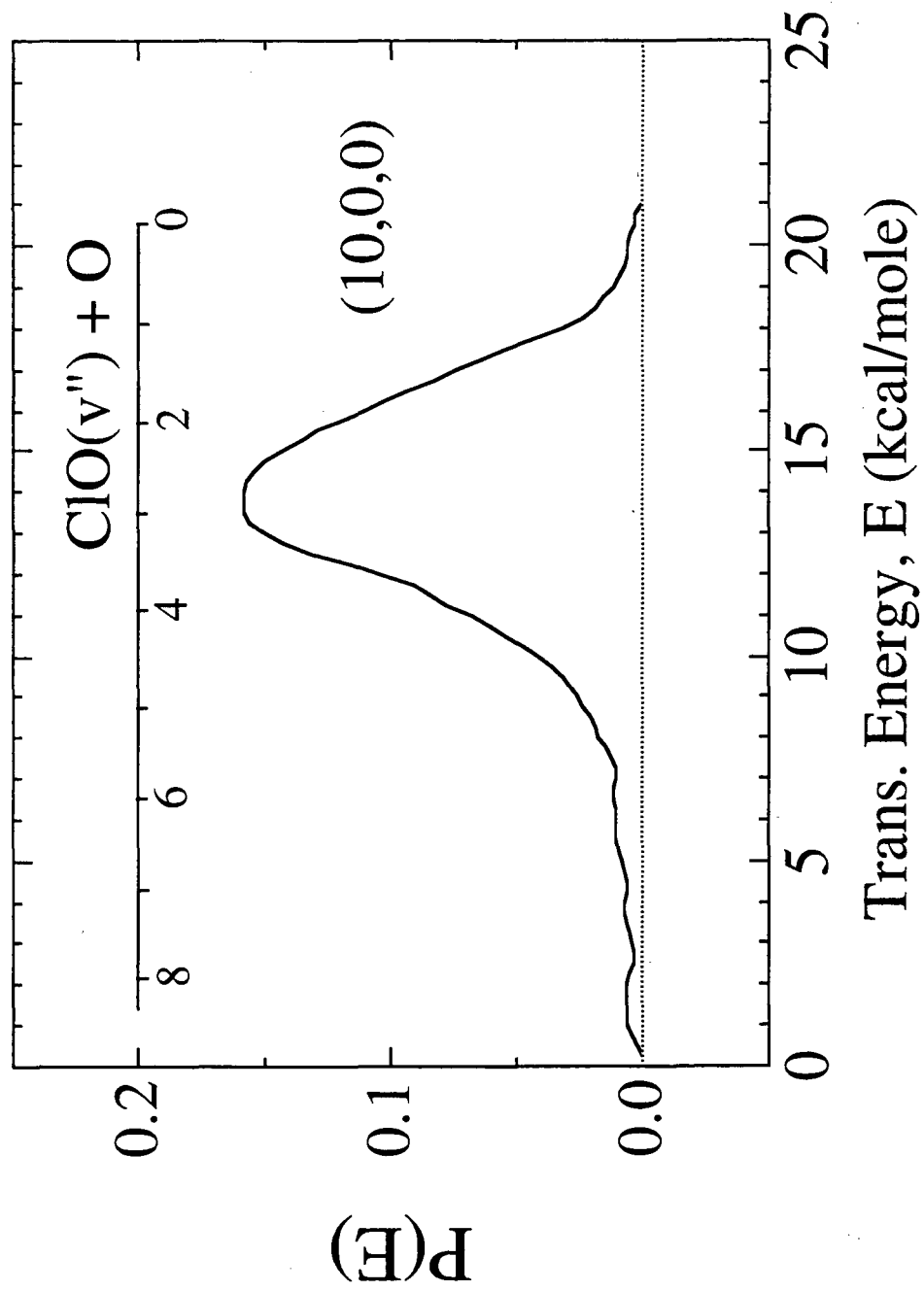
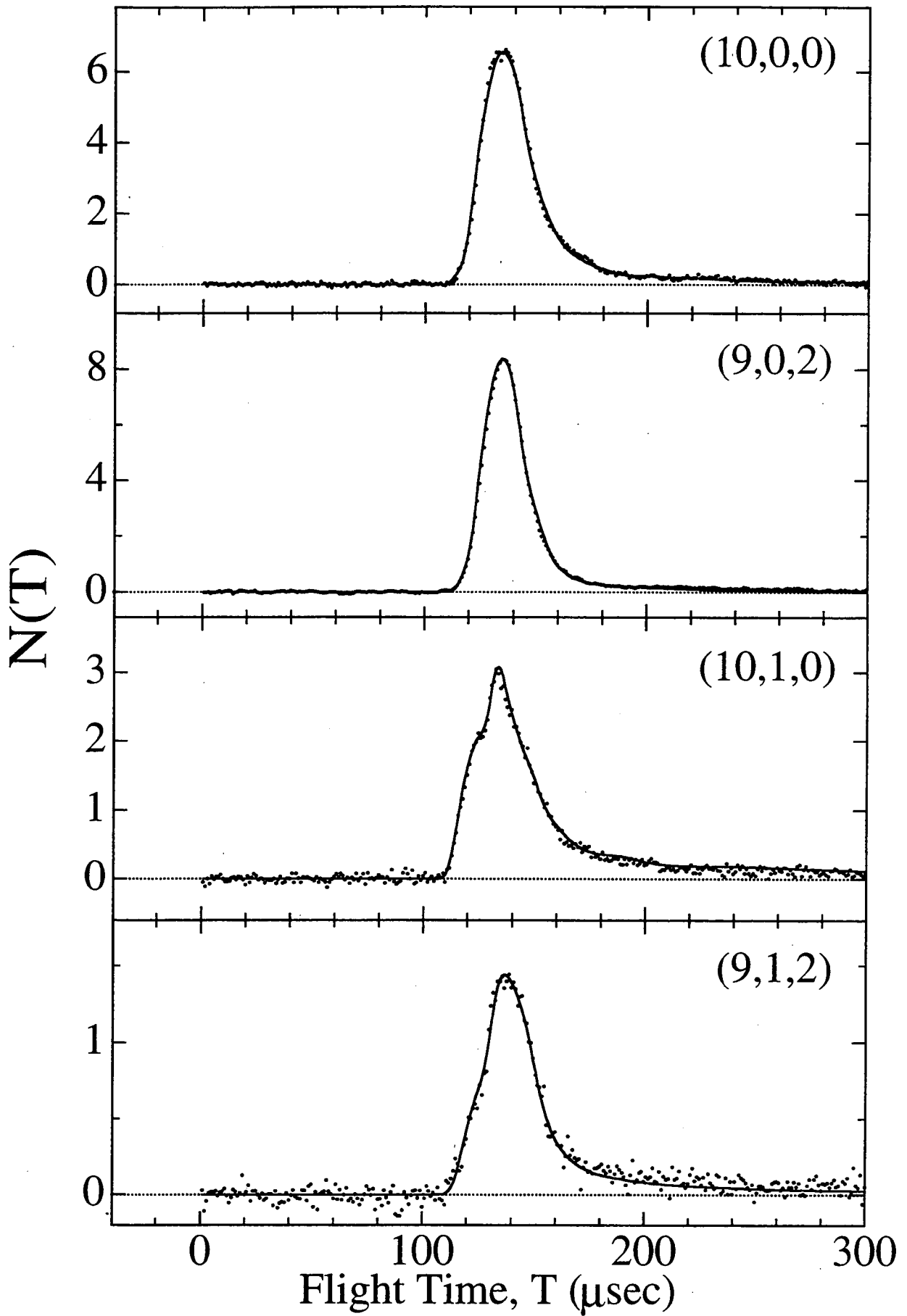Fig. 24
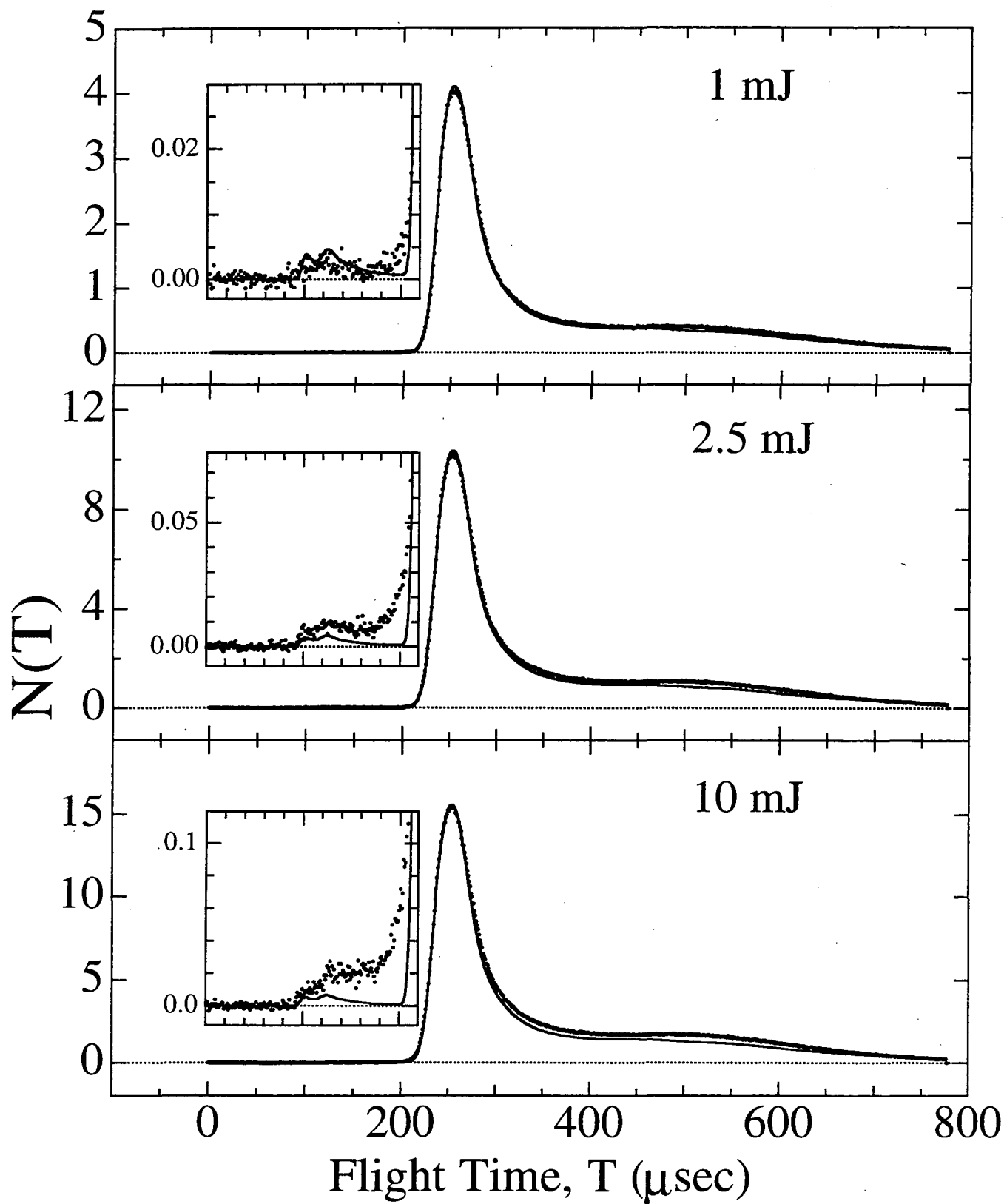
Fig. 25
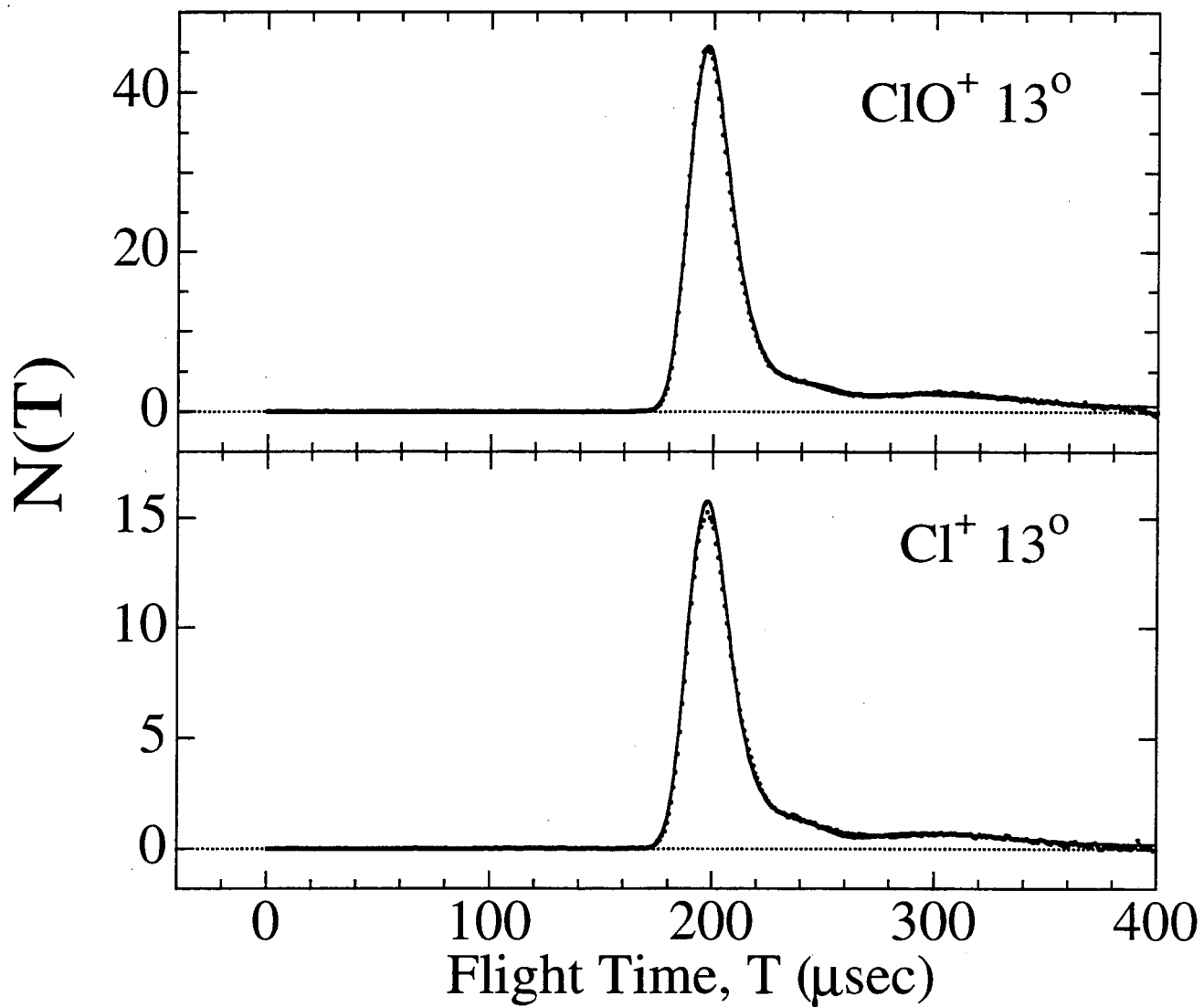
Fig. 26
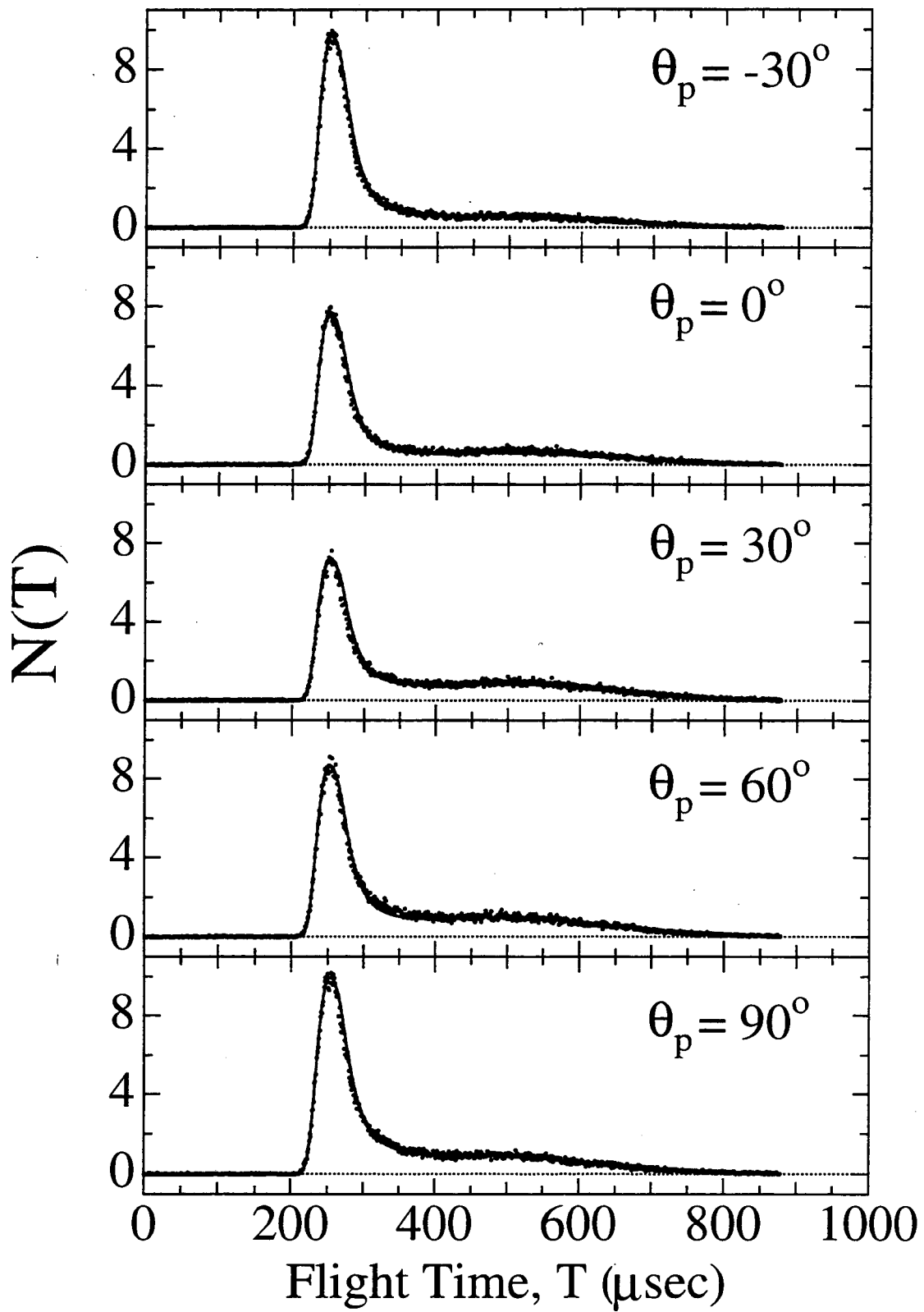
Fig. 27
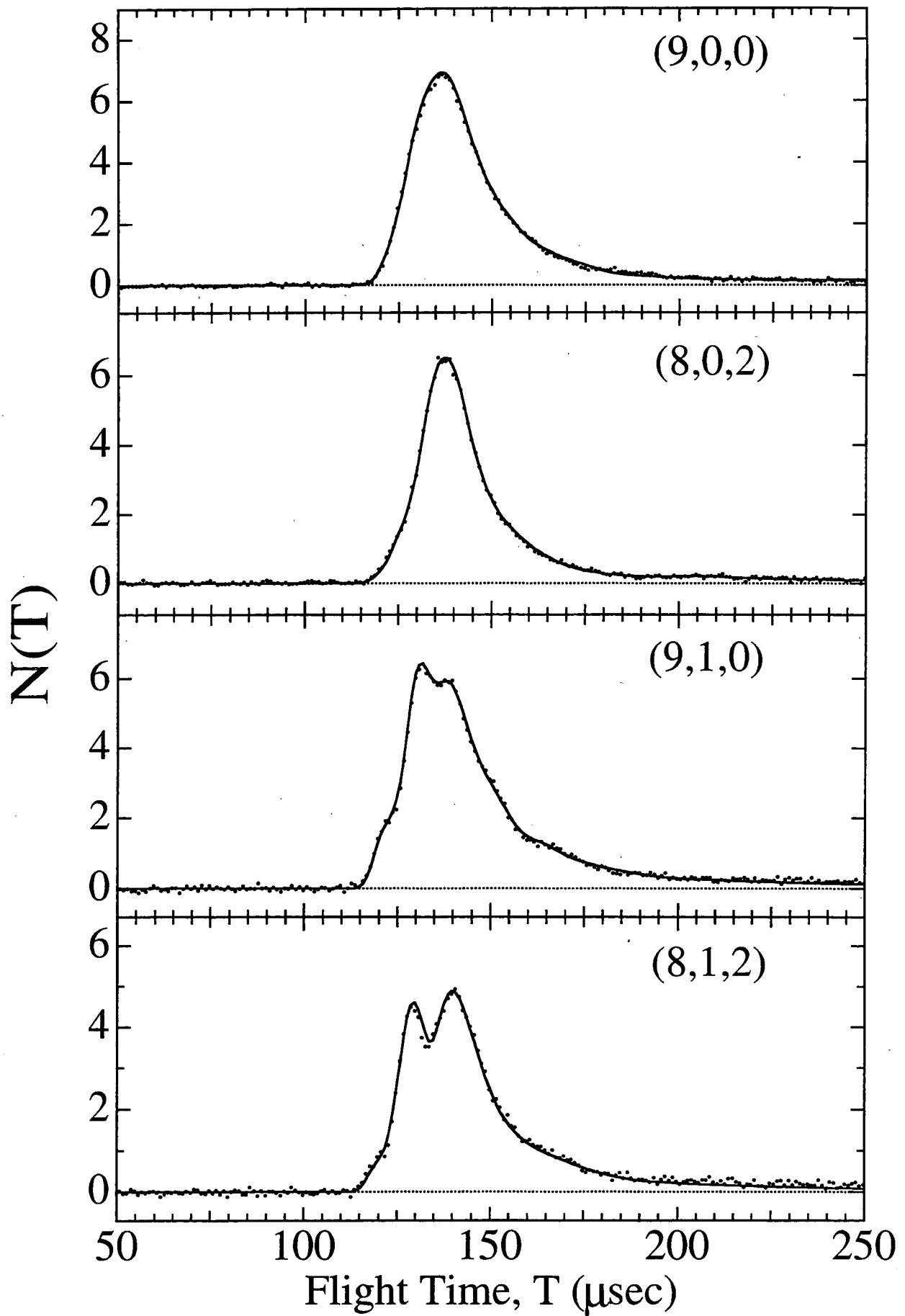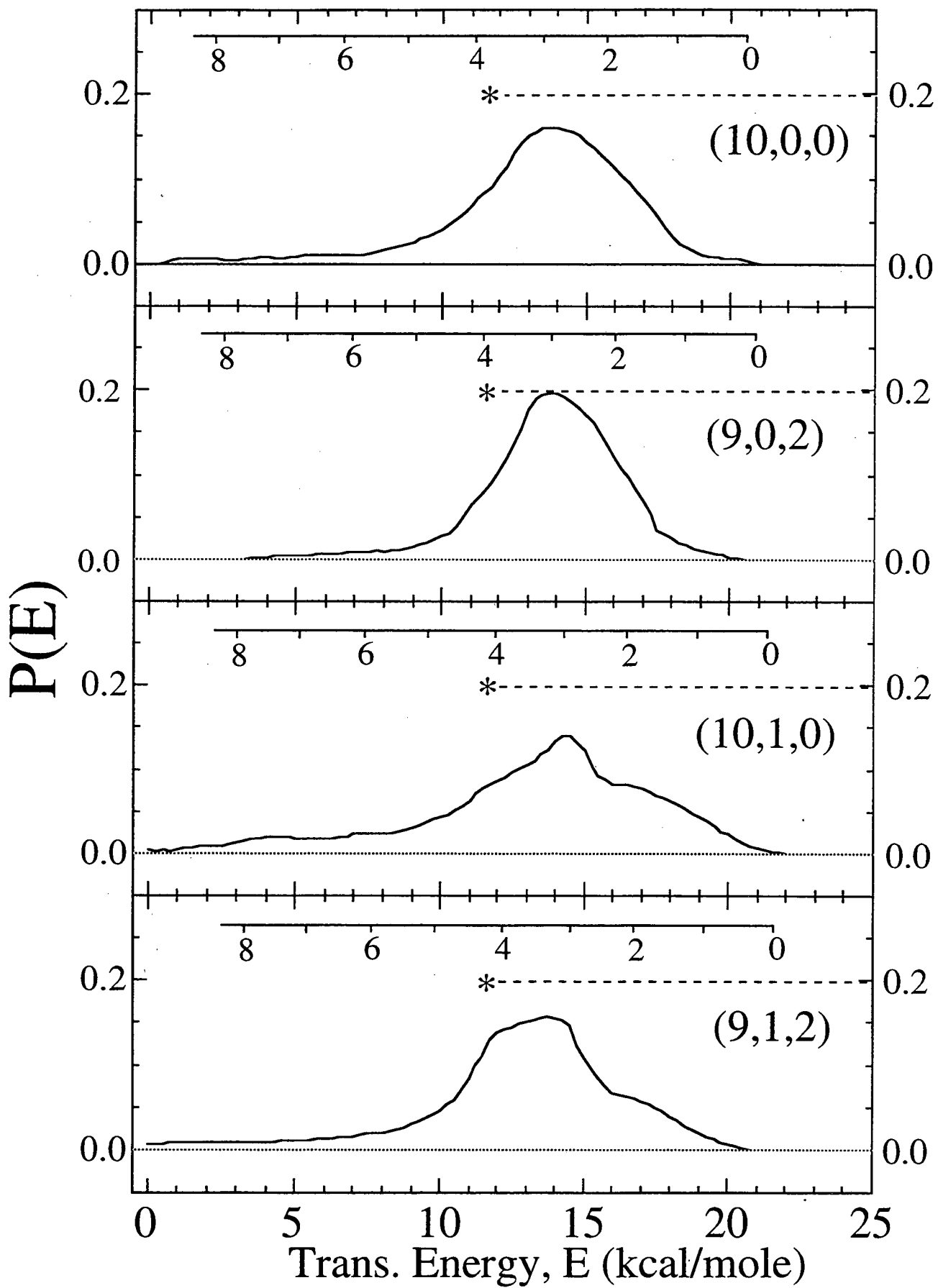
Fig. 28
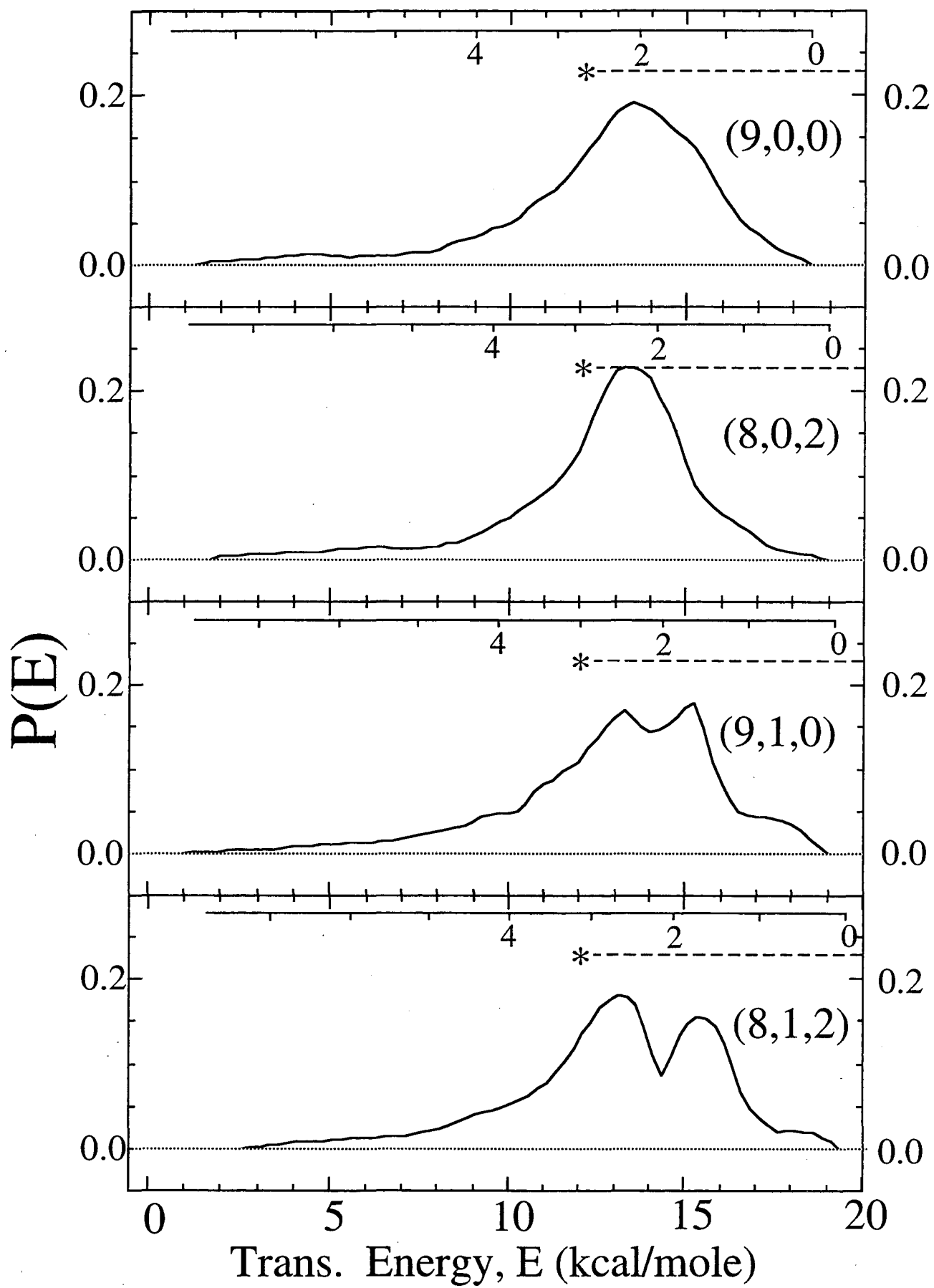
Fig. 29

Fig. 30

Fig. 31

LAWRENCE BERKELEY NATIONAL LABORATORY
UNIVERSITY OF CALIFORNIA
TECHNICAL & ELECTRONIC INFORMATION DEPARTMENT
BERKELEY, CALIFORNIA 94720